Model developments for *in silico* studies of the lumbar spine biomechanics

Tesi Doctoral

Jérôme Noailly

Universitat Politècnica de Catalunya

2009

Model developments for *in silico* studies of the lumbar spine biomechanics

- Tesi doctoral -

La present tesi investiga l'ús de la modelització amb elements finits per a l'estudi de la biomecànica lumbar per a l'avaluació clínica. Els estudis bibliogràfics del capítol 1 mostren relacions funcionals clares entre les forces externes i les estructures i formes del teixit lumbar. Els estudis clínics demostraren que independentment del seu origen, el dolor lumbar pot veure's empitjorat per sobrecàrregues dels teixits. Les mesures experimentals són insuficients per descriure la distribució de càrrega entre els diferents teixits lumbars, és així que s'han utilitzat models d'elements finits. No obstant, la fiabilitat dels models a l'hora de predir les càrregues locals en els teixits no ha estat demostrada, essent aquest un dels objectes d'estudi.

En el Capítol 2 s'elaborà un model bisegment de la columna lumbar. El model inicial es completà incloent el còrtex vertebral, una definició complerta de les juntes sinovials, les plaques terminals de cartílag i una descripció millorada de l'estructura de l'anell. Es van simular càrregues simplificades per als estudis in vitro per calcular les distribucions de tensions, deformacions i energia. El model bisegment és vàlid per interpretar les distribucions de càrrega funcionals a L3-L5 en el cas d'estructures conegudes de teixit, però el conjunt de la geometria L3-L5 necessitava ser millorat.

Així al Capítol 3 es creà un model geomètric bisegment precís de L3-L5. El nou model incloïa les corregides: dimensions i formes, alçades de disc, localitzacions del nucli, formes posteriors de l'os, i distribució dels lligaments. Després de comparar a nivell biomecànic l'antiga geometria amb la nova, els resultats mostraren que els rols relatius dels teixits modelats depenen de la geometria. En general, les distribucions de càrrega predites eren més fisiològiques en el nou model. En canvi, ambdós models, reprodueixen rangs experimentals de moviment, així doncs la seva validació hauria de tenir en compte les transferències de càrrega locals.

El Capítol 4 es centra en la variabilitat dels angles creuats del col·lagen de l'anell. Es crearen quatre models bisegment amb organitzacions d'anell fibrós basats en la bibliografia comparant-se sota diverses càrregues. A més es proposà un paràmetre d'estabilització de l'anell per analogia a un tub de parets gruixudes. La biomecànica del model depenia en gran mesura de l'organització de l'anell fibrós, però el paràmetre d'estabilització era sovint contradictori amb les tensions i forces predites. Així, s'assumí que la geometria de la columna i l'organització de l'anell fibrós estaven lligades. Les xarxes d'anell de col·lagen adaptades es poden determinar numèricament, però els models d'anell haurien d'estar bastats en relacions mecanobiològiques.

Al Capítol 5 es presenta un model de disc artificial acoblat amb el model de L3-L5. Models bisegment amb i sense implant van ser comparats amb càrregues controlades per força o desplaçament, incloent o no l'aproximació del pes del cos. La rigidesa de la pròtesi alterava generalment les distribucions de càrrega i les rotacions controlades per desplaçament conduint a grans efectes adjacents. Incloent el pes del cos les condicions de contorn semblaven més fisòlogiques que sense. Malgrat la rigidesa del nou disc, aquest sembla més prometedor que altres dispositius comercials.

En aquesta tesi s'han creat sis models nous elements finits de la columna lumbar osteoligamentosa. Les simulacions han mostrat que l'ús fiable dels models requereix d'una descripció precisa de les càrregues locals i respostes mecàniques de teixits. Les prediccions locals van estar limitades qualitativament degudes al desconeixement de les estructures de teixit tou, equacions constitutives i condicions de contorn. En canvi, els models poden ser emprats com a laboratoris in silico per superar aquestes limitacions. Basat en la informació numèrica i experimental, s'ha proposat un procediment jeràrquic per al desenvolupament qualitativament fiable de models elements finits de la columna lumbar.

Jérôme Noailly és MSc en Ciencia dels Materials (biomecànica) per la Universitat Politècnica de Catalunya (UPC, Barcelona), MSc en acústica per l'Institut National des Sciences Appliquées de Lyon (INSA-Lyon, Lyon, França), Enginyer de Materials per l'Ecole Européenne d'Ingénieurs en Génie des Matériaux (EEIGM,Nancy, França) i Llicenciat en Química-Física per la Université Pierre et Marie Curie (UPMC, París, França). En el moment d'escriure, l'autor compta amb set anys d'experiència en biomecànica i mecanobiologia computacional, compartides entre la UPC, l'Eindhoven University of Technology (TUe, Eindhoven, The Netherlands), i l'AO Research Institute (AO Foundation, Davos, Switzerland).

Model developments for *in silico* studies of the lumbar spine biomechanics

- PhD Thesis -

This PhD thesis investigated the use of finite element modelling to study lumbar spine biomechanics for clinical assessment. Bibliographic studies reported in the first Chapter showed clear functional relations between external forces and lumbar spine tissue structures and shapes. Clinical research revealed that independently of its origin, low back pain may be worsened by altered tissue mechanical environments. Experimental measurements alone cannot truly describe the load distributions between the different lumbar spine tissues. Thus, finite element models have been used in the past. But model reliability in predicting local tissue loadings is still not manifest and has been explored in this thesis as described in the following chapters.

In Chapter 2, a L3-L5 lumbar spine bi-segment model was built. An initial model was completed to include the vertebral cortex, a full definition of the facet joints, the cartilage endplates, and an improved description of the annulus fibre-reinforced structure. Simplified load-cases used for *in vitro* studies were simulated to calculate stress and strain energy distributions. Predictions within the L3-L5 lumbar spine bi-segment model could be interpreted in terms of functional load distributions related to known tissue structures, but the overall L3-L5 bi-segment model geometry needed further update.

Thus, in Chapter 3, a geometrically accurate L3-L5 lumbar spine bi-segment model was created. The new model included corrected L3 and L5 body shapes and dimensions, corrected disc heights and nucleus placements, corrected posterior bone shapes, dimensions, and orientations, and corrected ligament distributions. The new and old geometries were biomechanically compared. Results showed that the relative roles of modelled tissues greatly depend on the geometry. Predicted load distributions were generally more physiological in the new model. However, new and old models could both reproduce experimental ranges of motion, meaning that their validation should take into account local load transfers.

Chapter 4 focuses on the variability of the annulus collagen criss-cross angles. Four bi-segment models with literature-based annulus fibre organizations were created and compared under diverse loads. Moreover, an annulus stabilization parameter was proposed by analogy to a thick walled pipe. Model biomechanics greatly depended on the annulus fibre organization, but annulus stabilization parameter was often contradictory with the predicted stresses and strains. Spine geometry and annulus fibrous organization were hypothesized to be linked together. Adapted annulus collagen networks may be numerically determined, but annulus modelling should be based on mechano-biological relationships.

In Chapter 5, a case-study of a novel artificial disc design coupled with the L3-L5 lumbar spine model is presented. Bi-segment models with and without implant were compared under load- or displacement-controlled rotations, with or without body-weight like load. Prosthesis stiffness generally altered the load distributions and displacement-controlled rotations led to strong adjacent level effects. Including body weight-like loads seemed to give more realistic results. Although the novel disc substitute is too stiff, it is more promising than other existing commercial devices.

In this thesis, six new osteoligamentous lumbar spine bi-segment finite element models were created. Simulations showed that reliable use of lumbar spine finite element models requires precise descriptions of local tissue loading and response. Local predictions were qualitatively mainly limited by a lack of knowledge about soft tissue structural organisations, constitutive equations, and boundary conditions. However, models can be used as *in silico* laboratories to overcome such limitations. A hierarchical procedure for the development of qualitatively reliable lumbar spine finite element models was proposed based on available numerical and experimental inputs.

Jérôme Noailly is MSc in material science (biomechanics) from the Technical University of Catalonia (UPC, Barcelona, Spain), MSc in acoustics from the Lyon's National Institute of Applied Sciences (INSA-Lyon, Lyon, France), Material Engineer from the European School of Material Engineering (EEIGM, Nancy, France), and has a four-year university degree in Physical Chemistry from the University Pierre et Marie Curie (UPMC, Paris, France). At time of writing, the author has seven years of full time research experience in computational biomechanics and mechanobiology, shared among the UPC, the Eindhoven University of Technology (TUe, Eindhoven, The Netherlands), and the AO Research Institute (AO Foundation, Davos, Switzerland).

Model developments for *in silico* studies of the lumbar spine biomechanics

Tesi Doctoral

Memòria realitzada per

Jérôme Noailly

Nascut en St Germain en Laye, França

Per optar al grau de Doctor en Ciències amb menció Europea per la Universitat Politècnica de Catalunya

Directors:
Dr. **Damien Lacroix** i Prof. Dr. **Josep Anton Planell**
Universitat Politècnica de Catalunya, Institut de Bioenginyeria de Catalunya

Programa de Doctorat:
Ciència dels Materials i Enginyeria Metal·lúrgica

Departament:
Departament de Ciència dels Materials i Enginyeria Metal·lúrgica

This research has been funded by the Spanish Ministery for Science and Innovation under the PhD grant AP2002-2395 of the University Professor Training (FPU) program.

I first would like to dedicate this book to Soraya, the only person really aware about how much fight, frustration, motivation, tears, laughs, angry, happiness, and satisfaction is behind each line of the presented work.

I am also proud to dedicate my efforts to my parents, my grand-mother, and Nanou who always trusted and supported me.

Jérôme.

Table Of Contents

MODEL DEVELOPMENTS FOR *IN SILICO* STUDIES OF THE LUMBAR SPINE BIOMECHANICS

Chapter1

"Caminante, son tus huellas
el camino y nada más;
Caminante, no hay camino,
se hace camino al andar"

(Antonio Machado)

Chapter 1

- LUMBAR SPINE FUNCTIONAL ANATOMY & STUDIES - STATE OF THE ART

A. The lumbar spine functional anatomy

In this section, a non-exhaustive anatomical description of the human spine is given with special focus on the lumbar spine. The objective of this introduction is to set some bases about the specific anatomy of the lumbar spine and how this anatomy is related to the back functional biomechanics. The information reported in the next pages will be necessary to ensure a good understanding of the numerical studies developed in this thesis, in terms of terminology and from a mechanistic point of view.

I. The whole spine

In all vertebrates, the spine has three biomechanical basic functions; first, it transfers the external loads through the body; to anterior and posterior members for quadrupeds and from the superior to the inferior extremities for bipeds. Second, it ensures a controlled flexibility between the head, the trunk and the pelvis, and third, it protects the spinal nerve roots from loads, shocks and excessive displacements (Pope *et al.*, 1991; Comín *et al.*, 1995).

a. The vertebrae

The normal human spine is composed of 33 or 34 vertebrae distributed into five distinct sections that are defined by specific anatomical and functional characteristics (Fig. 1). At the upper extremity, the atlas (C1) and the axis (C2) articulate the vertebral column with the head via the occipital also called C0. They are part of the cervical spine, which extends in the crania-caudal direction on seven vertebrae (C1-C7). The twelve following vertebrae (T1-T12) are attached to the rib cage and form the thoracic spine. The lumbar spine begins after the thoracic spine with the first vertebra without ribs (L1) and includes the four following ones (L2-L5). After the lumbar spine, five welded vertebrae (S1-S5) constitute the sacral which articulates laterally with the wings of the iliac and caudally with a lower block of three or four welded vertebrae called the coccygeal spine.

b. The spine curvature

As shown in Fig. 1.1, the vertebral column is not straight, but has a natural sinusoidal shape formed by three antagonist curvatures in the anterior-posterior plane also named the sagittal plane. The posterior faced concavities that are found in the cervical and in the lumbar spines are called lordosis, and the posterior faced convexity of the thoracic spine is called kyphosis.

The human foetal spine has no lordosis and looks like a quadruped spinal column. The cervical curvature appears at the end of pregnancy and becomes more pronounced between the sixth and the twelfth week following the birth when the baby begins to sustain its head (Comín *et al.*, 1995). The lumbar lordosis only gets fully developed with the walk about two years after birth (Comín *et al.*, 1995). From a structural point of view, when a vertical load is applied, the shape of the human spine allows aligning the head and trunk gravity centres with the pelvis reaction force. This configuration reduces the instabilities, since the muscle activity necessary to prevent buckling and to maintain an erected posture is minimized. Hence, although it is hard to decide wether function follows form or form follows function, the natural development of the vertebral column leads to think that cervical and lumbar lordoses both result from a genetic adaptation to the bipedal posture kinematics.

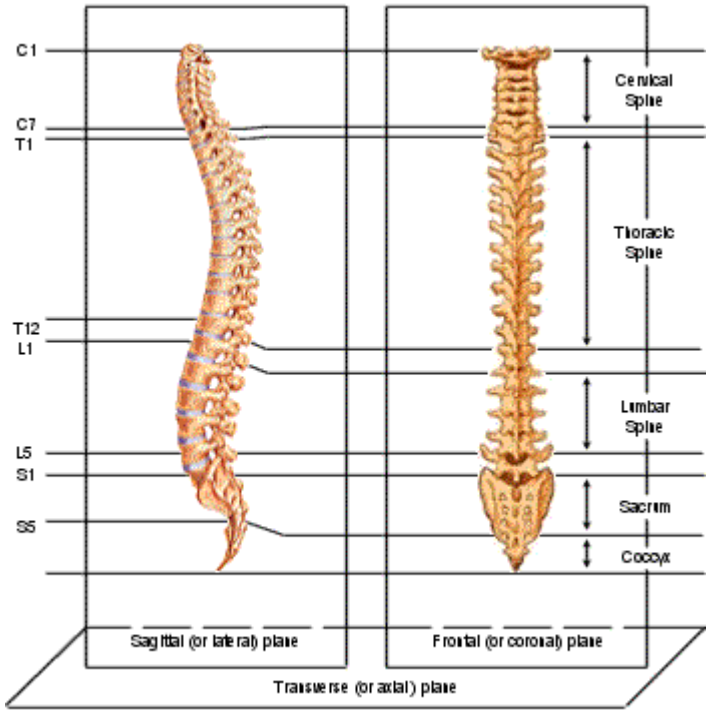

Figure 1.1: General presentation of the various parts of the spine and of its overall geometry.

c. The articulated spine

From C3 to sacrum, the vertebrae are constituted of an anterior vertebral body and posterior bony elements, namely the pedicle, the lamina and the processes (Fig. 1.2). Except in the sacral and coccygeal spines, the major link between the vertebral bodies is the intervertebral disc. The bony posterior elements of two adjacent vertebrae are linked together through the spinal ligaments and the facet articular contacts. The combination of these linking passive components with the muscles ensures the functional flexibility of the vertebral column.

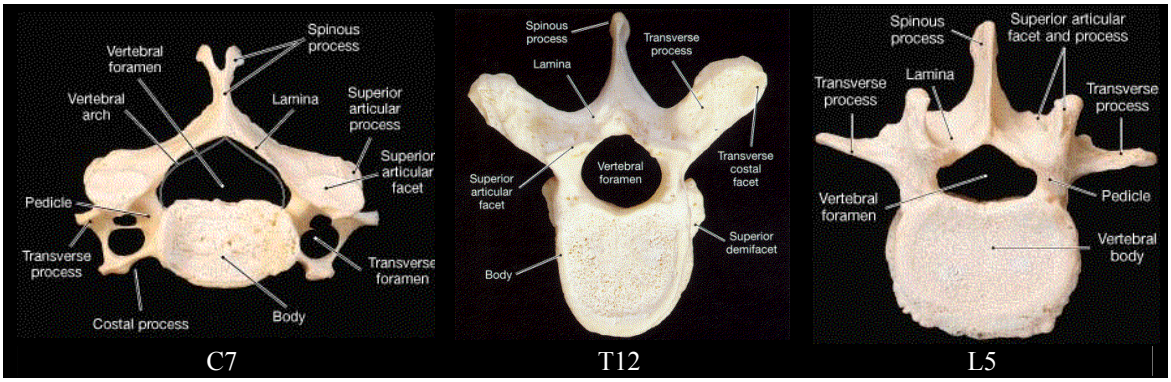

Figure 1.2: Cranial view of typical vertebral shapes in the cervical, thoracic and lumbar spine adapted from (Martini, 1998)

Figure 1.3 shows the ranges of motion in the different sections of the vertebral column and illustrates the following description of the functional spine kinematics. While the cervical and the lumbar spines have to be rather flexible to allow respectively the mobility of the head with respect to the trunk and the mobility of the trunk with respect to the pelvis, the thoracic spine has to be sufficiently rigid to prevent excessive deformations in the rib cage that contains vital organs such as the heart and the lungs. The flexibility of the lumbar spine has to be combined with a great mechanical resistance, since this lower part of the vertebral column supports the whole upper body weight including any extra weights that may be carried during the daily life.

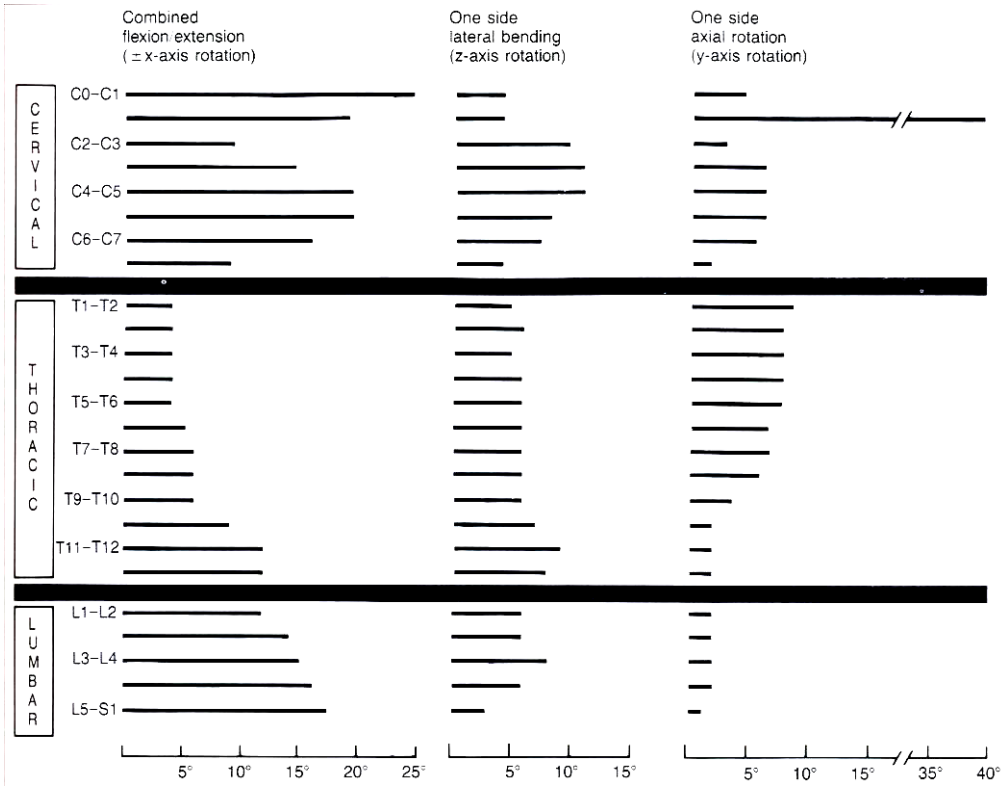

Figure 1.3: Ranges of motion at the different levels of the whole spine in sagittal, frontal and axial rotations (reproduced from (White III and Panjabi, 1990))

The functional mobility in each region of the back is firmly correlated with the local anatomy of the vertebrae and the intervertebral discs. For example, the intervertebral disc height plays an important role; in the thoracic spine, intervertebral discs represent about 20% of the total section height (McInerney and Ball, 2000), whereas in the cervical and lumbar spine, intervertebral discs contribute to about 30-35% of the section height (Frobin *et al.*, 2002; Frobin *et al.*, 1997; Rauschning, 1991). The shape of the vertebrae is also an important morphological factor which interacts with the rachis mobility. As shown in Fig. 1.2, the width (frontal plane) of the inferior cervical spine vertebral bodies (C3-C7) is approximately twice as the depth (sagittal plane). Combined with the important relative height of the intervertebral discs, this shape allows a great amount of flexion-extension ranging from 10º at the C2-C3 level to about 20º at the C5-C6 level (Fig. 1.3). In the thoracic spine, where the vertebral bodies are more or less cylindrical with a marked posterior concavity, the range of motion in flexion-extension varies between some 4º at the T1-T2 level and about 6º at T9-T10 (Fig. 1.3). At the lower thoracic levels, the intervertebral disc height relative to the adjacent vertebrae and the vertebral body width both increase, and the vertebral bodies become usually wider than deep when progressing down the lumbar spine. A consequence is that the lumbar mobility increases caudally in flexion-extension up to values ranging between 12º and 20º (Fig. 1.3).

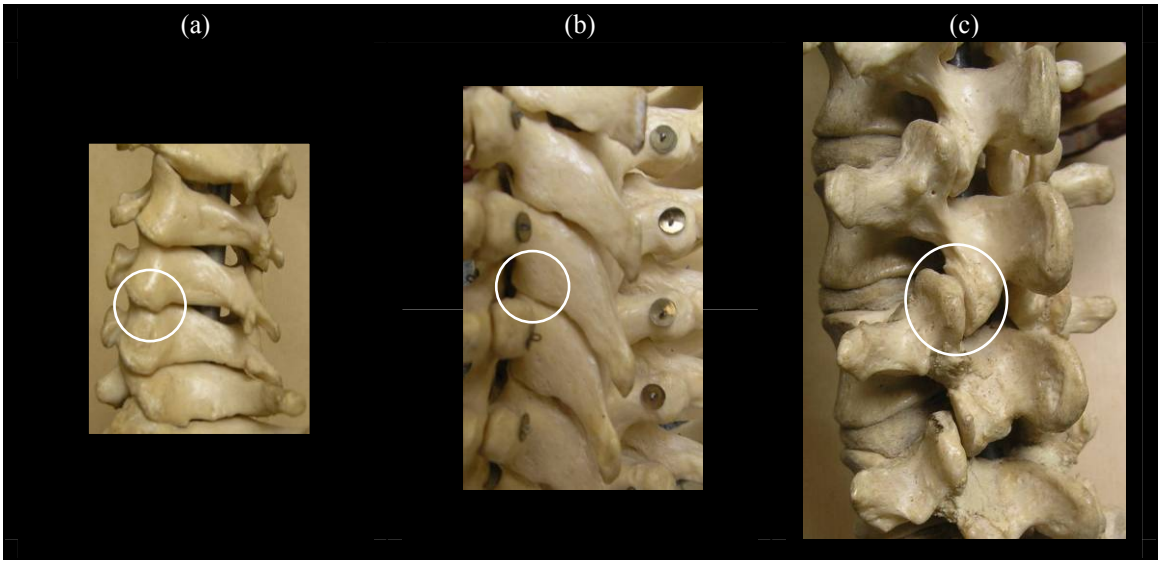

Figure 1.4: Postero-lateral views of samples of cervical spine (a), thoracic spine (b) and lumbar spine (c) with special emphasis of the zygapophysial joints

The vertebral articular processes are other elements whose morphology also rules significantly spinal motions. They support the zygapophysial joints (or facet joints) that articulate dorsally two adjacent vertebrae (Fig. 1.4). In this articulation, the orientation of the contact surfaces (articular facets) with respect to the anatomical planes has a major effect on the axial rotation: in the lower cervical spine, where the articular facets have a full frontal orientation and make an angle of 45º with the horizontal plane (Panjabi *et al.*, 1993), rotations up to 40º are allowed (Fig. 1.3). Caudally, the articular facets become more vertical and more sagittal. In the lumbar spine, facets are nearly vertical with an almost sagittal orientation (Panjabi *et al.*, 1993; Tulsi and Hermanis, 1993), which leads to an axial rotation mobility reduced to about 2º on both sides (Fig. 1.3). This severely restricted axial motion at the lower spine levels contributes to the stability of the bipedal locomotion.

Although articular facets and intervertebral discs do not control alone the functional mobility of the spine, they are of particular interest in clinical and biomechanical studies, as their morphology strongly interferes with the local segment kinematics.

II. Lumbar spine

a. Loads and muscle stabilization

The lumbar spine is the most caudal part of the articulated vertebral column and it normally supports the highest mechanical loads. In a person who does not carry extra weight, the lumbar structure bears at least 55% of the total body mass. Because of the spine curvature, external loads generate shear forces and rotational moments that must

be compensated by the action of the muscles in order to ensure mechanical stability. The muscles forces described in this paragraph will be limited to the case of upright standing, since this posture can be considered as an active equilibrium state of the spine where the intervertebral disc pressure is minimal (Kelsey *et al.*, 1984; Wilke *et al.*, 2001).

Table 1.1 gives an idea of the extension moments and compression forces magnitudes that might result from the muscular activity at the lumbar level by only considering the action of the major dorsal muscles (Fig. 1.5) (Bogduk *et al.*, 1992). The minor role of the ventral and intra-abdominal muscles was confirmed by the report of McNeill et al (McNeill *et al.*, 1980) who registered in vivo the maximum trunk moments from patients without pathology. The momentum values they measured in extension correspond to the values presented in Table 1.1, which points out the major role of dorsal muscles in agreement with other reported suggestions (Zander *et al.*, 2001; Bogduk, 1997).

Table 1.1: Values of total extension moments and total compressive force applied in the lumbar spine by the multifidus, the iliocostalis lumborum and the longissimus thoracis muscles (Bogduk et al., 1992).

Level	L1-L2	L2-L3	L3-L4	L4-L5
Maximum extension moments applied by muscles (Nm)	107	122	147	154
Maximum compressive force applied by muscles (N)	1823	2117	2497	2811

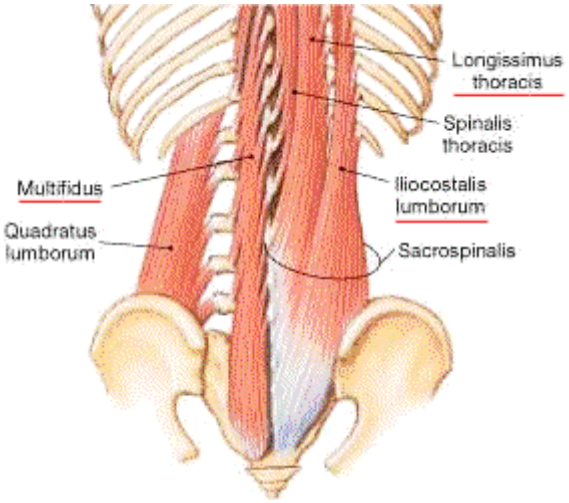

Figure 1.5: The spinal erector muscles acting at the lumbar level (Adapted from (Martini, 1998)) – Muscles whose action is represented in Table 1.1 are underlined)

As a response to axial external loads, the lordotic shape of the lumbar spine tends to be amplified and therefore lumbar back muscles have to stabilise the lumbar segments in the sagittal plane, exerting backwards moments, compression forces in the

vertebra axial axis, and shear forces perpendicular to the axis. While the axial forces remain compressive all along the lumbar spine, shear forces may be posterior or anterior depending on the spinal curvature and the spinal level (Fig. 1.6). Hence, as shown in Fig. 1.7, the stabilising posterior shear forces exerted by the multifidus and the erector spinae become less important at the L4-L5 level and pass to be anterior at the L5-S1 level. This indicates that the external loads applying on the lumbar spine are not uniform from level to level, and in the next paragraph, the interaction between the upright standing loading and the lumbar spine detailed geometry will be discussed.

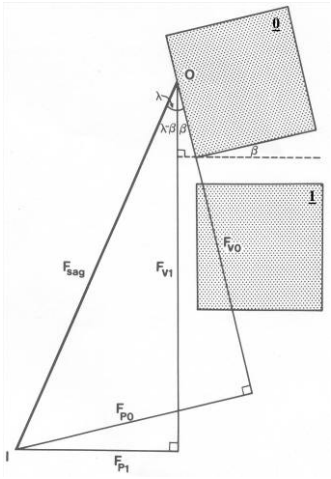

The fascicle is represented by the line OI, O being the origin and I the insertion point. F_{sag} is the force exerted by the fascicle in the sagittal plane, and F_v and F_p are the compressive and shear forces applied by the fascicle on the vertebrae. Sub indices 0 and 1 link respectively the forces to the vertebra of origin (0) and to the vertebrae below (1). λ is the orientation of the fascicle with respect to the vertebra of origin and β the intersegmental angle. Therefore, the compressive and shear forces are expressed as functions of F_{sag}, λ and β by the mean of the following relations: $F_{v0} = F_{sag} \cos \lambda$; $F_{v1} = F_{sag} \cos (\lambda - \beta)$, $F_{p0} = F_{sag} \sin \lambda$ and $F_{p1} = F_{sag} \sin (\lambda - \beta)$. Hence, while the compressive force has always the same sign, the shear force can be posterior or posterior, depending on the values of λ and β.

Figure 1.6: Schematic representation of the compressive loads and shear forces exerted by a muscle fascicle on its vertebra of origin and on the vertebrae located between the origin and the insertion of the fascicle (Adapted from (Bogduk et al., 1992)).

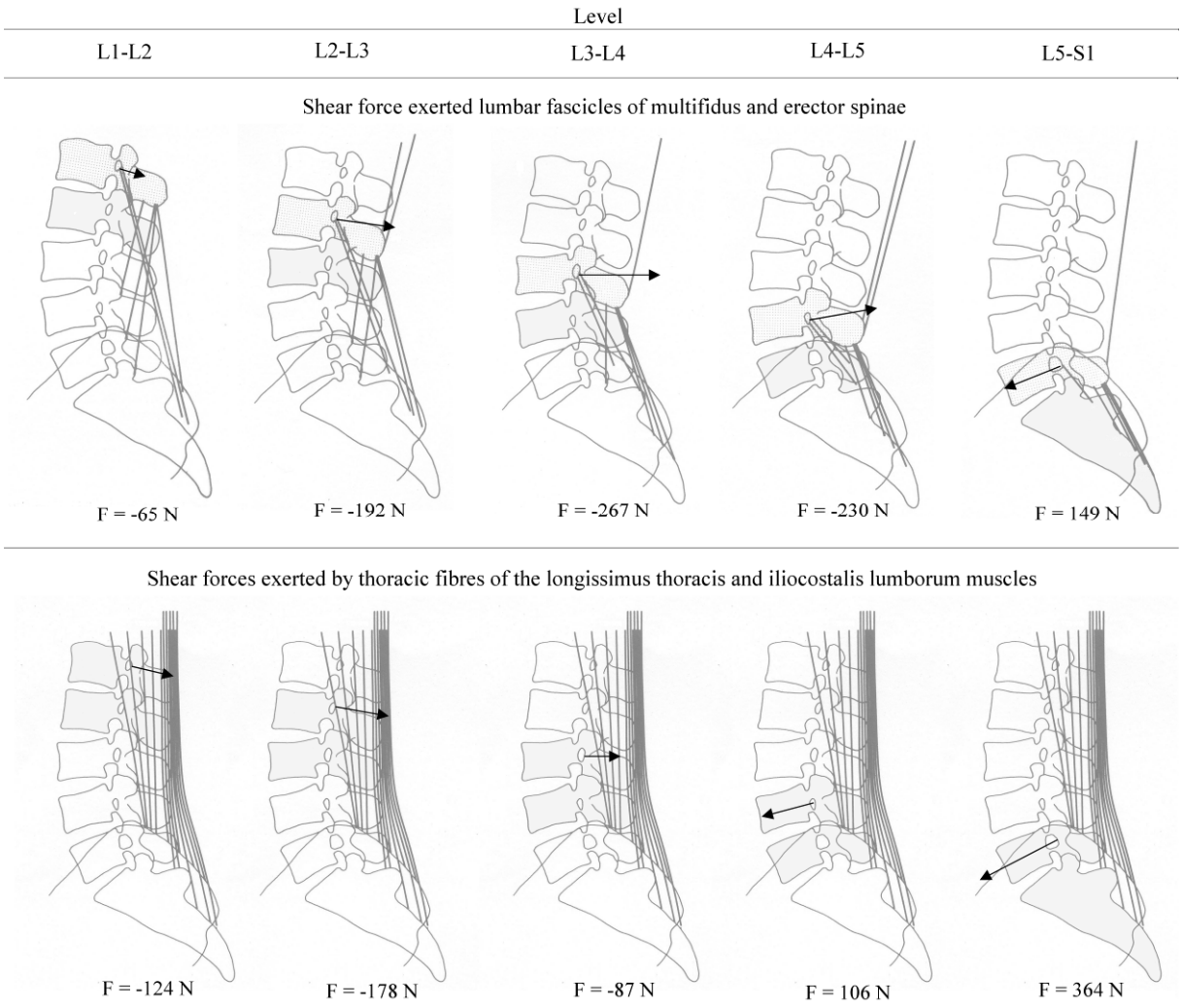

Figure 1.7: Shear forces exerted by the multifidus and the erector spinae muscles at different levels of the lumbar spine (Adapted from (Bogduk et al., 1992)). The forces were computed for each motion segment, from in vivo measurements, and considering the action of all the fascicles which cross the segment and originate at the first vertebra of the segment or at superior levels.

b. Normal functional anatomy & structure

1) Vertebrae

Due to their mechanical role, the lumbar spine vertebrae are the strongest of the whole articulated spine. A vertebra may be divided into three parts (Fig. 1.8); frontally, the first part is the vertebral body that is constituted by a block of trabecular bone enclosed in a cortex formed by the cortical shell, laterally, and by the bony endplates, upwards and downwards. The second part, namely the pedicles, links dorsally the vertebral body to the third part compound by the lamina and the processes (Fig. 1.2). These latter components are also referred to as the bony posterior elements.

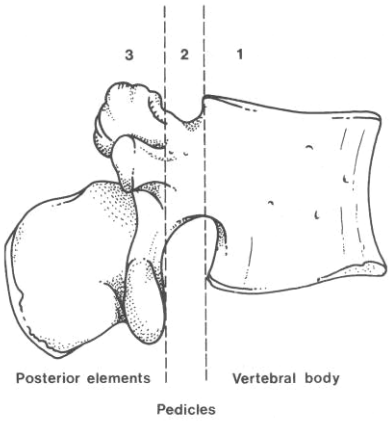

Figure 1.8: Division of a lumbar vertebra into three functional components (Adapted from (Bogduk, 1997))

In a vertebra, three types of bone can be found; the trabecular, the cortical and the subchondral bone. In the bony posterior elements, the subchondral bone is surrounded by the articular cartilage of the zygapophysial joints (Fig. 1.4c) and in the vertebral bodies, it is surrounded by the intervertebral disc and is more commonly called bony endplate. Both cortical shell and bony endplates are very thin (some fractions of millimetres) (Edwards *et al.*, 2001) and the trabecular bone represents the major component of the vertebral body (Fig. 1.9). From a morphological and kinematical point of view, the lumbar spine can be divided into three distinct regions; the transition zone from thoracic to lumbar, including L1, L2, the middle region, including L3 and a second transition zone from lumbar to sacral that includes L4 and L5 (Panjabi *et al.*, 1992; Bogduk, 1997).

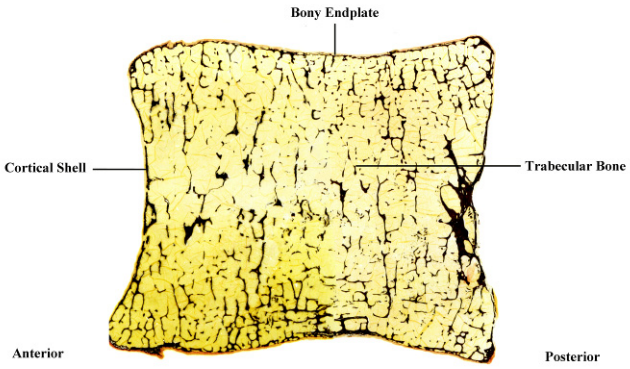

Figure 1.9: Histological sagittal cut of a lumbar vertebral body

(i) Vertebral bodies functional shape

Compared to the cervical or thoracic vertebrae, lumbar vertebral bodies have fairly flat superior and inferior surfaces (Bogduk, 1997), which seems to be optimal to withstand the large longitudinal compressive loads, usual at this level. From L1 to L5, the compressive force applied by muscles increases (Table 1.1), however, neither the elastic modulus nor the strength of the lumbar spine vertebrae is found to increase in the cephalo-caudal direction (Keller *et al.*, 1989). Hence, the mean resistance of the vertebrae to axial loads seems to come principally from their geometrical and structural characteristics.

From morphological measurements over 12 spines, Panjabi et al (Panjabi *et al.*, 1992) established that the vertebral body endplate areas tend to increase downwards. Nonetheless, from L4 to L5, a decrease of vertebral body depth which resulted in a more elliptical shape of L5 and in a slight decrease of the endplate area was observed (Panjabi *et al.*, 1992). Amonoo-Kuofi (Amonoo-Kuofi, 1991) measured the mean depth of the lumbar endplates for the intervertebral spaces of 615 spines and his results showed a similar tendency around the L5 vertebra. A priori, large endplate areas would lead to higher axial compressive resistance and this decrease around L5 seems to be in contradiction with the continuously increasing axial force from L1 to L5. Actually, the greatest endplate area was found for the lower L3 endplate (Panjabi *et al.*, 1992), at the centre of the lordotic curve where muscles exert the maximal posterior shear force during upright standing (Bogduk *et al.*, 1992). Between the segments L3-L4 and L4-L5, the posterior shear forces applied by the multifidus and the erector spinae fascicles (iliocostalis lumborum pars lumborum from L1 to L4 and longissimus thoracis pars lumborum from L1 to L5) decrease, while at the L4-L5 level, the thoracic fascicles of the erector spinae (longissimus thoracis pars thoracis from T1 to T12 and iliocostalis thoracis pars thoracis from T5 to T12) exercise an anterior shear force (Fig. 1.7). In fact, in the middle region of the lumbar spine, i.e. L3, the tip of the lordosis makes axial body loads to locally generate a maximum amount of anterior shear that muscles need to counteract. Therefore, a greater antero-posterior endplate diameter with an increased area may be designed to resist both the body loads and the muscles stabilizing forces. In the lower lumbar region, body and muscles forces are inverted, which may explain the decrease of endplate depth. Hence, although it is commonly accepted that the lumbar spine anatomy is principally shaped by the high compressive loads (Bogduk, 1997), the effect of other types of loads on the functional anatomy, such as shear forces, can not be ignored.

(ii) Vertebral bone functional structure

Smit et al (Smit *et al.*, 1997) studied the trabecular anisotropy within a L4 lumbar vertebral body and found that independently of the considered location, trabecular orientation was mostly vertical and consequently designed to support compressive axial loads. Nonetheless, around the endplates and close to the pedicles, transverse plane anisotropy was observed. It was even more pronounced in the pedicles surrounding areas, as a probable result of the previously cited shear forces. Pal et al (Pal *et al.*, 1988) found that from L1 to L3, posterior bone trabeculae run from the superior articular

processes toward the inferior articular processes through the lamina, but no particular orientation was found in the pedicles. Such result suggests that there is no particular transfer of normal load through the pedicle core; these components may work mainly under flexion due to two direct axial load paths, through the vertebral bodies and through the posterior elements via the facet contact (Fig. 1.10). Axial load transmission through the zygapophysial joints was put in evidence by in vitro experiments (El-Bohy *et al.*, 1989; Yang and King, 1984). El-Bohy et al (El-Bohy *et al.*, 1989) showed that it may be mainly due to the action of the superficial extensors of the spine (Fig. 1.5). Nevertheless, in upright standing, the zygapophysial joints only transmit about one sixth of the axial compressive forces and are not anatomically designed to resist high axial loads, as they lack a planar transversal contact area (Adams and Hutton, 1983). This indicates that the internal structure of the vertebral trabecular bone is quite sensitive to axial loads and assumes a primary role in resisting such kind of loads. In the 4^{th} and 5^{th} lumbar vertebrae, the trabeculae of the pedicles extend from the vertebral body to the inferior articular processes (Pal *et al.*, 1988). Here, axial compressive loads would also be transmitted directly through the intervertebral discs and the zygapophysial joints, but a specific normal load transfer from the body to the inferior zygapophysial joints takes place through the pedicles. This should be the result of the facet contact provoked by anterior shear exerted by the muscles at L4 and L5 (Fig. 1.6,1.7).

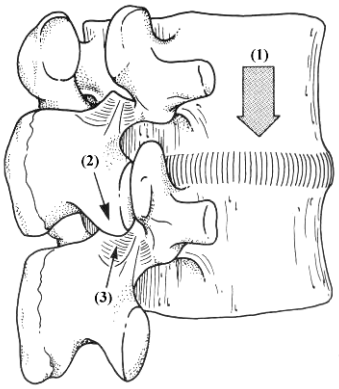

Figure 1.10: axial load transmission from body to body through the intervertebral disc (1) and from posterior elements to posterior elements through the tip of the inferior contact articular process of the lower vertebra (2) and the back of the lamina of the upper vertebra (3)(Adapted from (Bogduk, 1997)).

(iii) Neuronal arch functional shape

The normal loads transmitted through the lower lumbar pedicles could explain why the vertebral foramen transversal section tends from being ovoid at L1 to triangular at L5 (Panjabi *et al.*, 1992; Rao, 1994) (Fig. 1.11). Such load transmission may also justify the decrease of the spinal canal sagittal diameter, while the transverse diameter increases from the upper to the lower lumbar spine (Panjabi *et al.*, 1992; Rauschning, 1991). However, the lower neuronal arch configuration also helps the pedicles to resist

the bending moments occuring between the body and the posterior body elements resisting (Fig. 1.11, Table 1.1).

Panjabi et al (Panjabi *et al.*, 1992) found that both pedicle height and width increase from L3 to L5, which relies well with the transfer of axial load from the vertebral bodies to the inferior articular processes at the lower lumbar levels. Nevertheless, the decrease in pedicle height from L3 to L5 reported by Berry et al (Berry *et al.*, 1987) and Zindrick et al (Zindrick *et al.*, 1987) seems to indicate a need of greater resistance to lateral loads at the lower levels. Hence, together with the posterior shear, axial rotation may have a fair influence on the pedicle geometry. This is confirmed by the further anatomical study of the lumbar articular processes.

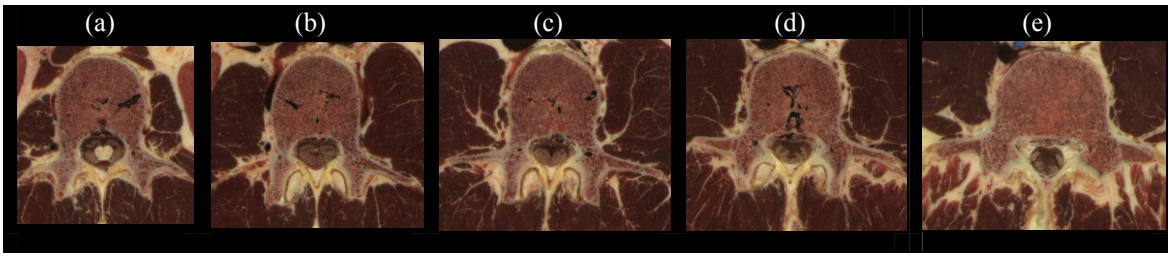

Figure 1.11: transverse plane histological cuts of the lumbar vertebrae from the same spine (Adapted from (Peitgen et al., 1998)). The cuts were chosen in order to show clearly the shape of the vertebral foramen (a) L1; (b) L2; (c) L3; (d) L4; (e) L5

(iv) Zygapophysial joints functional shape

Panjabi et al (Panjabi *et al.*, 1993) found that the lumbar articular processes have the major sagittal orientation of the entire spine, accounting for a greater resistance to the axial rotation induced by bipedal locomotion. Nevertheless, they also observed that the cephalocaudal increase of lumbar facet sagittal orientation was less for the spine than for the upper spine. Tulsi and Hermanis (Tulsi and Hermanis, 1993) even found more frontal facet orientations in the lower lumbar spine than in the upper lumbar spine. The anteroposterior shape of the lumbar superior facets is usually bilinear, and facets have two types of global shape; for a given mean orientation with respect to the sagittal plane, the J-shape facets (Fig. 1.12a) have a small anteromedial portion facing backwards, while the C-shape facets (Fig. 1.12b) have a larger area facing backwards. Hence, C-shape facets may offer a greater resistance than the former to forward relative displacements of the superior vertebra (Bogduk, 1997). Shape and sagittal orientation of the superior facets were respectively quantified as the depth of the joint cavity and the angle between the joint average plane and the sagittal plane (Tulsi and Hermanis, 1993). The analysis of such quantification is presented on Fig. 1.12c and can be correlated with the need of the facet to resist axial rotation and anterior shear. As stated before, at the L1-L2, L2-L3 and L3-L4 levels, the shear forces induced by the body weight are anterior, so that under muscle reaction forces, the zygapophysial joint facets tend to separate. Therefore at these levels, shear loadings only slightly involve the articulation and axial rotation is the most influent load. This results in highly sagittal oriented

superior facets which can be almost planar or J-shaped. At the L4-L5 level, muscles react to the posterior shear induced by external loads, and the L4 superior facets tend to be pressed against the L3 inferior facets along the antero posterior direction. The movement can be resisted both by a deeper L4 superior facet, preferentially associated to a C-shape geometry, and/or by an increased frontal orientation of the same facet. At the L5 level, the anterior shear forces might be so high that resistance is provided by a higher level of facet frontal orientation and since L5 facets do not need any pronounced C-shape, they can be flatter. The increasing facet contact area with progression down the lumbar spine (Panjabi *et al.*, 1993) and the posterolateral run of the L5 pedicles (Panjabi *et al.*, 1992; Rauschning, 1991) confirm the effect of a combination of axial rotation moments and posterior shear forces at the lower levels of the lumbar spine. Moreover, the present description of the zygapophysial joint functional anatomy is consistent with other geometrical features pointed out for the adjacent pedicles.

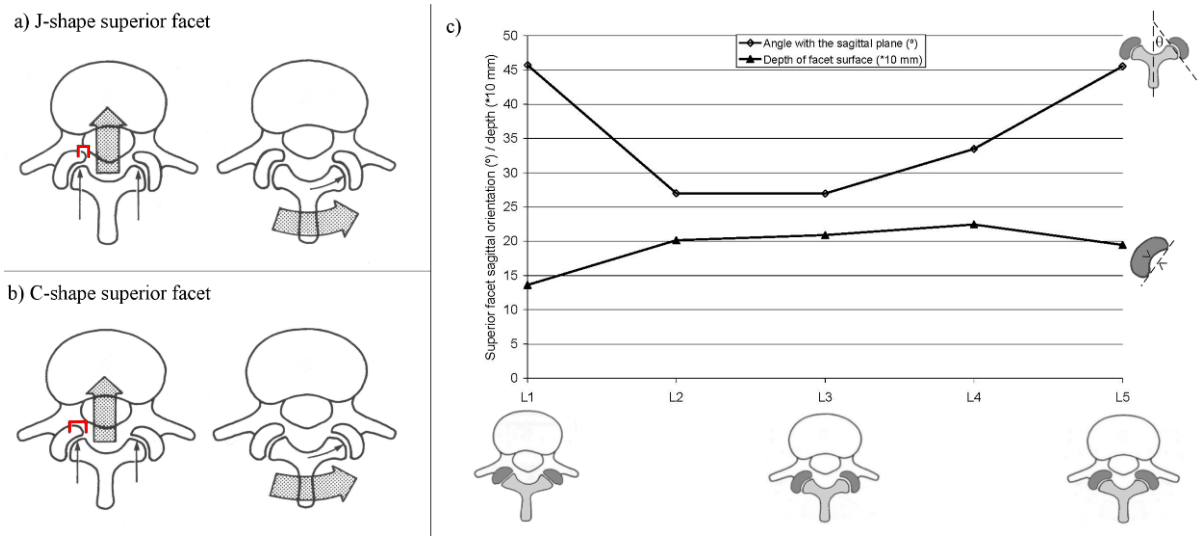

Figure 1.12: Functional morphology of the lumbar spine zygapophysial joint facets. a), b) Resistance provided either by a J-shape or C-shape superior facet of a zygapophysial joint in cases of anterior displacement and axial rotation imposed by the superior vertebra (adapted from (Bogduk, 1997)). The red square form represents the area of maximum resistance of the inferior vertebra's superior facet to the pressure exerted by the superior vertebra's inferior facet when this latter undergoes a forward translation (anterior shear). c) Illustrated quantitative morphology of a spine segment zygapophysial joint given at different levels of the lumbar spine by the orientation of the facet contact surfaces with respect to the sagittal plane, and the depth of the superior facets (Adapted from (Tulsi and Hermanis, 1993) and (Bogduk, 1997)).

2) Intervertebral discs

The intervertebral disc is a fibrocartilaginous structure that can be divided into three distinct parts; the central part, i.e. the nucleus pulposus, is enclosed by a lateral part, i.e. the annulus fibrosus, and by an upper and lower part, i.e. the cartilage endplates (Fig. 1.13). The dry matrix of the three components is partly constituted by

proteoglycans. This macromolecule represents about 65% of the dry weight in the nucleus pulposus, 20% in the annulus fibrosus (Bogduk, 1997) and 20% (mean value) in the cartilage endplate (Roberts *et al.*, 1989). The carboxylic (COO^-) and sulphate (SO_4^{2-}) functional groups of proteoglycans induce negative charges and contribute to absorb water via osmotic effects. Moreover, together with collagen II, the proteoglycans form a tri-dimensional matrix, whose dimensions emphasize swelling because of capillarity (Bogduk, 1997). The major implication of such a composition is that the percent of water present in the healthy intervertebral disc is rather high; 70-90% in the nucleus pulposus, depending on the age, 60-70% in the annulus fibrosus (Bogduk, 1997) and about 55% in the cartilage endplate (Roberts *et al.*, 1989). As stated before, the intervertebral disc is the principal articulation of the vertebral column and because of its position between the vertebral bodies it transfers the major part of the axial compressive loads. The hydrostatic pressure created by water makes the tissues to be able to bear high level of loads (Martin *et al.*, 2002) and as the fluid is able to flow in a controlled way, the deformability of the intervertebral disc is sufficient to ensure required the lumbar spine flexibility (Fig. 1.3).

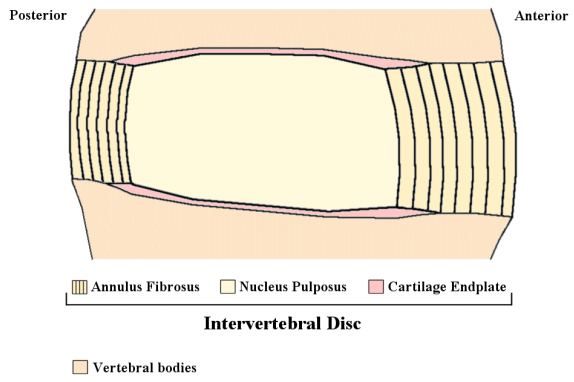

Figure 1.13: Schematic representation of the intervertebral disc structure in a sagittal cut view

(i) Nucleus pulposus

The nucleus pulposus is the intervertebral disc constituent with the highest dry weight fractions of proteoglycans and collagen II. Thus, hydrostatic pressure is maximal in this tissue, which seems particularly suited to withstand axial compressive loads (Hutton *et al.*, 2000). Moreover, in agreement with the lower lumbar spine biomechanics, it is not surprising that the nucleus fills a maximum proportion of the disc transversal area (Pooni *et al.*, 1986), i.e. 30-50% (White III and Panjabi, 1990), and that its location is found more posterior than central (Rao, 1994; White III and Panjabi, 1990), according to the adjacent trabecular bone areas of maximum axial orientation (Smit *et al.*, 1997). Compressive stresses in the vertebral body trabecular bone are not only induced by axial compressive forces, but also by backward extension (Smit, 1996), leading to think that the posterior location of the lumbar nucleus pulposus is optimal to ensure the anterior transfer of all the loads that typically increase caudally in the lumbar

spine (Table 1.1). All these observations are in agreement with the stress profilometries realized by Mc Nally and Adams (McNally and Adams, 1992), where the hydrostatic behaviour of the non-degenerated nucleus pulposus under compression was shown. Moreover, Bogduk and Twomey (Bogduk, 1997) stated that the high content of water and the randomly oriented collagen II are mostly related with compressive process.

(ii) Annulus fibrosus

Embriologically, the nucleus pulposus is a remnant of the notochord that had been surrounded by the circularly lamellar annulus fibrosus that comes from the perichordal mesenchyme (Humzah and Soames, 1988). According to this and to the compression resisting role of the nucleus, it is reported that the annulus fibrosus would be the result of a functional adaptation to the action of constant changing peripheral shear forces that depend on the instantaneous centres of rotation between adjacent vertebrae (Humzah and Soames, 1988). Hence, the structure of this tissue would be governed by other types of loads than direct axial compression. The influence of shear forces in the annulus is in agreement with its lamellar structure and with the results of Marchand and Ahmed (Marchand and Ahmed, 1990), who measured thinner lamellae in the outer annulus than in the inner annulus. Collagen organization within the annulus fibrosus also seems to support this theory. Collagen is after water the main constituent of the annulus fibrosus, since its amount rises up to 60% of the dry weight (Bogduk, 1997). Such content is principally related to collagen types I and II (Eyre, 1988). In the external annulus, collagen I represent 80% of the total collagen content, while collagen II quantity increases toward the centre, up to 80% of total collagen (Eyre, 1988). Collagen I is the stiffest of both types and is mostly related to a need for the tissue to resist tractions (Bogduk, 1997). In the annulus fibrosus, collagen I is organized in a criss-cross pattern within adjacent lamellae (Fig. 1.14a) and the angle made by the bundles with the anatomic planes is grossly defined but may vary along the periphery and/or along the thickness (Cassidy *et al.*, 1989; Marchand and Ahmed, 1990; Eberlein *et al.*, 2001). Humzah and Soames (Humzah and Soames, 1988) compared the anatomy of foetal and adult annuli fibrosi and concluded that the orientation of collagen within the lamellae may be the result of a mechanical adaptation, particularly due to axial torsion. In fact, the fibrous lamellar structure of the annulus should be particularly efficient to bear all type of shear deformation. Moreover, it has been shown that the shear stresses within the ground substance matrix should be even lower than the number of lamellae is high (Iatridis and Gwynn, 2004). Annulus collagen fibres are anchored to the top and bottom vertebrae and to the cartilage endplates (Inoue, 1981; Marchand and Ahmed, 1990). Therefore, by enclosing totally the nucleus pulposus (Fig. 1.14b), annulus fibres are able to resist the lateral pressure exerted by the nucleus (Fig. 1.15), which allows stabilizing greatly the intervertebral disc under the continuous daily axial compressive loads (Markolf and Morris, 1974). This stress transfer from the nucleus to the annulus is in agreement with the fact that the internal pressure exerted by the nucleus pulposus on the annulus fibrosus vanishes from inner to outer, according to the gradients of collagen I and II reported through the annulus thickness. Another example of adapted mechanical reinforcement by the collagen fibres can be seen in the posterior annulus fibrosus; since the nucleus pulposus is posterior located, the posterior annulus is much thinner than the anterior annulus. This structural weakness is locally compensated by higher collagen

contents (Brickley-Parson and Glimcher, 1984) that may stiffen the posterior annulus structure (Galante, 1967). The zygapophysial joints have also a protecting action on the intervertebral disc in backward extension (Yang and King, 1984; Schultz *et al.*, 1979) and in axial rotation (Ahmed *et al.*, 1990; Schultz *et al.*, 1979).

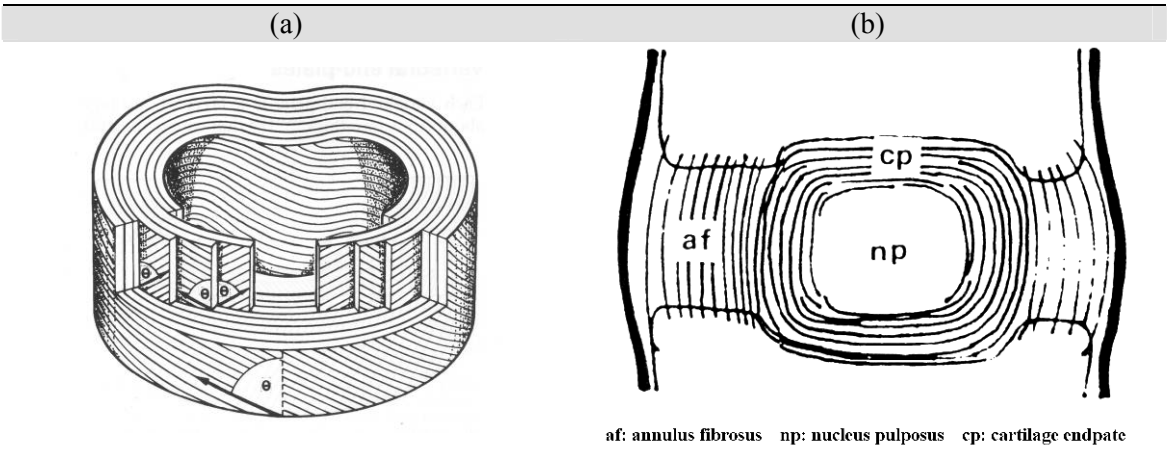

Figure 1.14: Concentric lamellar structure of the annulus fibrosus with collagen I fibre organization. (a) Fibre orientation in successive lamellae of the annulus fibrosus (Bogduk, 1997), (b) Sagittal view of annulus fibrosus collagen bony insertion and course within the cartilage endplate (Adapted from (Inoue, 1981)).

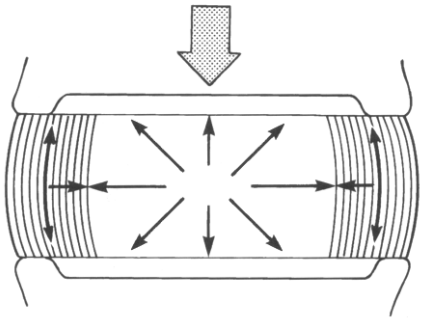

Figure 1.15: Action of the nucleus pulposus hydrostatic pressure on the annulus fibrosus under axial compression (Adapted from (Bogduk, 1997))

(iii) Cartilage endplate

The cartilage endplate is a thin structure that surrounds all the nucleus pulposus and about one third of the annulus fibrosus (Fig. 1.13). It is a hyaline cartilage, with a composition similar to that of an articular cartilage, but with less water. To some extend, cartilage endplates may resemble epiphyseal cartilage (Roberts *et al.*, 1989). Composition is heterogeneous and depends on the surrounding tissues; the collagen

content is higher in the annulus fibrosus neighbourhood and usually increases through the endplate thickness, from the disc to the vertebra, where water and proteoglycan contents generally decrease (Roberts *et al.*, 1989). The axial composition gradient of the cartilage endplate may be related to a reduction of pore size which prevents the proteoglycans to migrate into the vertebra and therefore preserves the integrity of the intervertebral disc hydrostatic pressure (Roberts *et al.*, 1996). However, small molecules such as nutrients can pass through the cartilage endplate from the vascularised vertebra to the avascular nucleus pulposus (Roberts *et al.*, 1996). This role of assuming a nutritive path for the inner part of the intervertebral disc, suits well with the fact that both cartilage and bony endplates are thinner at their centre (Roberts *et al.*, 1996; Roberts *et al.*, 1989; Edwards *et al.*, 2001). Moreover, the porous character of the bony endplate centre (Edwards *et al.*, 2001) is in agreement with this assumption. The collagen fibres of the cartilage endplate run parallel to the vertebral subchondral bone and there is no sign of anchoring with this latter (Inoue, 1981). Cartilage endplate mechanical role remains unclear.

3) Ligaments

From a topographic point of view, the spinal ligaments can be classified into four groups; the ventral or anterior ligaments that connect the vertebral bodies, the posterior or dorsal ligaments, connecting the bony posterior elements, the minor or "false" ligaments, and the iliolumbar ligament. The iliolumbar ligament will not be presented here, as it connects the ilium with L5 (Bogduk, 1997) and its action is out of the system we propose to study. This classification corresponds to that made by Bogduk (Bogduk, 1997) and Hayman et al. (Hayman *et al.*, 2000c; Hayman *et al.*, 2000b; Hayman *et al.*, 2000a).

(i) Ventral ligaments

The ventral ligaments are the anterior longitudinal and the posterior longitudinal ligaments. The anterior longitudinal ligament forms a continuous band with axially oriented fibres that cover all the anterior aspect of the lumbar spine. Through the ligament depth, the distinct fibre layers span over one intervertebral disc for the deepest ones or over up to five inter-body joints for the most outer fibres (Fig. 1.16a). Independently of the layer, the fibres are usually strongly attached to the cortical bone of the vertebral body margins. Some fibres normal to the axis of the ligament ensure a weak link between the deep longitudinal fibres that spread over the intervertebral disc and the annulus fibrosus (Tkaczuk, 1968). The fibres covering the vertebral bodies normally bridge the bone concavity and only few blend with the periosteum (Bogduk, 1997). According to the orientation of its fibres, the anterior longitudinal ligament can only restrict the vertical separations of the vertebral bodies and the anterior bowing due to the lumbar spine curvature (Bogduk, 1997). It may also reinforce the intervertebral disc during sagittal motions (Hukins *et al.*, 1990), especially under backward extension (Panjabi *et al.*, 1982). The fact that the ligament was found to be thinner over the

annulus fibrosus (Tkaczuk, 1968) shows that the mechanical resistance needed in this area is limited, probably due to the great thickness of the anterior lumbar annuli.

In the lumbar spine, the posterior ligament forms a narrow band over the posterior aspect of the vertebral bodies and intervertebral discs. Ligament fibres are attached to the superior margin of a vertebra and span up to the inferior margin of the first or fifth vertebra below, depending on the depth of the fibre layer (Fig. 1.16b). The great difference with the anterior longitudinal ligament is that the posterior longitudinal ligament is wider at the intervertebral disc level because its fibres spread laterally over the annulus fibrosus (Bogduk, 1997; Rauschning, 1991). Moreover they blend intimately with the annulus external layer and reinforce the posterior aspect of the disc, helping the thin posterior annulus fibrosus to support the loads (Rauschning, 1991; Bogduk, 1997; Tkaczuk, 1968).

The longitudinal ligaments are richly innervated (Tkaczuk, 1968; Rauschning, 1991) and as they deform with the intervertebral disc, they may serve as strain sensors for disc bulging and annulus traction (Rauschning, 1991). In fact, they are mainly composed by collagen fibres which give them a high stiffness but also some viscoelastic properties which suits well with the creep behaviour associated to the biphasic character of the intervertebral disc.

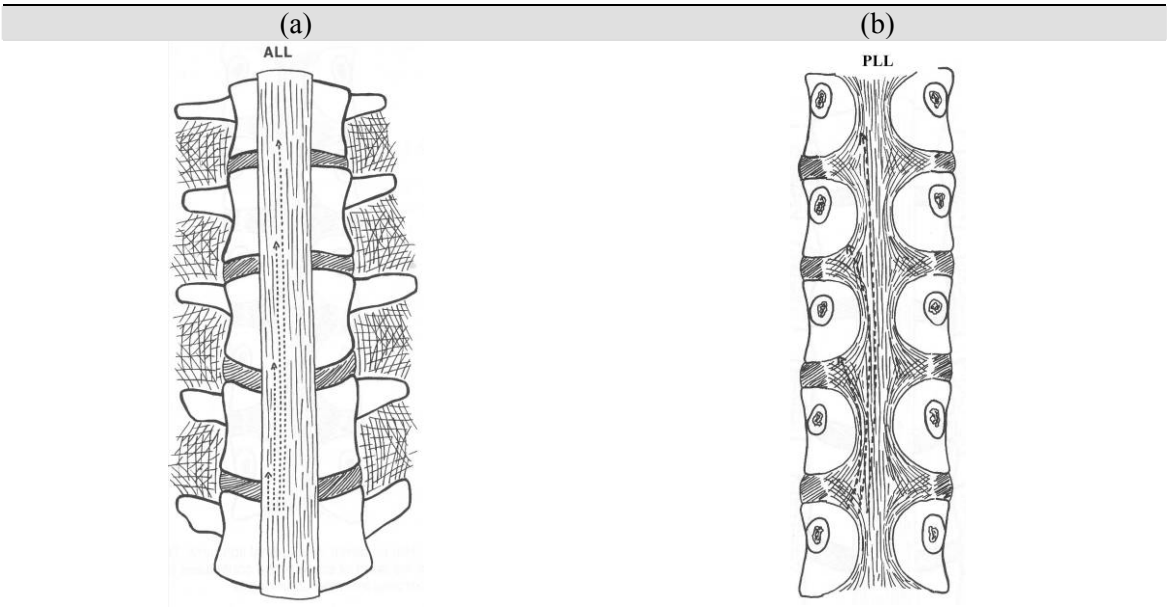

Figure 1.16: Schematic representation of the lumbar longitudinal ligaments (Bogduk, 1997). (a) Anterior view of the anterior longitudinal ligament (ALL). (b) Posterior view of the posterior longitudinal ligament (PLL). The arrows drawn on the ligaments represent the directions and the length of the different collagen layers.

(ii) Dorsal ligaments

In a postero anterior order, the dorsal ligaments are the supraspinous, the interspinous, the capsular ligaments and the ligamentum flavum. These ligaments form a continuous network (Fig. 1.17a) (Bogduk, 1997) and mostly resist external forward flexion moments (Adams *et al.*, 1980; Goel *et al.*, 1985).

The supraspinous ligament runs parallel to the spine longitudinal axis and bridges the interspinous spaces being attached to the tip of the spinous processes. This ligament has a complex structure which can be divided into three parts (Bogduk, 1997; Rissanen, 1960). The superficial layer, i.e. the most dorsal part, is subcutaneous and its fibres span up to four successive spinous processes (Bogduk, 1997; Yahia *et al.*, 1989). The middle layer is partially tendinous, acting as a link with the dorsal layer of the thoracolumbar muscles fascia (lies with the border of the iliocostalis lumborum and the spinous process) and the aponeurosis of the longissimus thoracis (Fig. 1.5). The deep layer of the supraspinous ligament can be clearly identified as the tendon derived from the aponeurosis of the longissimus thoracis. This part links the successive interspinous processes and runs caudally and ventrally from the tip of the superior process to the superior boarder of the inferior process, forming the posterior part of the interspinous ligament (Fig. 1.17b). All these parts are not separate entities; they are only used to describe the postero-anterior changes of the supraspinous ligament structure (Rissanen, 1960). Nonetheless, as the superficial part of the ligament is absent from the L4-L5 level, this space is rather occupied by a thick tendinous band which can be easily mistaken for supraspinous ligament (Rissanen, 1960). Figure 1.17b shows the supraspinous ligament without considering this lower tendinous part. Due to the higher content of collagen I in tendons (85-90% dry weight) than in ligaments (70% dry weight) (Woo *et al.*, 1997; Mow and Ratcliffe, 1997) and independently on muscles attachment, the tendinous – ligamentous aspect of the supraspinous ligament may provide a compromise of stiffness and strength that suits well with the ligament position at the maximum lever arm location in case of ventral flexion.

The interspinous ligament merges dorsally from the supraspinous ligament and connects the adjacent spinous processes (Fig. 1.17b). Its complex structure is composed by different fibrous layers whose orientations have been matter of many discussions (Rissanen, 1960); some authors observed a horizontal run of the collagen, whereas others defended the existence of a collagen vertical path. From L1 to L5, Rissanen (Rissanen, 1960) described four distinct antero posterior parts visible in the superficial layers from a lateral view of the spine, while Bogduk et al (Bogduk, 1997) only report the existence of three parts. Nonetheless, both descriptions state the existence of an antero-caudal run of the ligament fibres. Hukins et al (Hukins *et al.*, 1990) studied the interspinous ligament by X-ray diffraction, and found that most of the fibres run parallel to the spinous processes. About this principal direction the authors detected a fanlike fibre arrangement. Nonetheless, as pointed out in the report of the study, X-ray diffraction is equally sensitive to both the thickest and finest fibres and allows detecting fibre orientations throughout the ligament that did not obligatory correspond to the main ligament fibres. The composition of the interspinous ligament is mostly collagenous dorsally and there is an increasing amount of elastic fibres in the anterior direction that

comes to a maximum when the ligament lies ventrally with the ligamentum flavum (Yahia *et al.*, 1989).

The ligamentum flavum, also called interlaminar ligament is thick and lies between the adjacent vertebrae, closing dorsally the spinal canal. It connects the superior edge and the postero superior surface of the inferior lamina with the inferior edge and the antero inferior surface of the superior lamina (Ramsey, 1966) (Fig. 1.17c). Laterally, the ligament is attached to the articular processes and merges with the antero medial part of the capsular ligament. This lateral part of the ligamentum flavum is called the capsular portion (Nachemson and Evans, 1968). In the transverse plane, the ligament has a V-shape where the base is linked to the interspinous ligament and the concavity faces ventrally. The inside angle formed by the juncture of the two slabs of the V is somewhat less than 90º. At this point, some authors described a discontinuity of the structure, dividing the ligament into two distinct folds bounded together by a loose conjunctive tissue (Yahia *et al.*, 1989), however, Ramsey (Ramsey, 1966) could not observe such discontinuity and considered the ligament as a whole. Nachemson and Evans (Nachemson and Evans, 1968) also reported that the ligamentum flavum was a continuous structure, where the midline was only marked by the presence of small vessels. The medial area is the broader and the thickest part of the ligament that becomes thinner laterally as its merges with the zygapophysial joint capsules (Nachemson and Evans, 1968; Ramsey, 1966; Yahia *et al.*, 1989). Histologically, with 20% of collagen and 80% of elastin (Bogduk, 1997), the ligamentum flavum is probably the human ligament with the highest content of elastic fibres (Nachemson and Evans, 1968; White III and Panjabi, 1990). In fact, collagen fibres are not organized (Hukins *et al.*, 1990) in this ligament and are dispersed into a longitudinally oriented matrix of densely packed elastic fibres (Yahia *et al.*, 1989). The advantage of such structure is that when the ligament is stretched, the elastic fibres elongation is sufficient to allow a reorientation of the collagen in the stretching direction, giving an increasing stiffness with increasing strain (Hukins *et al.*, 1990), while when the ligament has to shorten, the elastic fibres impede it to buckle into the spinal canal (Bogduk, 1997; White III and Panjabi, 1990).

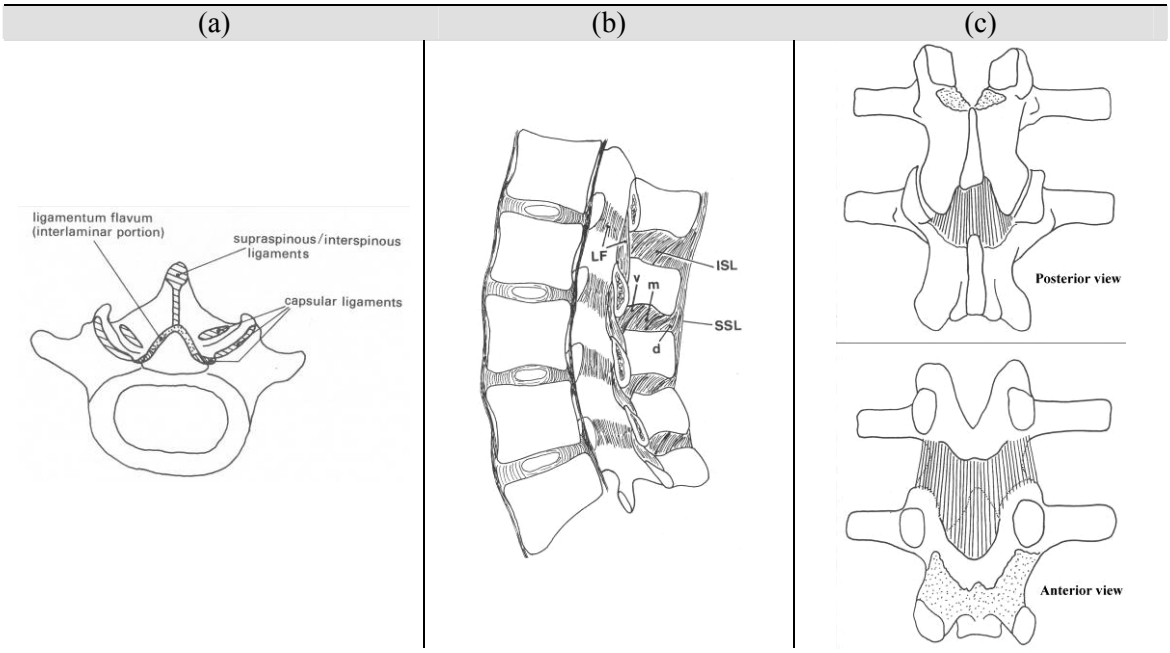

Figure 1.17: Schematic representation of the lumbar spine posterior ligaments. (a) Transversal view of the ligament position and interconnection (Adapted from (Adams et al., 1980)). (b) Sagittal cut with focus on the supraspinous ligament (SSL), interspinous ligament (ISL) and ligamentum flavum (LF); v, m and d respectively represent the ventral, medial and dorsal parts described by Bogduk and Twomey (Bogduk, 1997) for the interspinous ligament. (c) Representation of the bony posterior elements with posterior and anterior view of the ligamentum flavum (Adapted from (Bogduk, 1997)).

Because of the complexity of its morphology, the zygapophysial capsular ligament is the less well described of the lumbar spine dorsal ligaments. Nevertheless, it has been reported that in the lumbar spine, the ligament encloses the zygapophysial joint around its dorsal, superior and inferior margins (Bogduk, 1997; Yahia and Garzon, 1993). Ventrally, the joint is covered by the ligamentum flavum (Bogduk, 1997) (Fig. 1.18) that merges upward and downward with the capsule (Yahia and Garzon, 1993). The dorsal part of the capsular ligament is the thickest one and is reinforced by some of the deep fibres of the multifidus muscles (Yahia and Garzon, 1993; Bogduk, 1997). Through its thickness, the capsular ligament is constituted by two fibrous layers; the outermost layer consists of densely packed collagen fibres (Bogduk, 1997) running perpendicular to the joint line (Panjabi *et al.*, 1991), while the innermost layer contains irregularly oriented elastic fibres (Bogduk, 1997) that are probably related to the internal hydrostatic pressure of the articulation. The amount of elastic fibres increases ventrally in the superior and inferior parts at the transition zone with the ligamentum flavum (Yahia and Garzon, 1993). On one hand, Bogduk (Bogduk, 1997) reported that at the superior and inferior poles, capsule is thick and fairly loose, ballooning outside the joint. On the other hand, Yahia and Garzon (Yahia and Garzon, 1993) related the elastic fibre composition of theses zones to the flexibility required for segment sagittal extension. Both observations follow the same idea and seem to be complementary.

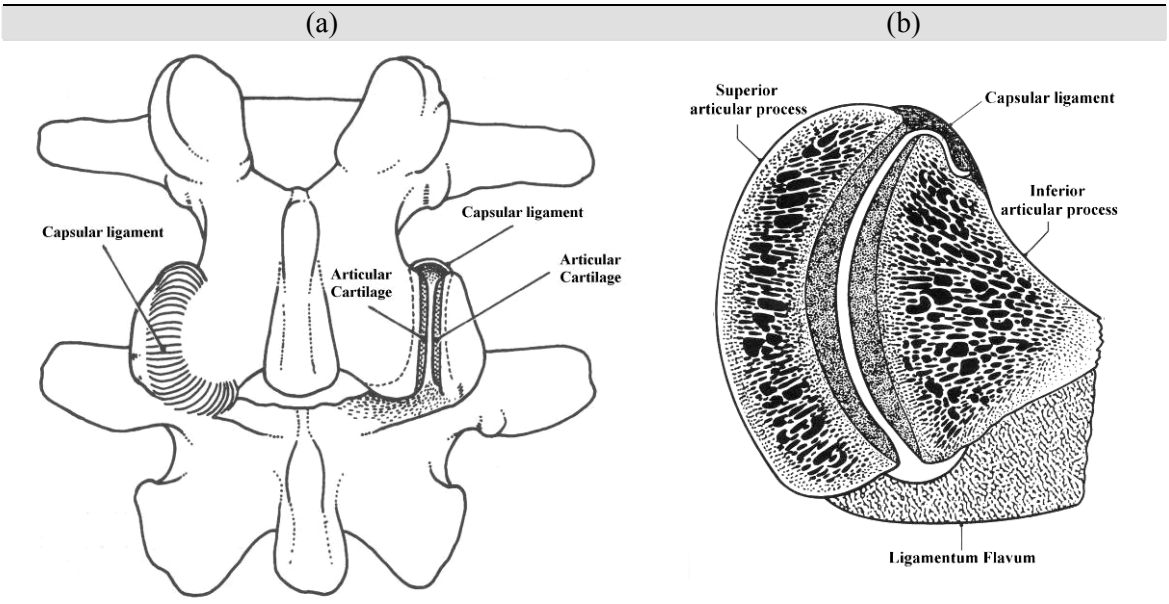

Figure 1.18: Schematic representation of the zygapophysial joint with special focus on the capsular ligament (Adapted from (Bogduk, 1997)). (a) Posterior frontal view. (b) Transversal cut of the zygapophysial joint.

(iii) "False" ligaments

The minor of "false" ligaments are the intertransverse, the transforaminal and the mamillo-accessory ligaments. They are called "minor" or "false" because they are too weak to play any real mechanical role or because they connect two distinct points of the same bone and do not act as passive restricting movement components.

The intertransverse ligament consists of sheets of connective tissue extending from the upper edge of one transverse process to the lower edge of the transverse process above (Fig. 1.19). The ligament has not any distinct border, and its collagen fibres are loosely packed and not so regularly oriented as the fibres of a true ligament (Bogduk, 1997). In the lumbar region, cross-sections are so small that the intertransverse ligaments look much more like membranes without any mechanical significance (White III and Panjabi, 1990). Toward the medial end of the intertransverse process, the ligament splits into two leaves (Fig. 1.19b); a dorsal leaf continues medially, attaches to the lateral part of the lamina, and blends inferiorly with the capsule of the adjacent zygapophysial joint. The second leaf curves forward and extends over the lateral surface of the vertebral body until it eventually blends with the lateral margins of the anterior longitudinal ligament (Bogduk, 1997). As shown in Fig. 1.19b, this part of the ligament closes laterally the intervertebral foramen and together with the medial continuation of the intertransverse ligament, this extension, rather than being true ligament, may be a part of a complex system of fasciae that serves to separate or demarcate some paravertebral compartments (Bogduk, 1997).

(a) (b)

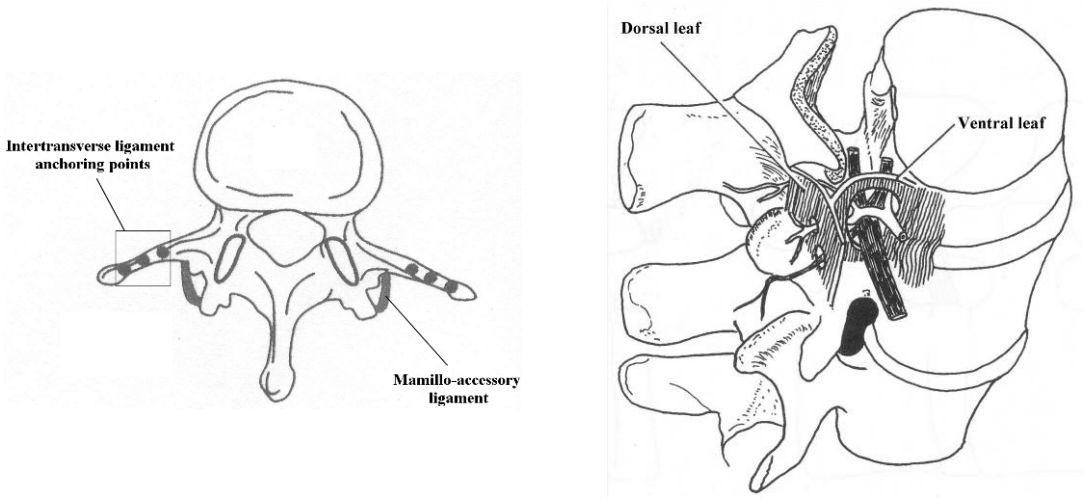

Figure 1.19: (a) Attachment points of the intertransverse ligament on the transverse processes and representation of the mamillo-accessory ligament (adapted from (Hayman et al., 2000a)). (b) Detail of the intertransverse ligament medial and antero medial extensions (reproduced from (Lewin et al., 1962)).

The transforaminal ligament consists of five types of narrow collagenous bands that are identified according to their respective attachments (Bogduk, 1997; Park *et al.*, 2001) (Fig. 1.20). These bands are all present in only about 47% of the cases (Bogduk, 1997). Curiously, the inferior corporotransverse ligament that is the only part connecting two adjacent vertebrae to each other and is therefore the best candidate to bear a certain mechanical role is not the most frequent band (Bogduk, 1997; Park *et al.*, 2001; Min *et al.*, 2005). Moreover, although the transforaminal bands are not always present, neither at all levels nor on both sides of the spine (Min *et al.*, 2005; Park *et al.*, 2001), they could be detected in foetal spinal column (Park *et al.*, 2001), which indicates the possible existence of another origin than mechanical adaptation. On the basis of their functional anatomy study, Park et al (Park *et al.*, 2001) suspected the transforaminal ligament to serve to partition the intervertebral foramen in order to support the transmission of the spinal and segmental artery branches and spinal nerves.

Finally, the mamillo-accessory ligament bridges the mamillary and accessory processes of each lumbar vertebra. Nonetheless this structure connects two points of the same bone and has, therefore, not the characteristics of a ligament, from a mechanical point of view (Fig. 1.19a).

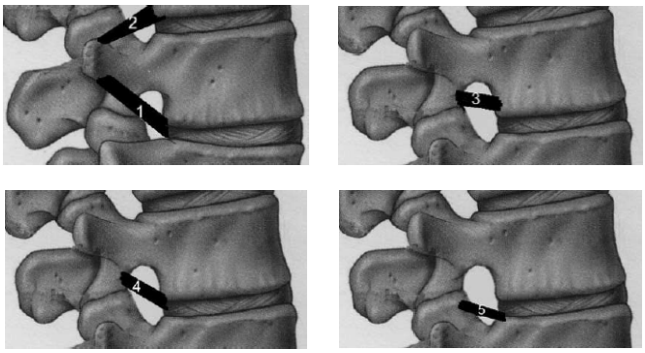

Figure 1.20: Representation of the different bands of the transforaminal ligament (Adapted from (Park et al., 2001)). (1) Superior corporotransverse ligament; (2) Inferior corporotransverse ligament; (3) Superior transforaminal ligament; (4) Mid transforaminal ligament; (5) Inferior transforaminal ligament.

B. Biomechanical studies of the lumbar spine

As presented in the previous section, the anatomy of the lumbar spine is fully functional, highly related to the upright standing and perfectly coherent. Hence, any structural defect in any part of the spine will make the anatomy of the surrounding tissues to lose its coherence with the mechanical environment and will be likely to provoke further structural changes. These changes can simply represent a functional adaptation of the tissues or/and a degeneration process.

I. Mechanical factors and low back pain

Together, heavy loading conditions and high flexibility make the human lumbar spine to be quite sensitive to daily poor ergonomic factors, and convert this part of the biped anatomy into a preferential site for mechanically induced traumas and degenerations. Low back pain disorders usually include intervertebral disc problems such as hernias, spondylolisthesis, but also facet arthritis, muscle and ligament injuries. Although low back pain has always affected human beings, it has turned into one of the major healthcare problem of the industrialized countries. At time of writing, one of the last studies of the European Agency for Safety and Health at Work (OpDeBeek and Hermans, 2000) reports that 30% of European workers suffer from back pain and suggests that between 60% and 90% of people will undergo low back disorders at some point in their life.

Efficient and durable treatments can be achieved only if the problem is well understood and if causes and consequence can be both clearly established and formulated. Even if mechanical loading is often considered as the greatest risk factor (Adams and Dolan, 1995), the origin of low back pain can also be biological (e.g. autoimmune diseases, tumours), psychological (Bigos *et al.*, 1991; OpDeBeek and

Hermans, 2000), congenital (e.g. spina bifida, functional or structural scoliosis), degenerative (e.g. spondylosis, degenerative arthritis), or unidentifiable. Nonetheless, because of the great adaptability of the tissues to their mechanical environment, even if mechanical factors are not directly linked to spine dysfunctions, they are likely to contribute to catalyse progressive degenerative processes as a response to an induced non reversible stimulus (Adams and Dolan, 1995). Note that in extreme cases, where surgery is involved, such stimulus may also come from the treatment itself, as in the case of spinal fusion, where the loading conditions generated by the treatment may be responsible for long term degeneration problems in the adjacent segments (Lee *et al.*, 1992; Kumar *et al.*, 2001). Therefore, low back problems have to be viewed as a chain of events where all spinal components may interact with each other, and where the mechanical role of these components, as well as their response to mechanical factors, must be understood.

II. Experimental biomechanical studies

Biomechanical studies on the spine began as early as in antiquity (Sanan and Rengachary, 1996); an Egyptian papyrus from the 17th century BC already described the differences between cervical strain, fracture and fracture-dislocation. In the 4th century BC, the concept of tissue remodelling was unconscientiously applied with the use of tractions or local pressures to correct spinal deformities. Between the 15th and the 16th century, spine stability was probably studied for the first time by Leonardo Da Vinci, and in 1680, Giovanni Borelli published the first analysis about the weight supported by the spine.

Measuring lumbar spine motions was first studied in 1827 by Weber on three cadavers, and the first systematic attempt to obtain load-displacement characteristics of motion segments under various load types was undertaken by Markolf in 1972 (Yamamoto *et al.*, 1989). Nonetheless, one of the greatest contributions to the knowledge in spine experimental biomechanics was brought by Panjabi and colleagues with *in vitro* studies that extend from the three dimensional movements of the normal spine (Yamamoto *et al.*, 1989; Panjabi *et al.*, 1977; Panjabi *et al.*, 1989) to the computation of ligament strain (Panjabi *et al.*, 1982) and the effect of disc degeneration (White III and Panjabi, 1990). In his review about experimental testing of the spine, Adams (Adams, 1995) reported that it was meaningful to study the *in vivo* spine biomechanics by using *in vitro* experiments. By this way, he indicated the reliability of numerous publications about *in vitro* tests on undamaged ligamentous spines (Yamamoto *et al.*, 1989; Nachemson *et al.*, 1979; Schmoeltz *et al.*, 2003; Rohlmann *et al.*, 2001). However, the absence of muscles from such tests induced instabilities that can be reduced by applying compressive preloads (Patwardhan *et al.*, 2003) and obtain more physiologic boundary conditions (Rohlmann *et al.*, 2001; Patwardhan *et al.*, 2003). While Panjabi et al (Panjabi *et al.*, 1977) and Rohlmann et al (Rohlmann *et al.*, 2001) found that preload increased sagittal rotational movements and reduced axial rotations (Fig. 1.21), Padtwardhan et al (Patwardhan *et al.*, 2003) observed a higher stiffness for sagittal rotations and Yamamoto et al (Yamamoto *et al.*, 1989) did not detect any effect of preload. As reported in (Patwardhan *et al.*, 2003), the absence of

preload effect may be due to a too low value of the compressive force. Nevertheless, it appears less important knowing the absolute effect of compressive preloads on the ranges of motion, than understanding why preloads could affect these ranges of motion and which spine components would be responsible. In this sense, many mechanical tests were performed in order to corroborate or further investigate the functional anatomy of the spine. For example, El-Bohy et al (El-Bohy *et al.*, 1989) performed in vitro experiments on lumbar spine bi-segments simulating the effect of the extensor muscles of the spine. The authors measured facet and disc pressures for different manitudes of of axial compression, forward flexion and muscles forces. Both facet and intradiscal pressures occurred as a result of muscle action in order to maintain the lumbar lordotic curve when flexion or compression were applied. However, in case of sudden release of extension or flexion, while intradiscal pressure decreased, facet contact increased. Hence, their work allowed putting in evidence the interaction between facet contact and intradiscal pressure, as well as the role of the zygapophysial joints when muscles are active.

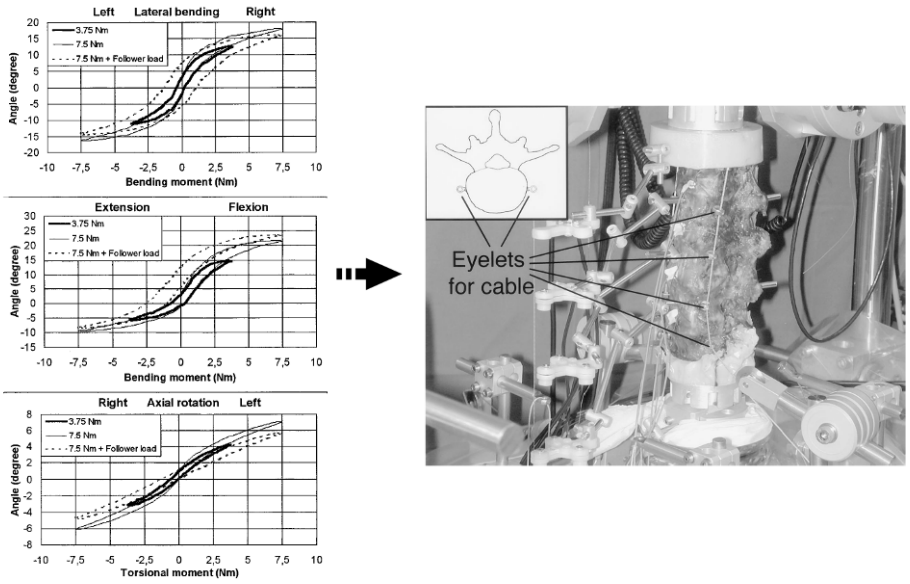

Figure 1.21: comparison of the rotation obtained experimentally on a L1-L5 specimen with pure moments with and without compressive preload. The preload was applied by means of a follower force driven by cables running axially along the spine segment (Adapted from (Rohlmann et al., 2001)).

At the end of the 50s, Brown et al (Brown *et al.*, 1957) found that under axial compression, lumbar motion segments without posterior elements invariably failed in the cartilaginous endplate and they suspected that the failure was more related to the condition of the bone than to the disc itself. Both Tencer et al (Tencer *et al.*, 1982) and El-Bohy et al (El-Bohy *et al.*, 1989) confirmed experimentally that in a general manner, the intervertebral disc was the main load-bearing element in axial compression and anterior shear, while the zygapophysial joints had a major role in posterior shear and axial torque. By the use of successive resections of ligaments and bony posterior elements, some authors could identify the specific mechanical role of some components

(Fig. 1.22). Twomey and Taylor (Twomey and Taylor, 1983) found that capsular ligaments were the most resisting ligaments to full sagittal motions (from full flexion to full extension). This confirmed the findings of Adams et al (Adams *et al.*, 1980) who focussed their study on flexion. Moreover, Adams et al (Adams *et al.*, 1980) found that the supraspinous and interspinous ligaments did not offer many resistance until half of the full flexion has occurred, which indicated a modest role of these ligaments in resisting flexion. They attributed such observation to the farthest positioning of the ligaments with respect to the centre of rotation, allowing resisting flexion with minimum effort. Such interpretation is understandable because in the reported experiment, the supraspinous and interspinous ligaments were the first ligaments to be cut, but related results are in contradiction with the experimentally based ligament force computations performed by Goel et al (Goel *et al.*, 1985). Discrepancy may come from the fact that Goel et al (Goel *et al.*, 1985) introduced a cost function to solve a statically indeterminated system, which had an unknown influence on the results. Nevertheless, both studies agreed in pointing out that capsular ligaments do play a significant role under sagittal flexion. Panjabi et al (Panjabi *et al.*, 1982) indirectly determined the strains in the lumbar spine ligaments from *in vitro* experiments, subjecting functional segment units to shear forces and rotational moments. This was useful in terms of spine kinematics knowledge, but to truly study the ligament resisting capacities, results need to be completed with data about the mechanical behaviour of each ligament. Such task has been performed by several authors (Myklebust *et al.*, 1988; Chazal *et al.*, 1985; Pintar *et al.*, 1992), but results generally show large deviations over the different experiments. This is certainly due to differences in the experimental methods and to the particular character the individually tested tissues. Actually, the material properties of the spine tissues ensure the mechanical integrity of the whole structure and their variability is probably related to geometrical and structural variability of the normal spine. This emphasises the importance of attempting to find out the mechanical influence of the spinal components, one by one and under various load cases.

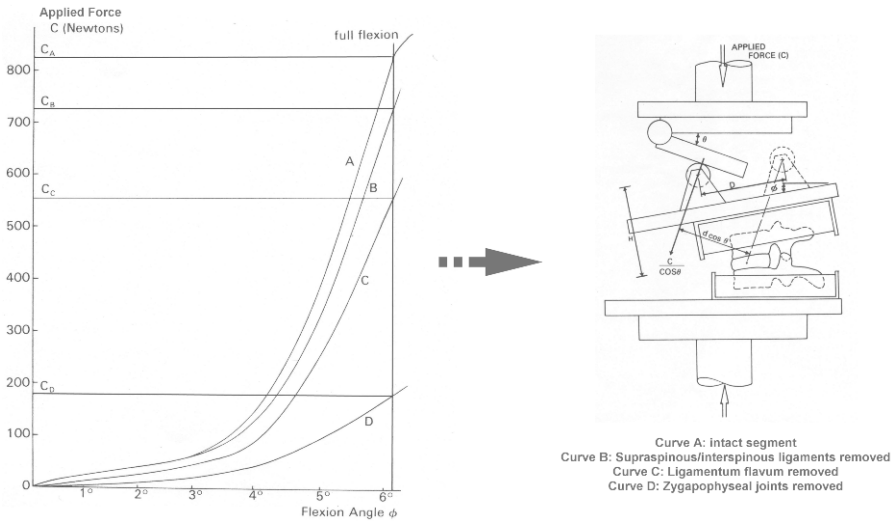

Figure 1.22: example of experimental study allowing studying the relative effect of isolated components on the biomechanics of a lumbar spine segment (Adapted from (Adams et al., 1980)).

At the end of the 70's, a series of three papers (Nachemson *et al.*, 1979; Berkson *et al.*, 1979; Schultz *et al.*, 1979) showed that both motions and intradiscal pressures are disc level dependent and increase when the posterior elements are excised. However, principally because of the morphological differences between the specimens, the effect of disc degeneration was hard to interpret and they concluded that it was not so significant. From a morphological point of view, Berkson et al (Berkson *et al.*, 1979), who measured the in vitro response of lumbar motion segments under compression and shear, argued that a greater intervertebral disc cross sectional area was significantly associated with a lower intradiscal pressure change. However, they could not observe any influence of the disc height. More recently, Heuer et al (Heuer *et al.*, 2007a; Heuer *et al.*, 2007b) measured the ranges of motion, the vertebral translations, and the intradiscal pressures of L4-L5 lumbar spine specimens after successive anatomical resections. Results highlighted the important mechanical role of the nucleus pulposus under sagittal, frontal, and axial rotations. Coupled translations could be also studied for different segment stabilities. Unfortunately, the use of a single segment is still restrictive as the relative roles of the spine components are propably level-dependent and load transfers should depend on specimen lengths.

Since spinal components continuously interact mechanically, the influence of one parameter cannot be determined only on the basis of the results that are experimentally available. For example intervertebral disc geometrical or mechanical variations are not imperatively related to changes in range of motion or intradiscal pressure; the studied parameters may be compensated by other structural or mechanical factors at the zygapophysial joints, ligaments or at the bony endplates level. Thus, a parametric stress analysis of the system becomes fully relevant.

III.Numerical biomechanical studies

Up to now, numerical modelling seems to be the most practical way to perform complete parametric studies of a biomechanical system, as specific data on the tissue stress state and load transfers can be obtained under any simulated boundary condition. Among the different methods of simulation, the finite element method proved its potential of accuracy and has the great advantage to allow the analysis of complex geometries. Finite element method was developed during the 50s for the aeronautic industry and it has been extended to diverse application domains such as electronics, material science, solid and fluid mechanics, bioengineering, etc… (Fagan *et al.*, 2002). Nowadays, the computational force is such that numerical studies represent an important part of the engineering studies and finite element modelling has a privileged place in the investigation of complex biomechanical problems.

The first finite element application in biomechanics was probably reported in 1972 by Brekelmans et al, who studied the biomechanics of different skeletal parts (Fagan *et al.*, 2002). Since this time, the number of biomechanical applications increased substantially, which allowed accessing always more detailed information about coupled biological-mechanical systems. The lumbar spine is one of the most studied of these systems and numerical works mainly focus on the behaviour of the

normal pine, the pathologic spine, the treated spine and the design of prosthetic materials (Fagan *et al.*, 2002). As shown in section B.II, the rachis is a very complex structure including many different tissues of various properties (anisotropic, composite, multiphasic, etc…). Hence, spine numerical models involve advanced continuum mechanics theories whith equation parameters that depend principally on possible experimental studies of isolated tissues. Therefore, mechanical approximations constantly coexist with the numerical and geometrical approximations inherent to any model. The relevance of all these simplifications must be studied through exhaustive validation tasks that should give confidence in the numerical results as possible extrapolations of the observable mechanical behaviour of biological systems.

The creation of a biomechanical finite element model is, therefore, a long and highly multidisciplinary task. Models are generally geometrically and mechanically non linear, resulting in large computational costs. For this reason, a compromise between the size of the model geometry and the complexity of the mechanical laws has to be found. Regarding the lumbar spine, depending on the author, the work may be rather focussed on one aspect or another. In this sense, the different models can be classified in the following way:

a. Models of vertebral bone
b. Models of intervertebral discs
c. Models of functional unit segments
d. Models of the whole lumbar spine

These models can be used to investigate the normal lumbar spine biomechanics, but may also represent pathological situations in order to study the mechanical implications of disorders and associated treatments. The models presenting some kind of disorders are generally directly focussed on clinical applications and the quality of the validation becomes fundamental.

a. Vertebral bone models

To our knowledge, one of the first three-dimensional models of a human vertebra was reported by Hakim and King in 1978 (Hakim and King, 1978). The geometry was acquired from direct measurements on vertebral cuts. Due to limited computer power, the model only contained 150 elements (Fig. 1.23a), just one type of bone was represented and all the materials were isotropic linear elastic. Hence, because of the great geometrical and mechanical approximations, numerical predictions were fairly far from the experimental data (Hakim and King, 1979). Thanks to medical imaging techniques, the geometries could be further better modelled and bone material properties could be adjusted. For example, in 1994, Bozic et al (Bozic *et al.*, 1994) reported the development of a cervical vertebra model from a series of Computed Tomography (CT) scans, where each pixel had been converted into an element. The great advantage of using CT scans is that the apparent density of bone can be deduced for any pixel and, with the help of experimental data, bone Young's modulus and strength values can be fitted for each element to the density data. Thus, the non homogeneity of the vertebral

tissue can be simulated. Around the same period of time, Mizrahi et al (Mizrahi *et al.*, 1993) defined the Young's modulus of the different materials of their L3 vertebral model as a function of density data obtained by CT analysis in normal and osteoporotic vertebrae. By this way, they could identify the probable weakness induced by the presence of osteoporosis at the bony endplate levels under compression. However, their model was geometrically too simple to investigate the real contribution of cortex shape and thickness.

In 1997, Silva et al (Silva *et al.*, 1997) modelled a L2 lumbar vertebral body and studied the effect of cortical shell stiffness, cortical shell thickness, and trabecular bone anisotropy, on the load shearing between vertebral and cortical bones. They found that any factor increasing the relative rigidity of the shell with respect to the centrum increased the force carried by the former. Their model was too simple to give a good description of the load sharing between the different bony parts. Nonetheless, it gave a better understanding on the reasons for discrepancy in experimental results about the effect of the cortical shell on the vertebral strength. Two years later, Overaker et al (Overaker *et al.*, 1999) reported the use of a beam mechanical model in order to construct a trabecular bone micro structural model. They used it in a L1 vertebral body finite element model and they simulated the effect of aging (trabecular bone porosity) and vertebral body lateral curvature. They concluded that the role of the shell increased with age, decreased with the vertebral body lateral curvature. Cortical shell thickness was also found to have a strengthening effect. The micro-structural approach reported by the authors aimed to mechanically represent the trabecular bone as a three-dimensional structure and not as a continuum, which gave without doubt a finer description of the tissue. However, coupling a structural model of beam elements to other tissue models requiring the use of solid brick elements may affect the computation of load transfers, due to a mismatch of degrees of freedom between beam and brick elements.

Inoue et al (Inoue *et al.*, 1998) modelled two lumbar vertebrae, (L4 and L5), to apply loads on their respective facet contact surface. They investigated stresses induced in the neuronal arch of each vertebra with respect to load orientation. They found that the maximum stress peak was distinct for each vertebra, and they showed the importance of the geometrical differences between L4 and L5. The modelled vertebrae came from a series of 2mm CT scan slices and had fairly accurate geometries. One of the last vertebra models to date was created by Nabhani and Wake (Nabhani and Wake, 2002): two casts of one L4 and one L5 human vertebrae were reconstructed numerically by sampling coordinate points across each side of the casts. The resulting meshed geometry appeared highly detailed (Fig. 1.23b). The models were used to study the respective roles of the cortical and trabecular bones under compressive load. To make the boundary conditions more realistic, the authors distributed the pressure applied on the vertebrae, so that 70% of load was applied on the upper vertebral body endplate and 30% on the superior articular process. They found that stresses in the vertebrae were mostly concentrated in the cortical bone around the pedicles, while the softer trabecular bone was not so heavily stressed but contributed to absorb energy. The importance of the posterior bony elements effect on the vertebral bodies stress distribution was also pointed out by Whyne et al (Whyne *et al.*, 1998) who modelled and studied a L1 vertebral body including successively the pedicles and the lamina.

(a) (b)

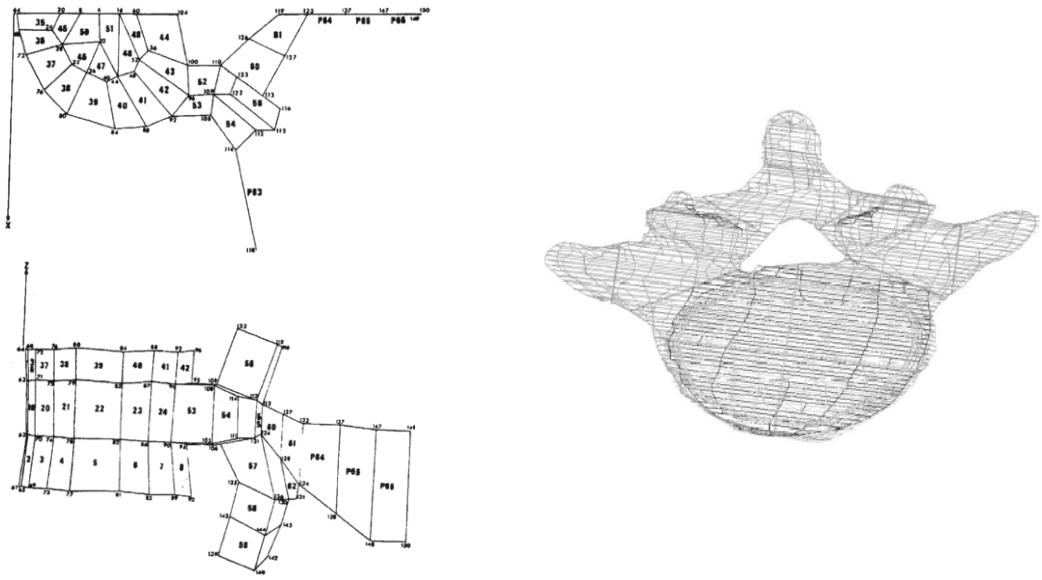

Figure 1.23: (a) Three-dimensional model f a human vertebra developed by Hakim y King (Hakim and King, 1978). (b) L5 vertebra model developed by Nabhani and Wake (Nabhani and Wake, 2002)

In other studies, although intervertebral discs were not the principal point of interest, they were modelled together with the studied vertebrae to introduce more realistic boundary conditions. For example Goel et al (Goel *et al.*, 1995b) used a simple L3-L5 bi-segment finite element model in order to implement a bone remodelling theory based on the strain energy density. From a homogeneous cylinder they could obtain the concave shape of a normal vertebral body (Fig. 1.24), as well as bone stiffness distributions corresponding to reported experimental values. In 1996, Smit (Smit, 1996) used a L3-L5 bi-segment model together with imaging anisotropy measurements and concentrated his work on the L4 trabecular bone functional anisotropy under simulated physiological load cases. He concluded that the bone microstructure was mainly designed to withstand compressive loads. These studies on the vertebral bodies clearly show the biomechanical importance of geometry, material properties, and the interaction between these two modelling parameters.

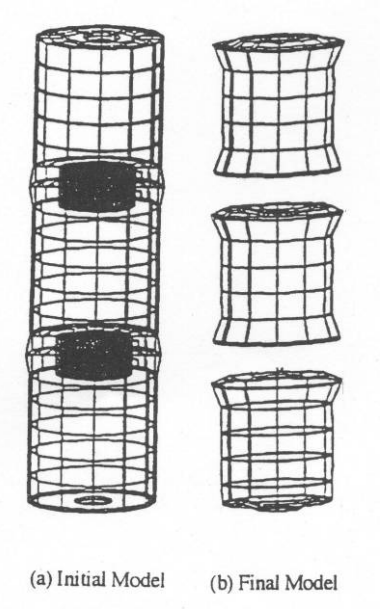

Figure 1.24: Effect of strain energy density based remodelling on cylindrical lumbar spine vertebrae (Goel et al., 1995b)

b. Intervertebral disc and functional unit segment models

In this section, intervertebral disc models and functional unit segment models are presented together because many authors who worked on the intervertebral disc used full unit segment models to simulate more realistic functional disc loadings.

The first finite element model, that described one segment composed by two vertebral bodies and one intervertebral disc, was probably published in 1973 by Belytschko and Kulak (Belytschko and Kulak, 1973). The model was axisymmetric with a horizontal plane of symmetry at the intervertebral disc mid-height and except this last part, all simulated tissues were isotropic and linear elastic. The intervertebral disc was modelled as an incompressible fluid and the annulus fibrosus was assumed linear orthotropic. Three years later, an update of the model was presented, where the non-linear orthotropic properties of the annulus fibrosus layers were introduced and fitted to experimental measurements on whole intervertebral discs (Kulak *et al.*, 1976). Nevertheless, the greatest contribution to intervertebral disc modelling was brought by Shirazi-Adl et al in 1984 (Shirazi-Adl *et al.*, 1984), with a L2-L3 disc body unit model including both geometric and material non linearities. The annulus was described as a ground substance matrix reinforced by collagen fibres. This was probably the first composite material model applied to the intervertebral disc. Annulus fibres were non-linear elastic and were distributed in 8 concentric layers (Fig. 1.25a). The collagen criss-cross pattern organization was modelled, but instead of jumping from negative to positive angle from layer to layer, each fibre layer was bidirectional and the absolute angle with respect to the horizontal plane was constant all over the disc. Moreover, although the symmetry of the model was fairly simple, it included the three types of vertebral body bone. In 1986, Shirazi-Adl et al (Shirazi-Adl *et al.*, 1986) completed

their model with ligaments and zygapophysial joints and studied the predicted behaviours under sagittal plane rotations, including the effect of intradiscal pressure loss and facetectomy. Results allowed putting in evidence the mechanisms of load transfer between different spinal components, such as the nucleus pulposus, the annulus fibrosus and the facet joints. However, although the segment model had been partially validated by means of comparison of the predicted results with in vitro experimental data, the geometry was approximated, the pedicles were represented by flexible beams and the lack of literature and appropriate techniques greatly limited both validation and geometrical updates. Some years later, Shirazi-Adl et al used their model to study more precisely the role of the zygapophysial joints (Shirazi-Adl and Drouin, 1987), the effect of the intervertebral disc modelling (Shirazi-Adl, 1989), and the effect of the pedicles bone compliance (Shirazi-Adl, 1994). In the first of these three studies, the importance of the facet geometry was pointed out, and in the second one the author compared a homogeneous orthotropic annulus fibrosus model with a non homogeneous model (Fig. 1.25b). It was found that the latter model gave a more realistic description of the annulus fibrosus biomechanical behaviour since tensile stresses were supported by the fibres, while the matrix was under compression.

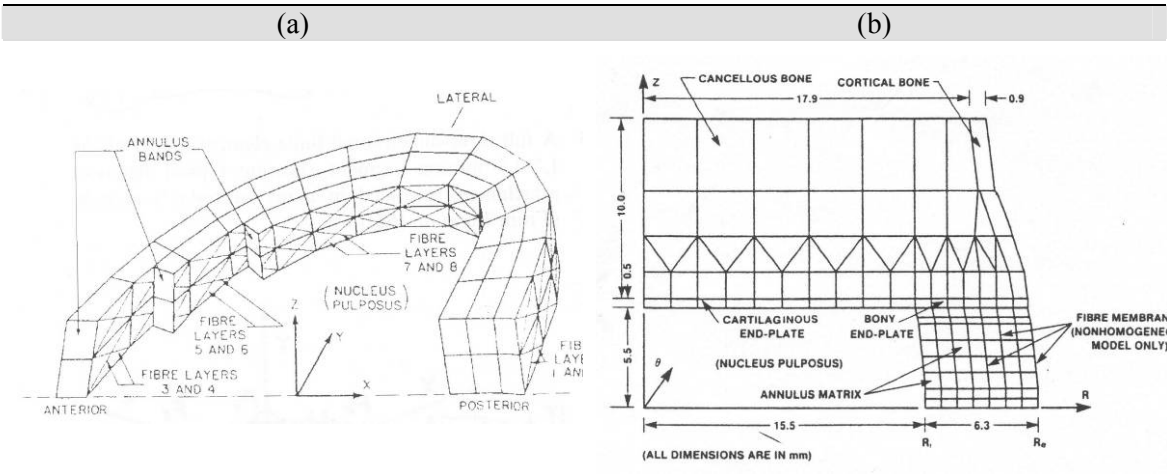

Figure 1.25: Shirazi-Adl's intervertebral disc models with the composite annulus fibrosus. (a) Composite with fibre layers modelled with unidirectional elements (Shirazi-Adl et al., 1984). (b) Fibres layers modelled with mono-oriented fibrous membranes (Shirazi-Adl, 1989).

At the end of the 80's and during the 90's, most of the relevant spine finite element studies were inspired by the structural modelling of Shirazi-Adl et al (Ueno and Liu, 1987; Goel and Kim, 1989; Sharma *et al.*, 1995; Smit, 1996; Natarajan and Andersson, 1999). Shirazi-Adl et al's model was also directly used as a basis for posterior studies of viscoelasticity (Wang *et al.*, 2000), poroelasticity (Argoubi and Shirazi-Adl, 1996), or coupled with experiments (Kasra *et al.*, 1992; Duncan and Ahmed, 1991). However, the geometry of the original model was fairly limited. In 1987, Ueno and Liu (Ueno and Liu, 1987) introduced the orthotropy in their bone material properties and studied the biomechanics of a three-dimensional L4-L5 model under axial rotation. They could analyse the distribution of stresses between the zygapophysial joints, the intervertebral disc and the vertebrae, and the amount of load

resisted by the facets was found to depend mainly on the gap between the articular surfaces. For simulated physiological load magnitudes, facets carried up to 40% of the torque and the highest stresses within the disc took place at the lateral margins of the annulus outer layer, indicating that torsion was unlikely to produce posterior or postero-lateral disc prolapse. These results gave a better understanding of the biomechanical role of the facets under axial compression but they can be only considered orientative since the L4 vertebral body was assumed to be the same as the L5 vertebral body. In 1995, Sharma et al (Sharma *et al.*, 1995) studied the role of the zygapophysial joints and ligaments in the stability of a L3-L4 functional segment unit and could identify the interactions between these components and the intervertebral disc. The role of facets in resisting flexion and rotation was limited by the capsular ligament. In extension, the facets played an important role only for large rotations, while for small moments the intervertebral disc was the main resisting component. The zygapophysial joints were also particularly important in order to withstand anterior shear forces. However, the geometry of the model was too basic to describe accurately the articular contact (Fig. 1.26a), lowering the level of confidence to the study performed about the effect of partial facet removal. Goel et al (Goel *et al.*, 1995a) used a L3-L4 lumbar motion segment model to investigate the effect of annulus injuries on motion, disc bulge and interlaminar shear stresses. They introduced the use of a composite element formulation, where annulus collagen fibres were not modelled by uniaxial elements, but were included in the element technology. The advantage of such formulation is that the anisotropy of fibre reinforcement and the control of the amount and orientation of the fibres can be independent of the element size. The limitation of the model was that the fibres were considered linear elastic. Although it remained simple, the global model geometry was more advanced than the previously published spine segment models (Fig. 1.26b). Moreover, the authors were probably the first to present a mesh sensitivity study.

One of the first accurate geometries that presented smooth outlines was acquired by Smit (Smit, 1996). A L3-L5 bi-segment model was created on the basis of a L4 vertebra CT scan. Because of the purpose of this study, simplifications were made on the geometry by using copies of L4 to generate L3 and L5. Nevertheless, the shapes of the vertebrae were much more realistic than in the other previously cited works. In 1996, Wu and Chen (Wu and Chen, 1996) reported the modelling of a L5 vertebra acquired from a sequence of CT slices taken every millimetre in the transversal plane. The L5 geometry looked very realistic, nonetheless, the authors only modelled a mid L5-S1 intervertebral disc and in order to reproduce a whole motion segment, they considered the disc mid-transversal plane as a symmetry plane. More recently, Polikeit et al (Polikeit *et al.*, 2003a) created a L2-L3 lumbar spine segment model based on CT scan data with detailed gross geometry and Rohlmann et al (Rohlmann *et al.*, 2006) presented a L3-L4 lumbar spine segment model adapted from Smit's model (Zander *et al.*, 2001). These models have fairly advanced geometries (Fig. 1.26 c,d) and are the result of a further step in computational methods. However, from the point of view of tissue mechanical modelling, they do not present great improvements when compared to the models of the Shirazi-Adl generation. Schmidt et al (Schmidt *et al.*, 2006; Schmidt *et al.*, 2007a), who also acquired an accurate CT scan-based geometry of a L4-L5 human lumbar spine segment, used a different approach to investigate the material properties of their particular model. They iteratively calibrated the material properties of

different modelled tissues by progressively incorporating these tissues into the whole model and comparing the predictions with in vitro experiments performed on geometrically reduced specimens. Interestingly, the authors found that ligaments should have non-linear mechanical behaviours, and in general, they were the first to introduce a whole set of material properties that specifically fit to a particular model geometry. Nevertheless, this optimization process involved a static calibration of material constitutive equations that were generally not different from those used in the above-cited studies.

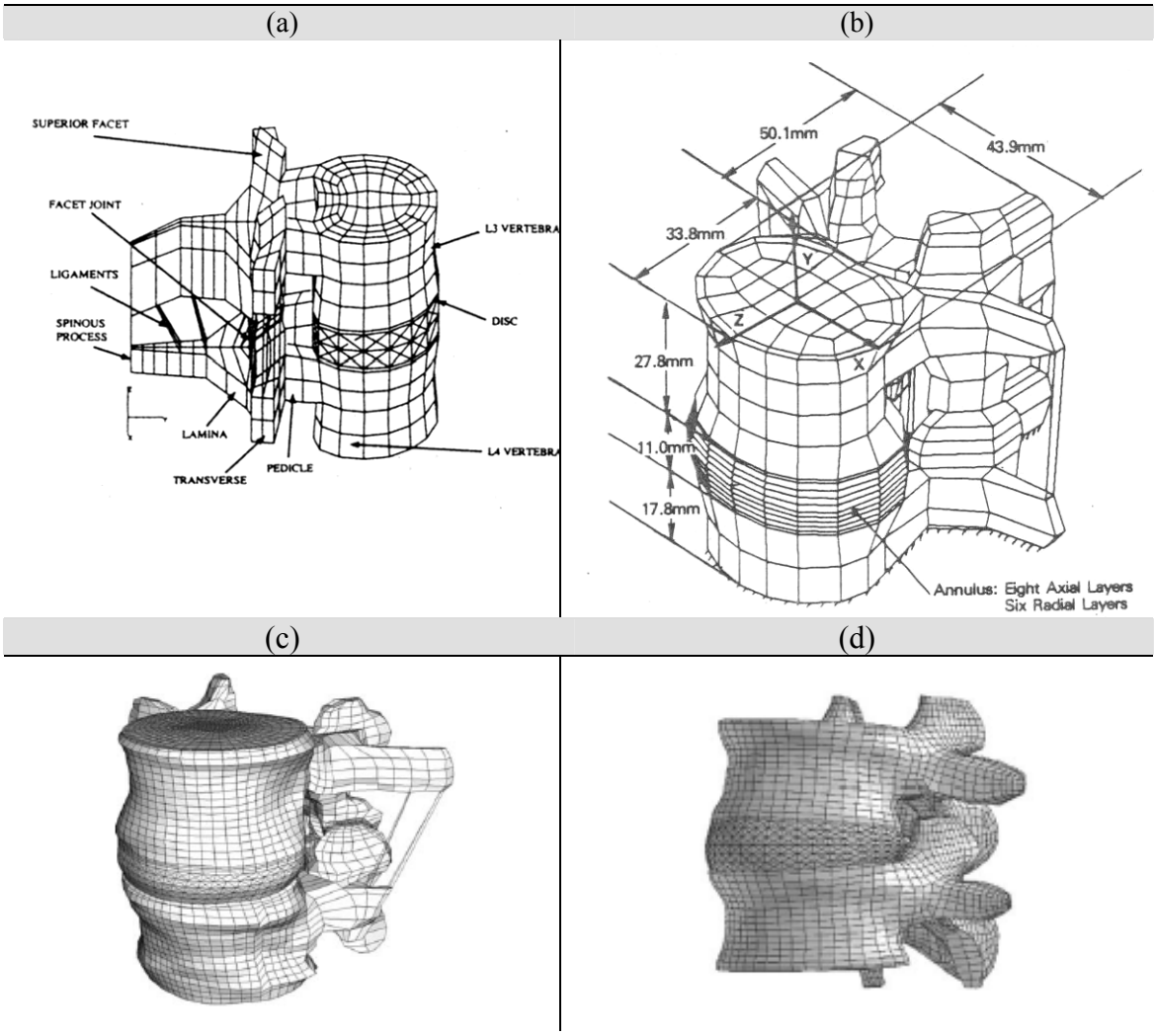

Figure 1.26: Different models of lumbar motion segment. (a) L3-L4 from Sharma et al (Sharma et al., 1995). (b) L3-L4 from Goel et al (Goel et al., 1995a). (c) L2-L3 from Polikeit et al(Polikeit et al., 2003a). (d) L4-L5 from Rohlmann et al (Rohlmann et al., 2006).

Other authors investigated others ways of modelling tissues. They focussed their research more on the application of new material constitutive equations than on direct clinical applications. Some authors intended to find an anisotropic stiffness matrix to simulate the mechanical effect of the annulus fibrosus fibrous organization. In 1986,

Spilker et al (Spilker *et al.*, 1986) created a simplified axisymmetric motion segment model where the annulus was composed of 10-12 concentric layers, each of them being described by a continuum linear orthotropic mechanical law. With such model, the authors could study the effect of fibre orientations but the determination of the orthotropic layer matrix components represented a great limitation. Elliott and Setton (Elliot and Setton, 2000) used a similar approach with the advantage to have access to experimental data for the determination of their equation parameters. Derived the stress-strain laws from a strain energy function, fibre angle could be used as an explicit variable, allowing studying the contribution of the different interactions fibre-fibre and fibre-matrix to the tissue mechanical behaviour. Results led to point out the importance of considering annulus fibre contributions, not only in the axial direction of the mono oriented layers, but also in the transverse planes. The authors further performed a series of experimental tests on differently oriented annulus samples and validated the model sensitivity to fibre angle (Elliot and Setton, 2001). Nonetheless, the proposed model was limited by its linearity and its inability to deal with large strains and rotations. Due to the gel-like aspect of soft tissue ground substances and to the high contribution of water in the biomechanical behaviours of biologic materials, most of the efforts were also turned toward hyperelastic and multiphase mechanical formulations. These formulations illustrate the non linear mechanical behaviour of the tissues and allow introducing the effects of hydrostatic pressures and incompressibility. Belytschko and Kulak (Belytschko and Kulak, 1973) were probably the first authors to model the incompressibility and hydrostatic stress state of the nucleus pulposus. Later, Simon et al (Simon *et al.*, 1985) introduced intervertebral disc poroelastic modelling. Their simulations led them to conclude that disc degeneration may be related with an increase of permeability. The normal and degenerated models studied by the authors behaved well when compared with creep experiments under compression, and steady state simulations were also consistent with the experience. However, the anisotropy of the annulus fibrosus was not represented and material properties had to be adjusted to pre-existing simulation results, rising up the uncertainty of the predictions. Poroelasticity was used in several studies to investigate the importance of the fluid solid interaction within the intervertebral disc. Laible et al (Laible *et al.*, 1993) published an adaptation of the axisymmetric model created by Simon et al (Simon *et al.*, 1985) where the swelling pressure was introduced into the Biot's poroelastic theory in order to represent the load carrying capability of fluid. Martinez et al (Martinez *et al.*, 1997) developed a poroelastic axisymmetric finite element model of the intervertebral disc that takes into account the variation of the permeability with strain, inducing a non linear material behaviour. They found that the nucleus principal stresses increased with annulus disruption, showing the lost of load bearing capacity of this last component. However, the modelling of the composite nature of the annulus fibrosus was not clearly explained and the effect of fibres could not be pointed out. Frijns et al (Frijns *et al.*, 1997) build and validated a one-dimensional model based on a quadriphasic mixture theory for the intervertebral disc annulus tissue. The effect of ions on the swelling properties was computed and it was found that the potential gradient contributed negatively to the fluid flow and could not be neglected. On similar bases, Iatridis et al (Iatridis *et al.*, 2003) used a bi-dimensional intervertebral disc finite element model to combine the poroelasticity with an electrochemical model in order to represent both the distribution and concentration of proteoglycans. They found that these factors had a great influence on the fluid flow and the tensional state. Fergusson et al (Ferguson *et al.*, 2004) used the

poroelasticity in a more clinical approach, by studying the molecules transport through the intervertebral disc during diurnal loading. With an axisymmetric intervertebral disc finite element model, they predicted that convective transport was not so important during diurnal loading, while it became significant during swelling. The importance of poroelasticity in finite element modelling was also stated by Whyne et al (Whyne *et al.*, 2001) through a simpler theory. They developed a two-dimensional finite element model of a L1 vertebra and adjacent intervertebral discs to study the effect of the presence of a tumour within the vertebrae on the model biomechanics. They compared the results given by a poroelastic formulation with those given by a fully elastic formulation. The type of mechanical modelling used for the intervertebral disc affected the boundary conditions of the vertebra and the authors found that the fully elastic formulation was not sufficient to represent an accurate stress state within the vertebra. In both cases, either the whole annulus fibrosus matrix or its solid phase alone (poroelastic model) was modelled as a hyperelastic fibre reinforced material. Hyperelasticity is another mechanical formulation that has been extensively investigated. Hyperelastic materials are non linear elastic materials whose stress-strain relationship can be described by the means of a strain energy function. In general, the hyperelastic laws used for soft tissues biomechanical modelling describe incompressible behaviours and depending on the number of terms of the strain energy functions, they have the great advantage to be intrinsically compatible with finite strain calculations. The incompressible hyperelastic approximation is understandable if one considers that the physiological loading rate is high enough so that fluid outflow does not occur (Smallhorn *et al.*, 2001). Moreover, the loading and unloading paths are similar with such law, so that the dissipative effects cannot be modelled. This implies that the parameters must be fitted to experiments performed after preconditioning where the testing strain rate should ensure that the individual tissue behaviour is representative of its response within the spine (sub)structure submitted to high-rate loads (Race *et al.*, 2000). Kulak et al (Kulak *et al.*, 1976) were the first authors to use a strain energy function in order to simulate the non linear mechanical behaviour of the intervertebral disc material. The mechanical parameters governing nonlinearity were fitted to intervertebral disc experimental axial deflexion curves and both intradiscal pressures and bulging predicted by the model were in good agreement with experimental data. Natali et al (Natali, 1991; Natali and Meroi, 1993) used hyperelasticity to describe the mechanical behaviour of the intervertebral disc ground substance and found good correlations with experimental results. Hence, they varied the compression coefficient in their hyperelastic formulation in order to simulate a degenerated disc, opening a new way to clinical applications. The vertebral bone was treated as an orthotropic material and similarly to their predecessors, Natali et al used one-dimensional elements for the annulus composite reinforcing fibres. However, the model geometry remained too simplified (Fig 1.27a) to allow any clinical prediction on the spine biomechanics. Some years later, Eberlein et al (Eberlein *et al.*, 2001) developed a fully hyperelastic intervertebral disc model, where the annulus fibrosus collagen fibres were included into an anisotropic continuum formulation. The model was also limited since it contained only two vertebral bodies (L2 and L3) and the intervertebral disc. Nonetheless, shapes were fairly accurate (Fig. 1.27b) and when comparing their formulation to the classical one where fibres are modelled by one-dimension elements, the authors found that the anisotropic continuum modelling allowed a more homogeneous distribution of strains around the annulus periphery. Poro- and hyper- elasticity were also mixed by

considering hyperelastic the solid phase of the poroelastic model. Duncan and Lotz (Duncan and Lotz, 1997) presented a porohyperelastic model of the annulus fibrosus whose predicting power under axial compression was greater than the simply poroelastic models previously published. The annulus fibre layers were simulated by using rebar elements, which represents a structural modelling of the annulus fibrosus. As presented before, the positive effect of combining poro- and hyper- elasticity was also pointed out by Whyne et al (Whyne *et al.*, 2001). Several multiphasic mixture theories were developed together with experimental protocols in order to take into account intrinsic incompressibility, and fluid effects in the intervertebral disc (Best *et al.*, 1994; Iatridis *et al.*, 1998; Klisch and Lotz, 2000). After that, some complete finite element porohyperelastic studies were presented with a full integration of knowledge about the influence of incompressibility, swelling, charge effect, etc… (Baer *et al.*, 2003; Sun and Leong, 2004; Schroeder *et al.*, 2008). At time of writing, the computational cost of formulations such as poroelasticity, hyperelasticity, poro-hyperelasticity, or osmo-viscoelasticity still limits the construction of extensive models, especially when requiring added degrees of freedoms for fluid pore pressure. For example, in 1996, Wu and Chen (Wu and Chen, 1996) integrated the poroelasticity in a half motion segment (Fig. 1.27c), but the condition of transversal symmetry represented a great limitation. In the first decade of the 21st century, increasing computational power made, however, that highly non-linear or multiphasic material formulations are being progressively integrated in complete finite element lumbar spine segment models. In 1996, Smit (Smit, 1996) used a mathematical analogy between the isotropic linear law and the hyperelastic Mooney Rivlin model to introduce a hyperelastic nucleus pulposus in his bi-segment model. Between 2001 and 2004, Eberlein et al (Eberlein *et al.*, 2001; Eberlein *et al.*, 2004) extended the use or hyperelasticity to the annulus fibrosus and ligament. Since then, hyperelasticity has quickly become a “gold standard” for the fluid filled almost incompressible nucleus and annulus materials (Noailly *et al.*, 2005; Rohlmann *et al.*, 2006; Schmidt *et al.*, 2007a; Bowden *et al.*, 2008). Nonetheless such formulation is still mostly phenomenological, and in 2007, Williams et al (Williams *et al.*, 2007) showed that they could increase the accuracy of their L4-L5 motion segment model by incorporating poroelastic formulations for the trabecular and subchondral bone, and for the intervertebral disc tissues.

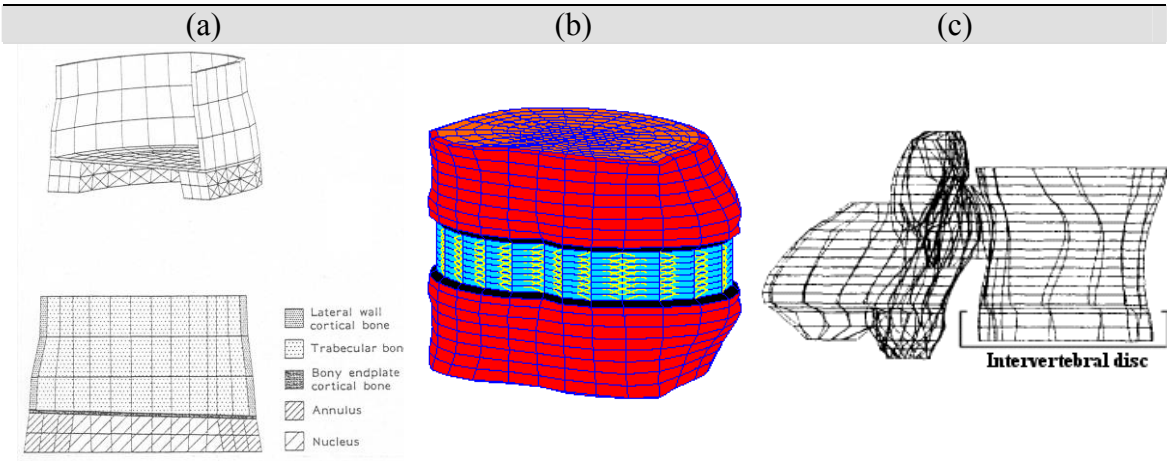

Fig. 1.27: Early models where special material laws were incorporated. (a) Natali et al. (Hyperelastic intervertebral disc ground substance) (Natali and Meroi, 1993). (b) Eberlein et al. (Fully hyperelastic intervertebral disc)(Eberlein et al., 2001). (c) Wu and Chen (Poroelastic model) (Wu and Chen, 1996).

c. Whole lumbar spine models

Whole lumbar spine models allow better studies of the lumbar spine biomechanics, since the number of motion segment units between the artificial boundary conditions is greater. However, the computational cost of the simulations is also greatly increased so that a compromise has to be found between simplification and accuracy with respect to the real biomechanical system.

In 1983, a PhD thesis presented by W. Skalli offered a bi-dimensional finite element modelling of the isolated lumbar spine. Ten years later, a paper on the three-dimensional modelling of the whole lumbar spine (Lavaste *et al.*, 1992) was published by the same researchers. The geometry was determined by X-ray morphological analyses with the help of a custom made program that took into account characteristic linear dimensions for vertebra heights, depths, widths and vertebral body curvatures. However, this geometry was fairly approximated and the defined mesh was very coarse (Fig. 1.28a). In 1995, Gardner-Morse et al (Gardner-Morse *et al.*, 1995) studied the role of muscles in the lumbar spine stability by using another modelling approach where the vertebrae were rigid bodies and the passive soft tissues were simulated by means of beam elements whose stiffness was fitted to experimental values. The use of rigid bodies and beam elements allows creating very large models; nonetheless, this type of numerical approximation is limited to kinematics studies, since the biomechanics of the tissues cannot be investigated. Shirazi-Adl and Parnianpour (Shirazi-Adl and Parnianpour, 2000) also developed a full lumbar spine model using rigid bodies for the vertebrae, but the intervertebral disc and ligaments were deformable bodies. The intervertebral discs included an annulus fibrosus composite model similar to that presented by Shirazi-Adl (Shirazi-Adl, 1989), and a fluid filled cavity that represented the nucleus pulposus. The ligaments had non-linear material properties and the zygapophysial joints were treated as a non-linear and frictionless contact problem (Fig.

1.28b). With such model and by using wrapping elements, the authors could study the lumbar spine stability and tissue stresses with and without follower loads as boundary conditions. Zander et al (Zander *et al.*, 2001) presented a fully deformable lumbar spine finite element model based on a L4 vertebra model previously acquired by Smit (Smit, 1996). They modified the vertebra in function of reported quantitative anatomical data and reconstructed a whole set of lumbar spine vertebrae. The bony parts of the model were isotropic linear elastic and the soft tissues were modelled according to the studies from Smit (Smit, 1996), Shirazi-Adl et al (Shirazi-Adl *et al.*, 1986) and Goel et al (Goel *et al.*, 1995a). Although the material properties remain relatively simple, this model was one of the first complete lumbar spine model with accurate geometry and where full stress analyses can be performed (Fig. 1.28c). Moreover with such extensive structure, the authors could complete the analytical study performed by Bogduk et al (Bogduk *et al.*, 1992) where the forces induced by lumbar muscles were investigated segment per segment. In this sense, both Shirazi-Adl and Parnianpour (Shirazi-Adl and Parnianpour, 2000) and Zander et al (Zander *et al.*, 2001) found that the follower force induced by the muscular activity increased the stability of the spine and the soft tissue stresses. Eberlein et al (Eberlein *et al.*, 2004) created a L2-S1 lumbar spine model which is one of the last published to date (Fig. 1.28d). The objective of the study was to investigate the mechanical behaviour of the lumbar spine soft tissues, which were described by means of hyperelastic laws. Nonetheless, the model had its limitations which were the modelling of the bony parts (tetrahedral elements, inaccurate description of the cortical bone layer and isotropic material properties) and the fact that a fully validation could not be obtain. At time of writing, the full lumbar spine finite element model reported by Chen et al. (Chen *et al.*, 2008) (Fig. 1.28e), could roughly reproduce various experimental ranges of motion, but still used limited tissue models and boundary conditions.

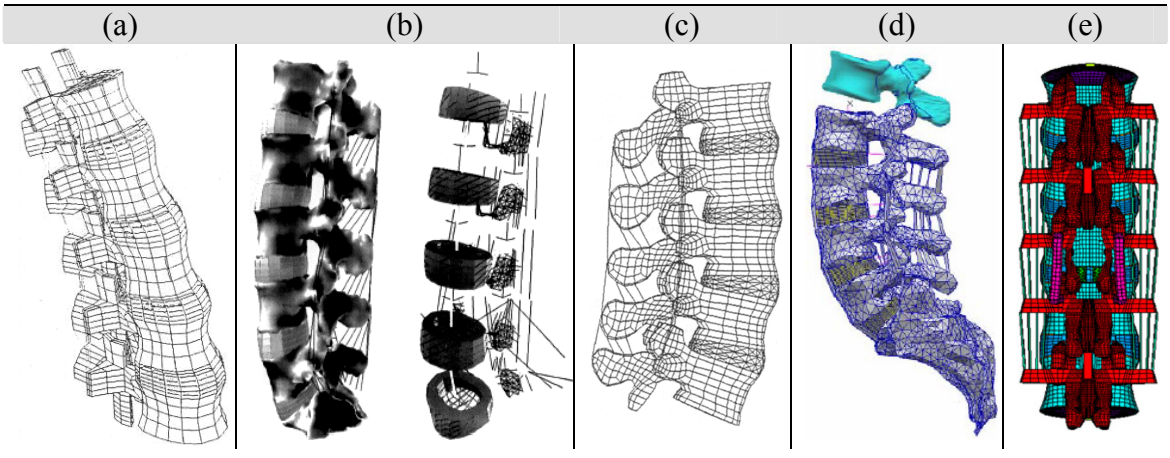

Figure 1.28: Presentation of some full lumbar spine finite element models from the literature. (a) L1-L5 fully deformable model (Lavaste et al., 1992). (b) L1-S1 with vertebrae modelled as rigid bodies (Shirazi-Adl and Parnianpour, 2000). (c) L1-L5 fully deformable model (Zander et al., 2001). (d) L2-S1 fully deformable model with hyperelastic soft tissues (Eberlein et al., 2004). (e) L1-L5 fully deformable model (Chen et al., 2008)

d. Examples of clinical conclusions made from numerical studies

Apart from being used for a better understanding of the spine biomechanics, lumbar spine finite element models have allowed simulating various types of internal boundary conditions as controlled deviations from the normal intact structure. Such models can be very useful to predict the effect of surgical treatments or structural pathologies. The information obtained from the simulations can be experimentally inaccessible, though valuable to assess surgeons for clinical outcomes and decisions. Nonetheless, the results of these works are to be considered carefully keeping in mind the limitations given by the degree of complexity and the level of validation of the models. Table 1.2 presents some examples of such numerical studies.

Table 1.2: Summary of the principal characteristics of some numerical studies used for clinical assessment

Authors & date	Type of model – Boundary conditions	Model dimension	Studied characteristics	Conclusions / Outcomes
Goel and Kim (Goel and Kim, 1989)	L3-L4 complete motion segment with sagittal plane symmetry. Simulation of total denucleation in the intact model and in a model with a bilateral total discectomy.	3D	The ranges of motion, facet contact forces and disc bulge were compared for the different models.	Facets played an important role in protecting the injured disc and the load born by this structure increased by 80% after denucleation. However, vertebral body stresses did not increase significantly and disc bulge decreased indicating the beneficial effect of chymopapain. There were contradictions with clinical findings and the model needs to be improved.
Langrana et al. (Langrana *et al.*, 1991)	L3-L4 intervertebral disc model where the choice of material properties allowed taking the model as an intervertebral disc prosthesis or as a natural organ	3D	Determination of the optimum geometrical and material properties for the disc substitute and study of local disc injury effect when the model simulates a physiologic intervertebral disc.	Finite element analysis provided proper material properties and geometrical data for synthetic disc manufacturing. In the physiologic disc model, single layer local injuries in the posterolateral annulus regions had always greater effect on disc bulge increase than injuries in anterior or lateral regions.
Skalli et al. (Skalli *et al.*, 1993)	Lumbar spine bi-segment model with simulation of a vertebral fracture in the middle vertebra and modelling of a Cotrel Dubousset osteosynthesis implant type with an anterior bone graft. Compressive forces and torsion moments were applied.	3D	Study of the loading effect with variation of fracture grade, geometry and material properties of the implanted material. Simulation of the segment mobility, stress analysis within the device and study of the bone graft influence.	The efficiency of the osteosynthesis systems varies with the boundary conditions and the treatment technique.
Natarajan et al (Natarajan *et al.*, 1994)	Intact and damaged L3-L4 Body-disc-body unit under axial compressive load and sagittal force momentum. For the damaged model, initial annulus tears modelled by local volume reductions.	3D	The anulus failure initiation and propagation were studied under the different load cases.	Failure always started at the endplate indicating that this zone is the weak link of the body-disc-body unit. Compressive load are not expected to produce failure in the annulus failure, but in the endplate. Finally, annulus initial peripheral tears enlarged tears in the inner annulus rather than at the periphery.

Authors & date	Type of model – Boundary conditions	Model dimension	Studied characteristics	Conclusions / Outcomes
Sharma et. al (Sharma *et al.*, 1995)	L3-L4 functional unit model under pure rotational moments and shear forces.	3D	Study of the ranges of motion and facet joint loads with and without ligaments and/or articular facets.	Pronounced facet sagittal orientation could be linked with spondylolisthesis problems or extension instability. Localised facet excision could allow restoring the spinal foramen size with a minimum amount of instability.
Kong et al. (Kong *et al.*, 1998)	Finite element model of the thoracolumbar spine and rib cage under sagittal flexion and extension, and with optimization-based force model in order to predict the forces in the lumbar region muscle fascicles.	3D solid elements for the lumbar part and beam elements for the thoracic part	Study of muscles effect on the lumbar spine model part during static lifting in the sagittal plane.	Muscles stabilize the spine and may induce height stresses in the endplate postero-lateral regions and at the pedicle-vertebral body junction. Shear stresses peaks were found in postero-lateral region of the intervertebral discs and due to the anterior shear forces, the lower lumbar zygapophysial joints and ligaments experienced significant loads, while the upper lumbar facet joints did not contribute to load transfer which increased the intradiscal pressures.
Natarajan et al. (Natarajan *et al.*, 1999)	L3-L4 lumbar spine functional unit under axial rotation.	3D	Influence of progressive removal of the facet joints on the segment range of motion	The segmental rotational behaviour became perturbed when more than 75% of the facet is removed.
Kim (Kim, 2000)	Comparison of two L3-L4 lumbar spine segment models with different intervertebral disc areas and model properties representing, either young, or old adults. Angular displacements applied under extension, with compressive preload	3D	Effect of ageing on annulus displacements, and principal strains, parallel, transversal, and normal to the fibres. Fibre breakage, folding, failure, folding, and interlaminar delamination interpreted in terms of tensile strain directions	Annulus of the young spine more susceptible to layer failure than annulus of the old spine. Layer failure likely to occur in anterior annulus. Independent of ageing, layer folding due to axial compressive strains was likely to occur in outer posterior annulus areas and interlaminar delamination at the posterolateral inner annulus.
Zander et al. (Zander *et al.*, 2002)	L1-L5 lumbar spine model with internal fixators and interbody bone graft at the L2-L3 level. Anterior sagittal flexion and lateral bending motions simulated.	3D	Effect of the bone graft size, placement and stiffness on the lumbar spine biomechanics.	Stresses in the endplates adjacent to bone graft increased. Overloading increased with bone graft stiffness. Sagittal flexion led to the lowest stress increases. Large grafts with low stiffness should be biomechanically preferred.

Authors & date	Type of model – Boundary conditions	Model dimension	Studied characteristics	Conclusions / Outcomes
Eberlein et al (Eberlein, 2002)	L2-L3 lumbar spine segment with Dynesys™ posterior stabilizing device.	3D	Comparison of the ranges of motion obtained with the implant with or without nucleusectomy, with the ranges of motion obtained for the non treated segment, intact, and without facet and ligaments.	Great stiffening effect of the device on the motion segment and non-physiological biomechanical response in axial rotation.
Polikeit et al.(Polikeit et al., 2003b)	L2-L3 lumbar spine segment with material properties adapted to an osteoporosis case simulation and modelling of PMMA cement augmentation. Sagittal flexion, lateral bending and axial compression loads were simulated.	3D	Influence of PMMA cement injection on the load transfers within the segment.	The treatment reinforces the osteoporotic vertebra, but both stress and deflections were increased within the adjacent endplates as well as intervertebral disc pressures.
Polikeit et al (Polikeit *et al.*, 2004)	L2-L3 functional unit model with changes in the vertebral bone and intervertebral disc Young's moduli in order to simulated respectively osteoporosis and disc degeneration.	3D	Influence of the osteoporotic conditions on the vertebral bone strains and their interaction with the degenerated discs.	The presence of a degenerated disc in an osteoporotic segment might produce more realistic overall strain distributions and the presence of a healthy disc might be considered as the worst-case scenario.
Goel et al (Goel *et al.*, 2005)	L3-S1 lumbo-sacral tri-segment model with virtual implantation of a Charite® artificial disc model at the L5-S1 level. Flexion and extension moments with axial compressive follower force applied to both intact and implanted models. Additional hybrid boundary conditions studied, where pure moment magnitudes were increased until rotations equalled those of the intact model.	3D	Ranges of motion and facet loads were computed at each level of both the intact and the implanted models. Shear stresses calculated in the endplates adjacent to the prosthesis and compared to the stresses predicted in the corresponding endplates of the intact model.	Compared to the intact model, ranges of motion generally increased at the implanted level and slightly decreased at the adjacent levels. Facet forces at the implanted level could either increase of decrease, depending on the way external loads were applied. Under extension, high stresses in the implanted model L5 endplate indicated that, depending on local lordosis, L5-S1 prosthesis loosening could occur at the device upper endplate.

Authors & date	Type of model – Boundary conditions	Model dimension	Studied characteristics	Conclusions / Outcomes
Noailly et al (Noailly *et al.*, 2005)	L3-L5 lumbar spine bi-segment model based on a L4 vertebra CT scan. Flexion, extension, axial rotation, and axial compressive loads simulated on both an intact and a treated model with a L4-L5 novel composite disc substitute. Both peripheral and full contact between prosthesis and adjacent vertebrae were studied.	3D	Ranges of motion, facet contact forces, and stress distributions in the intervertebral discs and vertebral trabecular bones, were analyzed for both the intact and implanted models.	Under load control, composite disc substitute might, neither induce traumatic stresses at the implanted level, nor significantly affect the adjacent level. Nevertheless, important bone remodelling may be expected in the vertebrae adjacent to the implant, depending on contact conditions between bone and implant. Generally full contact between the prosthesis and the vertebral endplates should be preferred.
Lacroix et al (Lacroix *et al.*, 2006)	L3-L5 lumbar spine bi-segment model based on a L4 vertebra CT scan. L4 and adjacent intervertebral discs replaced by different bone grafts, i.e. femoral, tibial, and fibular. Cartilage endplate was eventually left between vertebrae and grafts. Compression, extension, and flexion loads simulated for both intact and treated segments.	3D	L3-L5 bi-segment stiffness, and stress distributions in the vertebrae studied for both implanted and intact models. Effect of bone graft type, bone graft number and location was analyzed.	Bone grafts considerably stiffened the lumbar spine bi-segments and modified stress distributions in adjacent vertebrae. Generally, fibular grafts had major stiffening effect. Femoral grafts best preserved the stress-strain distributions in adjacent vertebrae and could be seen as the best solution to limit long-term bone remodelling. Due to axial asymmetry, tibial graft made results to depend on initial placement. Presence of cartilage endplate was positive from a biomechanical point of view.
Rohlmann et al (Rohlmann *et al.*, 2006)	L3-L4 lumbar spine motion segment with disc degeneration modelled by means of disc height reduction, non-linear ligament stiffness curves offset, and nucleus pulposus compressibility increase.	3D	Comparison of ranges of motions, intradiscal disc pressures, annulus von Mises stresses and facet joint forces between healthy model and models with various degrees of disc degeneration.	Due to disc height reduction, annulus fibrosus stress and facet joint forces increased with disc degeneration. However, as ranges of motion decreased with the grade of degeneration, facet joints increase was not proportional to degeneration degree.
Moumene and Geisler (Moumene and Geisler, 2007)	L4-L5 lumbar spine motion segment based on a L4 vertebra CT scan. Non-pathologic intervertebral disc replaced, either by a Charite®, or by a Prodisc® artificial disc model. Extension, axial rotation, and lateral bending motions simulated with prostheses differently placed in the intervertebral space.	3D	Comparison of facet contact forces obtained with intact disc and with the two types of modelled disc substitutes. Influence of prosthesis placement on facet contact forces was analyzed and stresses in both prosthesis models were computed.	Charite® mobile core artificial disc generally reduced facet contact forces with respect to the intact model. Facet overload unlikely, even with prosthesis misplacement. Conversely, Prodisc® disc fixed core led to frequent facet load increases, depending on prosthesis location. Lower stresses within the mobile core should be beneficial for device life time.

Authors & date	Type of model – Boundary conditions	Model dimension	Studied characteristics	Conclusions / Outcomes
Natarajan et al (Natarajan *et al.*, 2008)	L4-L5 lumbar spine motion segment with poroelastic endplates and intervertebral disc tissues. Swelling taken into account. Three mass lifting activities, including time history, simulated, and taking into account muscle forces.	3D	Intervertebral disc translational and rotational motions, disc and endplate von Mises stresses, and annular shear and fibre stresses, computed for each lifting activity. Facet contact forces and fluid exchange between disc and surrounding tissues were reported.	Lifting activities involving lateral bending gave higher disc stresses and motions, and might increase low back pain risk. Disturbances of fluid exchange because of sclerotic subchondral bone may increase intradiscal pressures and disc bulge, possibly contributing to back pain.
Chen et al (Chen *et al.*, 2008)	L1-L5 lumbar spine finite element five-segment model. Flexion, extension, axial rotation and lateral bending motions simulated with and without implants. Implants, inserted at the L3-L4 level, were either interbody fusion cage with posterior pedicle screws, or Prodisc® disc substitute. Tissue removals imposed by implantation procedure modelled.	3D	Segmental ranges of motion, annulus von Mises stresses, and facet contact forces computed at both implanted and adjacent levels.	Interbody fusion induced high stress concentrations in the annuli adjacent to the implanted levels. Adjacent levels particularly affected under flexion extension. Prodisc® device destabilized the implanted level, induced large annulus stress in the remaining annulus tissue, and large facet contact forces.
El-Rich et al (El Rich *et al.*, 2009)	L5-pelvis patient-specific geometrical model acquired by *in vivo* CT-scan. Load conditions involved in spondylolisthesis modelled as axial force, axial force with flexion moment, and axial force with extension moment.	3D	von Mises and shear stresses calculated in S1 and in the pedicles and pars articularis of L5.	Pedicle region and dorsal wall of the L5 pars articularis were particularly loaded suggesting that pedicular stress fracture may be associated with spondylolisthesis. Results qualitatively agreed with clinical observations. Model could be used to study risks of spondylolisthesis associated to peculiar geometries of the pelvis.

Chapter2

"I start from one point and go as far as possible."

(John Coltrane)

Chapter2

- STRESS ANALYSIS OF THE LUMBAR SPINE - MECHANICAL INTERACTIONS & ROLE OF THE INTERNAL COMPONENTS

A. Introduction

As presented in Chapter 1, low back problems should be viewed as a chain of events where all the spinal components interact with each other and where their mechanical role, as well as their response to mechanical factors must be understood. This was clearly established by several clinical studies and by *in vitro* experiments on lumbar spine specimens. For example, Tencer et al (Tencer *et al.*, 1982) demonstrated that a cooperative mechanism exists between facets and intervertebral disc in the case of annulus fibrosus injury. On one hand, Nachemson (Nachemson, 1963) showed that the pressure changes measured in the nucleus pulposus under various load magnitudes depended principally on the annulus fibrosus tissue behaviour. On the other hand, *in vivo* magnetic resonance studies may indicate that the deformation mode of the annulus fibrosus under flexion and extension changed with disc degeneration and depended on the nucleus pulposus tissue state (Fennell *et al.*, 1996). Facet cartilage layers were also found to be affected by disc degeneration (Vernon-Roberts and Pirie, 1977), and more generally, various types of measurements and observations on human tissues revealed that the mechanical condition of the intervertebral disc state affects other tissues of the lumbar spine such as the vertebral endplates (Grant *et al.*, 2002; Keller *et al.*, 1993), or vertebral bone in general (Pollintine *et al.*, 2004; Adams *et al.*, 2006), or the ligaments (Ruiz Santiago *et al.*, 1997; Neumann *et al.*, 1994). An illustration of mechanically induced pathological situation is given by the case of spinal fusion where the new mechanical environment given by the outcome of the surgery is likely to participate in the further degeneration of adjacent levels (Lee *et al.*, 1992; Kumar *et al.*, 2001; Lehmann *et al.*, 1987; David, 2002). This is probably due to the major issue of spinal fusion which is the loss of mobility of the treated segment. A known tissue configuration and a well identified set of possible external loads could give an estimation of the risks of different pathology, which would contribute to optimize the techniques of treatment and prevent post-operative complications. In this sense, finite element analysis is adequate, since it is probably one of the most suitable methods to predict stresses in non linear complex structures, providing information hardly accessible through experimental testing.

Up to now, many different models of the spine have been published. One of the greatest contributions to lumbar spine finite element modelling was brought by Shirazi-Adl and colleagues who used a geometrical L2-L3 lumbar spine segment and studied the influence on the segment motion of components such as posterior bony elements (Shirazi-Adl, 1994), and intervertebral disc and facet cartilage (Shirazi-Adl *et al.*, 1986; Shirazi-Adl and Drouin, 1987; Shirazi-Adl and Drouin, 1988; Shirazi-Adl, 1991). Goel et al (Goel *et al.*, 1988) were other great providers of knowledge on the spine biomechanics. They used their model to study the biomechanics of spine instrumentation, or to determine the effect of different types of annulus fibrosus injuries (Goel and Kim, 1989). The criteria used by Shirazi-Adl, Goel and colleagues for the determination of the tissue material properties, facet contact simulation or intervertebral disc structure modelling served as basis to many further lumbar spine numerical studies (Ueno and Liu, 1987; Duncan and Ahmed, 1991; Kasra *et al.*, 1992; Lavaste *et al.*, 1992; Wang *et al.*, 1997; Sharma *et al.*, 1995; Natarajan and Andersson, 1999; Smit, 1996; Zander *et al.*, 2001; Schmidt *et al.*, 2006). Among them, Ueno and Liu (Ueno and

Liu, 1987) analysed the stress distribution within the intervertebral disc and the vertebral bodies of a L4-L5 motion segment model under combined axial compression and rotation. They found that the annulus fibrosus fibres bore principally tensile stresses transmitting the shear stresses from a vertebral body to another, where the cortical shell plays a prominent role. Sharma et al. (Sharma *et al.*, 1995) performed a parametric motion study of a L3-L4 lumbar spine segment model and identified the relative contributions of ligaments, intervertebral disc and zygapophysial joints in resisting different sagittal motions. These studies gave a good idea about the biomechanical function of the different tissues of the lumbar spine. However, the geometries and material properties were fairly simplified. Among the most recent and most accurate lumbar spine model geometries, the model of Zander et al (Zander *et al.*, 2001) was based on a three dimensional L4 vertebrae geometry reconstituted by Smit (Smit, 1996) from a series of CT scans. It was then used to study the effect of modelled implants on the load transfer through the vertebrae (Zander *et al.*, 2002), and to study the influence of different grades of simulated disc degeneration on the load path through the ligaments, the facet joints and the intervertebral disc components (Rohlmann *et al.*, 2006). Regarding the biomechanical behaviour of normal motion segments, they investigated the influence of muscles on the annulus fibrosus stress state (Zander *et al.*, 2001), and the load distribution in the spinal ligaments as a function of the ligament stiffness and load cases (Zander *et al.*, 2004). Nonetheless, the type of material constitutive equations and the level of refinement of some substructures, such as vertebral bodies, annulus fibrosus, or cartilage endplates were not so adequate to the study of the mechanical interactions that exists between the different lumbar spine tissues. Polikeit et al (Polikeit *et al.*, 2004) used a fairly accurate CT scan based geometry of a L2-L3 lumbar spine segment to identify the differences of load transfer between the intervertebral disc and the vertebral body trabecular bone. However, the study was primarily focussed on the effect of modelling osteoporosis; the individual role of components such as the vertebral bony cortex, the ligaments, or the posterior bony elements was not discussed. Moreover, both ligaments and annulus fibres were defined as linear elastic, which may influence notably the load transfers. Apart from the nucleus pulposus that was modelled as a fluid filled impermeable cavity, all the soft tissues of the model of Eberlein et al (Eberlein *et al.*, 2004) were non-linear elastic (hyperelastic formulations) (Eberlein *et al.*, 2001; Stadler and Holzapfel, 2006) The model was adapted to the assumed mechanical laws, and the authors used a stress analysis to determine the optimal regional stiffness variations of the annulus fibrosus collagen fibres (Eberlein *et al.*, 2001), or even the best type of mesh refinement and analogical surface fit for the modelling of the facet joints contact layers (Stadler and Holzapfel, 2006). With this approach, they optimized their model, fitting the mechanical and numerical approximations with the expected stress distributions in the different tissues. Nonetheless, the interactions between the different components of a whole spine mono- or multi-segment were not studied. From the point of view of material properties, as stated in Chapter 1, many models offered solutions for a more mechanistic description of the spine tissues behaviour. Nonetheless, these advanced constitutive laws were mainly used in reduced and simplified geometries and implementations in large models such as complete three dimensional spine functional units are still fairly limited.

Each model has its own specificity and numerical results usually provide thorough information on the biomechanics of the spine structure and substructures. However, it seems that up to now, there is not any detailed model that integrates all the accumulated knowledge for a further advanced description of the multiple interactions between the spinal components. Therefore, the objective of this chapter was to summarize some of the latest lumbar spine modelling techniques into a full L3-L5 bi-segment model in order to identify the mechanical interaction between the different lumbar spine components through a stress analysis under static conditions. By this way, it is expected to establish specific relations between the structure and the mechanical integration of each component, which along with comparisons with previous numerical and experimental studies would efficiently guide further developments of the model, essential for future clinically relevant predictions.

B. Model definition

I. Geometry

A L3-L5 bi-segment finite element model created and validated by Smit (Smit, 1996) was taken initially. In this model, the L4 vertebra was obtained from a CT scan of a 44 year old man without pathology and was duplicated to represent L3 and L5. In order to make possible the qualitative study of the biomechanical role played by each tissue in the structure, all the spinal components that were not represented in the original geometry were modelled by local modifications of the mesh. Then, the vertebral cortex (cortical shell and bony endplates) and the intervertebral disc cartilage endplates were introduced, and the definitions of the posterior articular contact facet cartilage layers and annulus fibrosus composite structure were refined (Fig. 2.1).

a. Vertebral cortex

The thickness values of cortical shells and bony endplates were principally determined from literature (Silva *et al.*, 1994; Ritzel *et al.*, 1998) and verified by histological cut measurements performed at the Royal Free Hospital, London, England (Fig. 2.2). The pictures were acquired under the software Axiovision 3.0 with an optical microscope Axioskop 2 MOT (Zeiss) and a digital built-in camera AxioCam (Zeiss). As shown in Figure 2.2, the cortex thicknesses are not constant within the sagittal plane. Nonetheless, the available samples came from pathologic spines (osteoporotic bone, osteophytosis at joint margins, bony endplate sclerosis) and the thickness variations did not follow a specific pattern that could have been reported in the model. Therefore, the cortical wall was divided into a posterior and an anterior part, each of them having a given constant thickness (Fig. 2.3, Table 2.1).

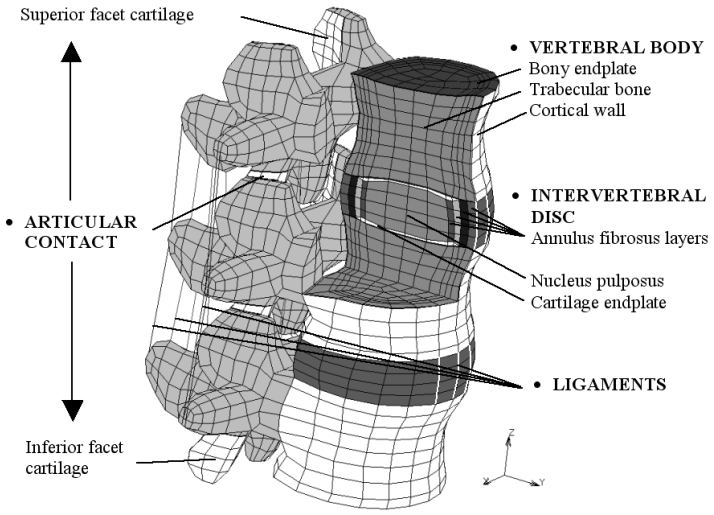

Figure 2.1: Global geometry of the modelled L3-L5 physiologic lumbar spine segment

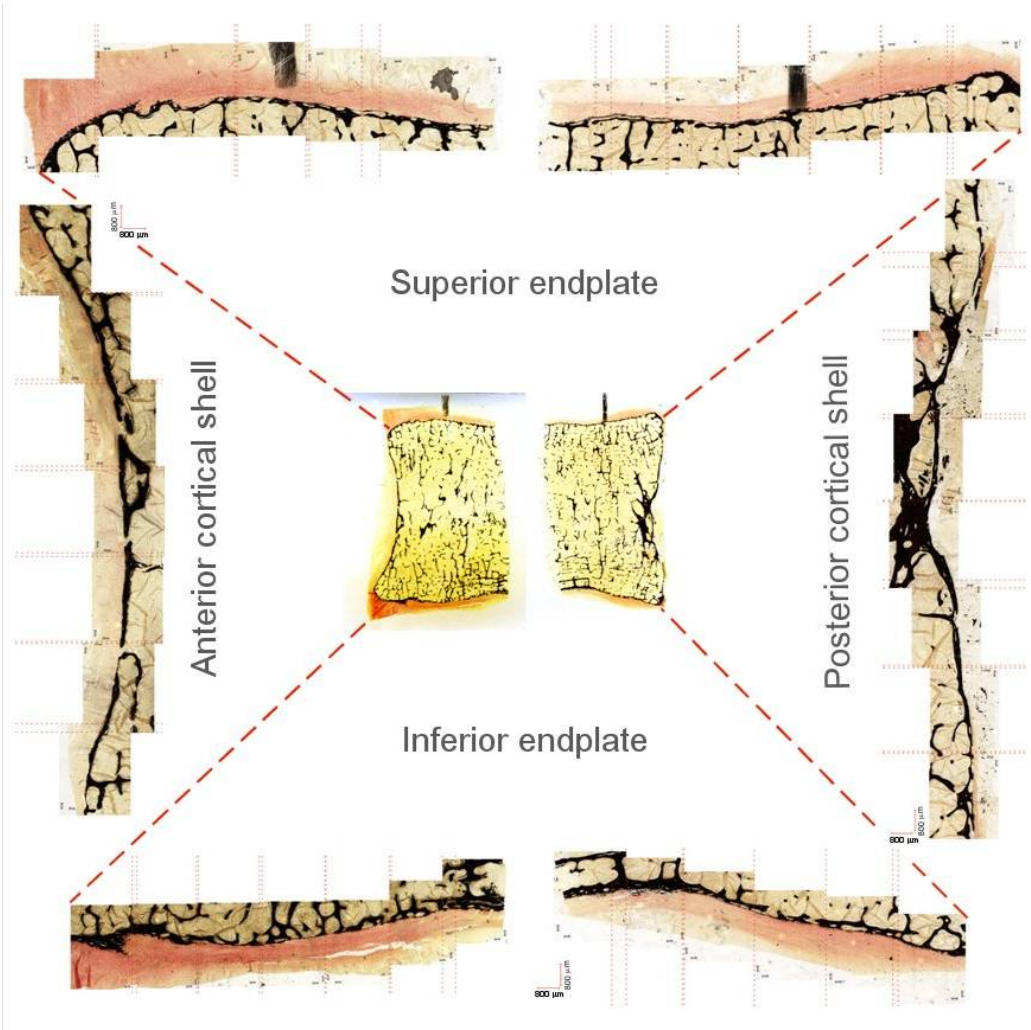

Figure 2.2: Histological mid-sagittal cut of a lumbar vertebra with magnification of the different parts of the cortex.

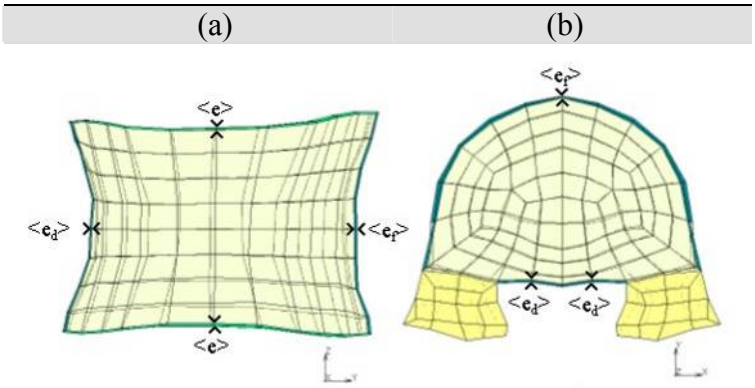

Figure 2.3: Modelled L4 vertebral body including cortex (Thickness values are given in Table 2.1). a) Mid-sagittal cut lateral view. b) Transversal cuts cranial view

Table 2.1: Averaged values for bony endplates and cortical shell thicknesses

	Cortical shell		Bony endplate
	$<e_f>$ (µm)	$<e_d>$ (µm)	<e> (µm)
L3	300	255	167
L4	300	290	177
L5	375	320	209

b. Cartilage endplate

As with the bony cortex, the intervertebral disc cartilage endplates were studied through histological cuts and they were found to cover the whole nucleus pulposus and spread over the annulus fibrosus up to between one third and a half of annulus thickness (Fig. 2.4). This finding corresponded well to the scanning electron microscopy observation of the intervertebral disc three dimensional structure performed by Inoue (Inoue, 1981). According to our measurements and to the literature (Humzah and Soames, 1988; Saunders and Inman, 1940; Roberts *et al.*, 1996), the thickness of the modelled cartilage endplate varied from 1mm to the periphery to about 0.6mm in the centre.

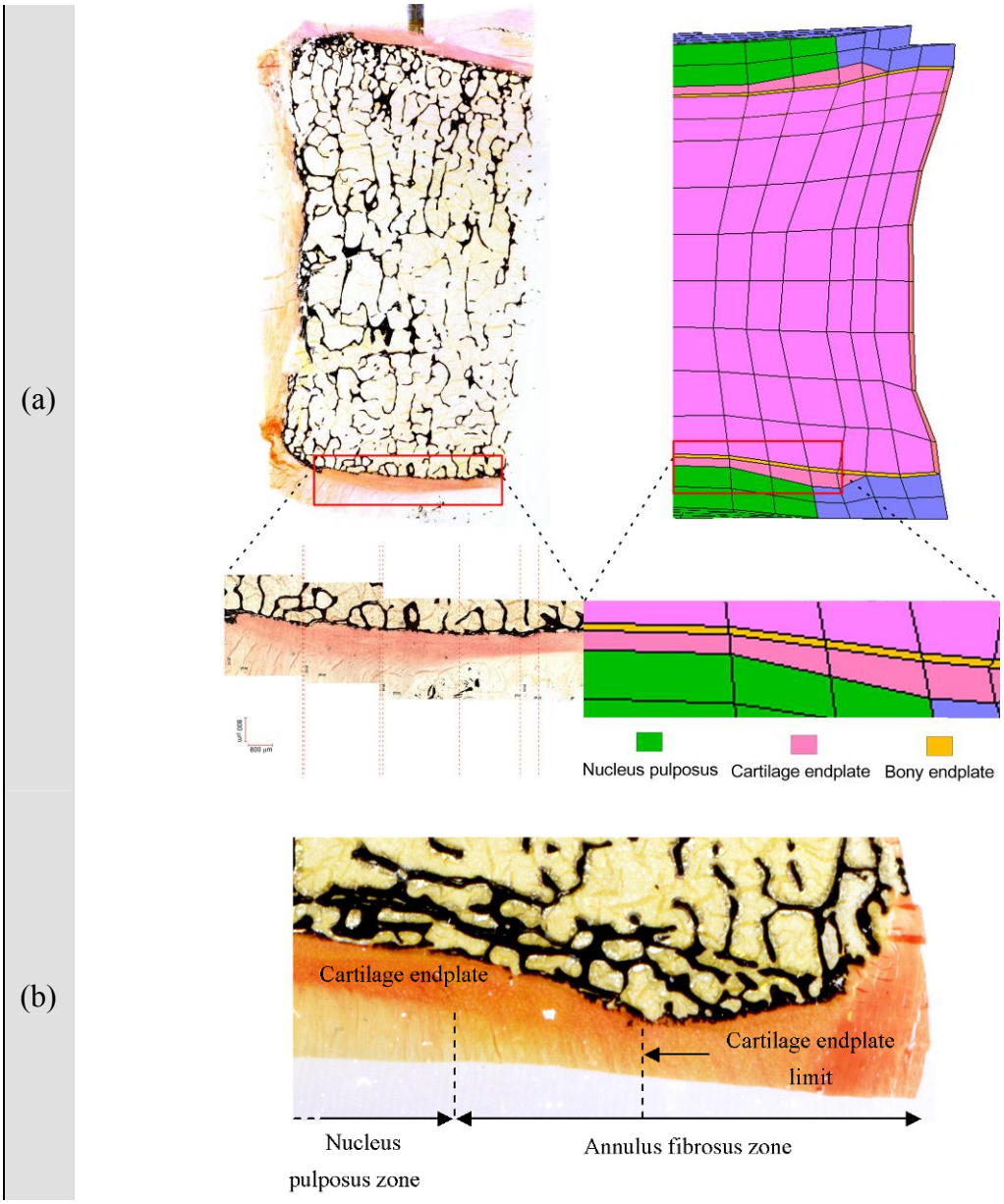

Figure 2.4: Cartilage endplate modelling from histological cut observations. a) General shape. b) Detail of the peripheral zone.

c. Annulus fibrosus

The annulus fibres defined by Smit (Smit, 1996) were represented by three-dimensional unidirectional truss elements that crossed the axial planes of the hexahedral elements used for the annulus matrix modelling (Fig. 2.5). The disadvantage of such fibre reinforced material model is that the fibres orientation and distribution are mesh-dependent and can hardly be modified. Hence, a new definition of the annulus composite structure was introduced through the use of the so-called rebar elements. This type of elements consists in three-dimensional empty bricks in which up to five parallel

mono-oriented cord (fibre) layers can be defined (Fig. 2.6a). Every layer is characterized by the cords cross section area, orientation, material properties and by an equivalent thickness related to the volume fraction of the fibres. The composite material becomes fully defined after the superposition of each rebar element to a solid hexahedral element that represents the matrix (Fig. 2.6b).

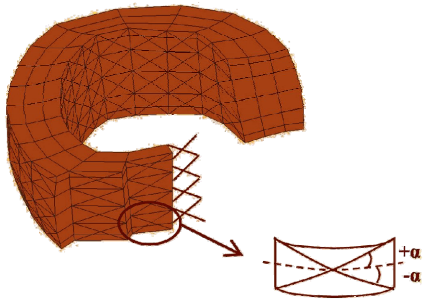

Figure 2.5: Original definition of the annulus fibrosus composite structure, where the fibres are modelled with truss elements attached to the hexahedral solid elements of the matrix.

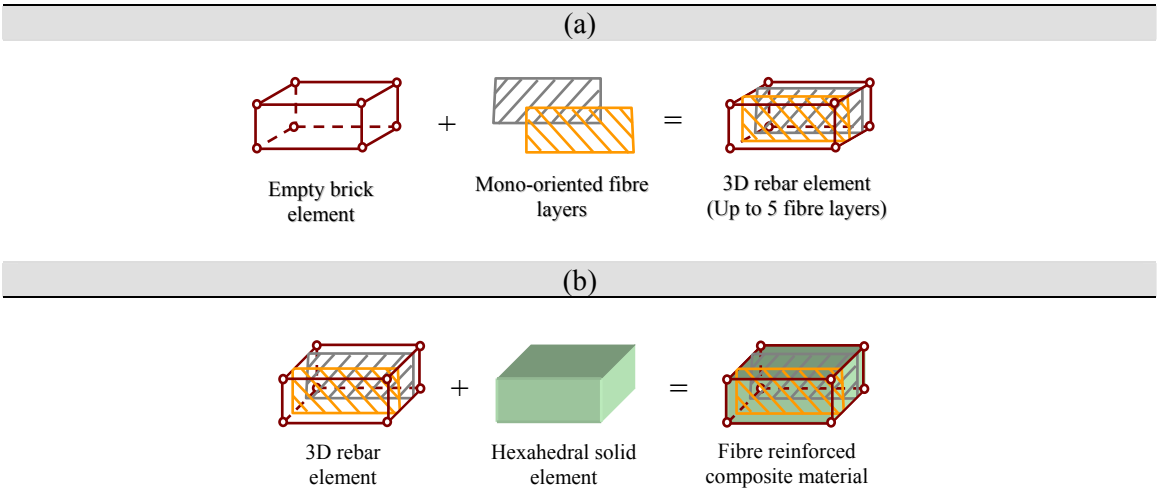

Figure 2.6: Construction of the fibre reinforced composite material for the lumbar spine model annulus fibrosus; a) 3D rebar element technology, b) Composite material based on rebar formulation

In the annuli fibrosi of the modelled bi-segment, the fibres were distributed within four radial layers of three-dimensional rebar elements, giving in total 20 mono-directional layers uniformly distributed along the annulus fibrosus thickness (Fig.2.7a). Such configuration may be considered as a fairly good approximation of the lumbar annuli fibrosi anatomical descriptions, since these latter report the identification of about 20-35 unidirectional collagen layers (Marchand and Ahmed, 1990; Cassidy *et al.*, 1989). According to Cassidy et al (Cassidy *et al.*, 1989), the fibre orientation changed in the radial direction in a criss-cross pattern and the absolute value of the angle between the fibres and the annulus axial axis decreased from 62º in the outer annulus to 45º in

the inner annulus (Fig. 2.7b). In order to represent the variations of fibres section and volume percent, the annulus fibrosus was divided into four radial and tangential areas (Fig. 2.8a). Rebar layers were fairly equidistant. Nonetheless, according to Brickley-Parson and Glimcher (Brickley-Parson and Glimcher, 1984), the cross-section of the modelled collagen bundles varied in function of the layer radial position within each tangential quadrant of the annulus (Fig. 2.8b). Furthermore, Marchand and Ahmed (Marchand and Ahmed, 1990) measured different values of collagen mass content in the radial direction. These values were associated to the different radial sections. Hence, the relative amount of collagen in each radial zone was determined, and the corresponding volume contents were computed, so that the total fibre volume content was 16% (Best *et al.*, 1994; Galante, 1967) (Fig. 2.8c).

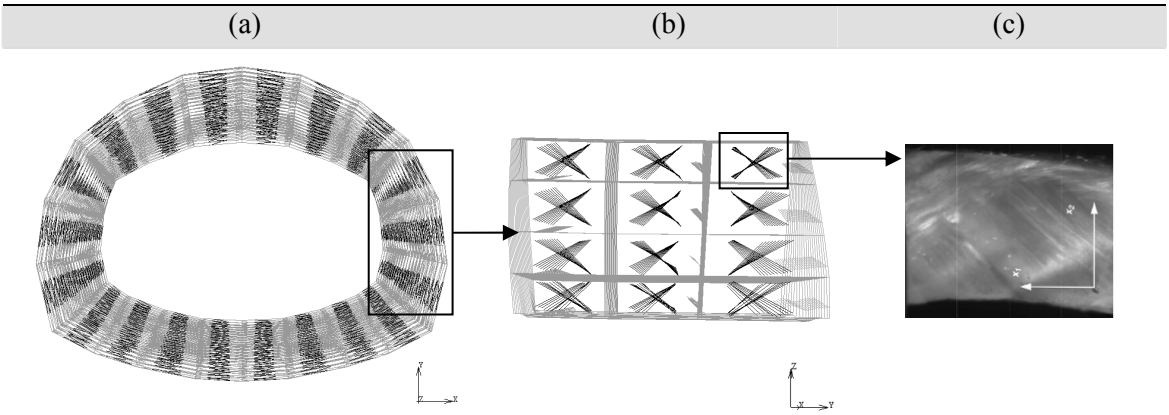

Figure 2.7: Rebar elements technology. a) Annulus fibrosus fibres represented by rebar elements. b) Fibres view across annulus thickness. c) Optical microscope image from an outer annulus multilayer sample (Adapted from (Guerin and Elliot, 2006))

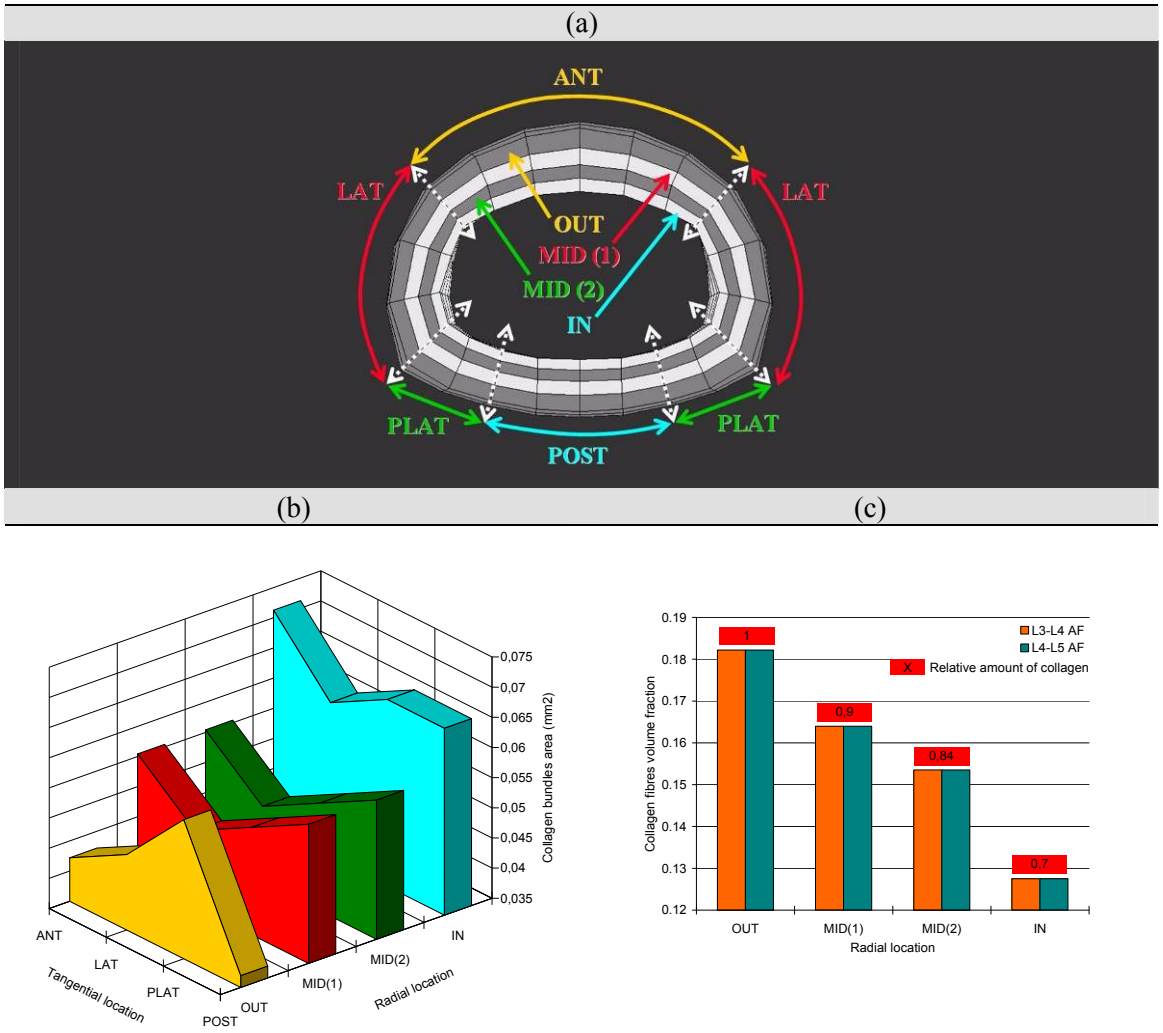

Figure 2.8: Collagen fibres content data in different areas of the modelled annuli fibrosi. a) Definition of different tangential and radial geometrical areas b) Variation of the collagen bundles area through the annulus. c) Relative quantity of collagen in the different annulus radial sections and variation of the corresponding collagen volume fraction through the L3-L4 and L4-L5 annulus thicknesses.

d. Facet cartilage layers & ligaments

Articular facets were represented by three-dimensional hexahedral elements (Fig.2.9), and the contact areas were interpolated by Coon surfaces. The ventral and dorsal ligaments that correspond to the six major spinal ligaments were modelled with truss elements whose directions were the main line of action of the soft tissue according to the previous modelling performed by Smit (Smit, 1996) (Fig. 2.1). The sectional areas were taken from the literature (Panjabi *et al.*, 1991). The intertransverse ligament was the only minor ligament introduced in the model, since no information could be found on the mechanics of other minor ligaments that could participate in stabilizing the spine segment, such as the transforaminal ligaments (Chap. 1).

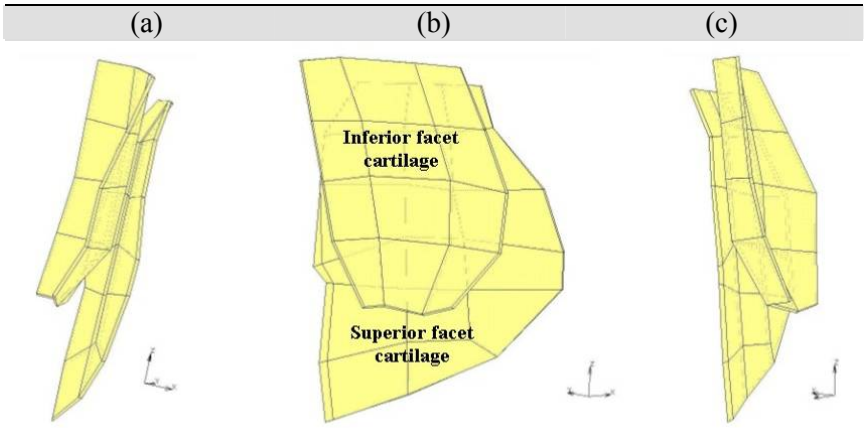

Figure 2.9: Modelled zygapophysial joint facet cartilage layers. a) Dorsal view; b) Lateral view; c) Frontal view

II. Material properties

All the constitutive laws and material parameters values used for the modelled tissues are summarised in Table 2.2. The stress-strain relationships were calculated for large displacement and large strain in the scope of a total Lagrange mechanical formulation. The unidirectional experimental engineering strains and stresses that were taken from the literature in order to compute the tangent stiffness of the elastic non linear materials (hypoelastic materials) were respectively converted into Green strain and 2nd Piola-Kirchhoff stress. These variables ensure that, under large displacements, no strain is added by rigid rotations (Crisfield, 1996) and were related to the experimental reported engineering data by the following equations (one dimension):

$$E_{11} = \varepsilon_{11}(1 + 0.5\,\varepsilon_{11}) \tag{2.1}$$

$$S_{11} = \frac{\sigma_{11}}{(1 + \varepsilon_{11})} \tag{2.2}$$

where E_{11}, S_{11}, ε_{11} and σ_{11}, are respectively unidirectional components of the Green-Lagrange strain, 2nd Piola-Kirchhoff stress, engineering strain, and engineering stress. The above relations show that for a given stress-strain engineering data list, the large displacement stress-strain curve in tension will be located under the engineering curve. An example is shown in Figure 2.10 for the anterior longitudinal ligament.

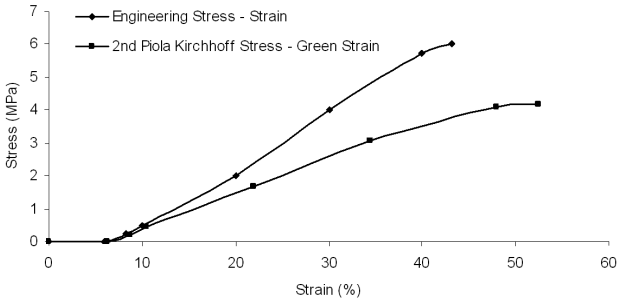

Figure 2.10: Difference between engineering and large displacement stress strain relationships: example of the Anterior Longitudinal Ligament in tension (Engineering data taken from (Sharma et al., 1995))

Table 2.2: Summary of the material properties used for the model

Material	Constitutive laws	E (MPa)	ν	G (MPa)
Trabecular bone	Isotropic transverse, Linear elastic (Whyne *et al.*, 2001; Ueno and Liu, 1987; Cowin, 2001)	140 * 140 250	0.45 * 0.176 0.315	48.276 * 77 77
Cortical bone	Isotropic transverse, linear elastic (Ueno and Liu, 1987; Natali and Meroi, 1993)	8000 * 8000 12000	0.4 * 0.23 0.35	2857.14 * 2400 2400
Bony endplate	Isotropic, linear elastic (Whyne *et al.*, 2001)	1000	0.3	-
Bony posterior elements	Isotropic, linear elastic (Shirazi-Adl *et al.*, 1986)	3500	0.3	-
Cartilage endplate	Isotropic, linear elastic (Shirazi-Adl, 1989; Whyne *et al.*, 2001; Natali and Meroi, 1993)	24	0.4	-
Facet cartilage	Tension: isotropic linear elastic	11 (Sharma *et al.*, 1995)	0.2 (Li *et al.*, 2000)	-
	Compression: hypoelastic	From 11 at 0% strain to 3500 at 0.7% strain	From 0.2 at 0% strain to 0.4 at 0.7% strain (Li *et al.*, 2000)	-
Ligaments	Hypoelastic	Experimental data (Myklebust *et al.*, 1988; Chazal *et al.*, 1985; Pintar *et al.*, 1992)		
	$dS = \left(\frac{\partial^2 \varphi}{\partial \varepsilon^2}\right) dE \quad ; \quad \varphi = \int S\, dE$ (Crisfield, 1996)			
Annulus fibrosus fibres	Hypoelastic	Collagen I: Experimental data (Sharma *et al.*, 1995)		
	Collagen I : $dS = \left(\frac{\partial^2 \varphi}{\partial \varepsilon^2}\right)_{Collagen\ I} \times dE$ Collagen II : $dS = 0.77\left(\frac{\partial^2 \varphi}{\partial \varepsilon^2}\right)_{Collagen\ I} \times dE$			
Annulus fibrosus matrix	Neo-Hookean incompressible (Eberlein *et al.*, 2001)	μ = 0.5MPa		
	$W = \frac{\mu}{2}\left(\bar{I}_1 - 3\right) \quad ; \quad dS = \left(\frac{\partial^2 W}{\partial E^2}\right) dE$ (Holzapfel, 2000) ‡			
Nucleus pulposus	Mooney-Rivlin incompressible (Smit, 1996)	C_{10}=0.12MPa, C_{01}=0.03MPa		
	$W = C_{10}\left(\bar{I}_1 - 3\right) + C_{01}\left(\bar{I}_2 - 3\right) \quad ; \quad dS = \left(\frac{\partial^2 W}{\partial E^2}\right) dE$ (Holzapfel, 2000) ‡			

* The Young's moduli are presented respectively in the 11, 22 and 33 directions. The Poisson's ratios and the Coulomb's moduli are given respectively in the 12, 23, and 31 directions; 1: coronal plane horizontal direction, 2: sagittal plane horizontal direction, 3: axial direction

‡ I_1 and I_2 are respectively the 1st and the 2nd invariant of the right Cauchy-Green tensor isochoric (deviatoric) part.

a. Isotropic transverse vertebral bone

For Cortical and trabecular bone isotropic transverse properties, the sets of Poisson's ratios and shear moduli found in the literature had to be adapted according to the Young's modulus values in order to respect the symmetry of the stiffness matrix. According to Cowin et al (Cowin, 2001), the following relationships were used:

$$\frac{\nu_{12}}{E_1}=\frac{\nu_{21}}{E_2} \quad ; \quad \frac{\nu_{13}}{E_1}=\frac{\nu_{31}}{E_3} \quad ; \quad \frac{\nu_{23}}{E_2}=\frac{\nu_{32}}{E_3} \qquad \text{(2.3a),(2.3b),(2.3c)}$$

$$\nu_{12}=\nu_{21} \quad ; \quad G_{12}=G_{21}=\frac{E_1}{2(1+\nu_{12})} \quad ; \quad \nu_{13}=\nu_{23} \quad ; \quad \nu_{31}=\nu_{32} \quad ; \quad G_{23}=G_{31}$$

(2.4a),(2.4b),(2.4c),(2.4d),(2.4e)

where $\nu_{i,j}$, G_{ij} and E_i ($i,j = 1,2,3$) are respectively the Poisson's ratio, the shear and Young's moduli of the material. Equations (2.3) represent the conditions of symmetry on the compliance (or stiffness) matrix for an orthotropic material, and equations (2.4) are additional conditions due to the existence of an isotropic transverse plane defined by the directions 1 and 2.

b. Zygapophysial joint cartilage layers

The facet cartilage stiffness increased non-linearly, driven by the contact-induced strains. The application of an isotropic tangential law allowed computing all the stress components of the three-dimensional solid elements from the tangential stiffness changes in the contact direction (Fig. 2.11). Moreover, it has been experimentally shown that the compressibility of articular cartilage layers was depth dependent (Woo *et al.*, 1979). As in the first stages of compression, the superficial layer deformed most (Schinagl *et al.*, 1996), the apparent Poisson's ratio of the modelled cartilage was considered to vary with the compressive strain, from 0.2 to 0.4 (Li *et al.*, 2000). According to the type of indentation experimental curve and modelling reported by Sharma et al (Sharma *et al.*, 1995), the tangent stiffness of the facet cartilage layers was fitted to a power law and varied from 11MPa to the stiffness value of the adjacent bone (Fig. 2.11).

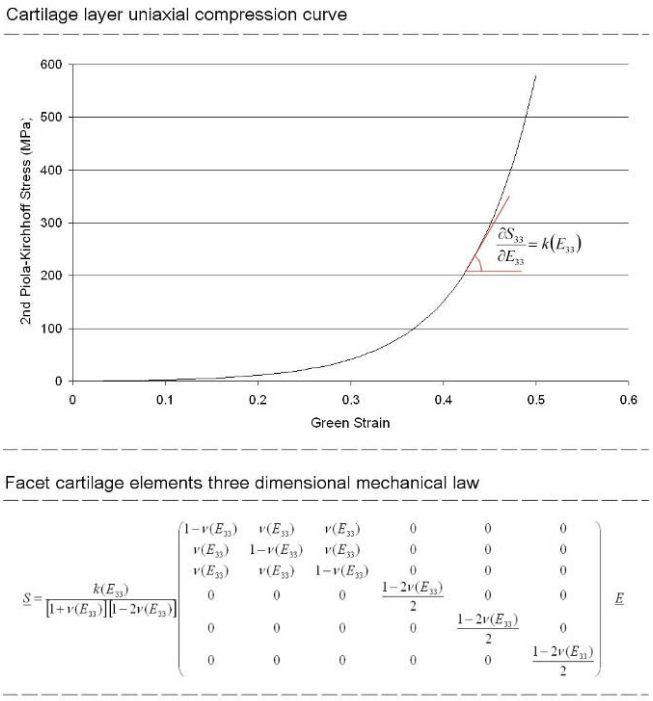

Figure 2.11: Mechanical modelling of the articular facet cartilage layers.

c. Ligaments

Since in the original Smit's model, the stiffness of the supraspinous and interspinous ligaments were arbitrarily modified in order to validate the simulated behaviour under flexion (Smit, 1996), the strain stress relationships of the posterior ligaments were reviewed. Their relative contribution to resist flexion was evaluated from experiments of Adams et al (Adams *et al.*, 1980), where force-rotation curves up to full flexion of lumbar functional units were determined after the successive resections of the supraspinous/interspinous ligaments, the ligamentum flavum and the facet joints (Fig. 1.22). The authors determined that in the context of their experimental protocol, the facet joint removal effect could be directly associated to the capsular ligament removal effect alone. Moreover, if it is assumed that the action of the spinal ligaments is governed by their main unidirectional collagen bundles, the softening of the segment measured by the testing apparatus of Figure 1.22 might fairly correspond to the principal resisting force offered by the removed ligament. Note that the way of loading used in the experiment did not only involve a flexion momentum on the segment, but also an anterior shear force. Nonetheless, it has been found that the posterior ligaments are hardly sensitive to such load (Tencer *et al.*, 1982). Berkson et al (Berkson *et al.*, 1979) studied the effect of anterior shear with and without posterior ligaments and pointed out that most of the observed effect was due to the associated bending because of the manner they applied the shear force. Hence, the differences between the experimental curves of Adams et al (Adams *et al.*, 1980) were directly associated to the response of each removed ligament to the measured rotation (Fig. 2.12a,b). After that,

the ligament strain data determined by Panjabi et al (Panjabi *et al.*, 1982) as a function of the segmental rotation were used to associate the rotations reported in Figure 2.12 with the strain level in each ligament (Fig. 2.12c). In the study of Adams et al (Adams *et al.*, 1980), the supraspinous and interspinous ligaments were treated together and no individual deformation curves could be obtained for these two entities. In fact, while they compared their results with those of Myklebust et al (Myklebust *et al.*, 1988), Chazal et al (Chazal *et al.*, 1985) reported the existence of a factor of about two between the forces beyond the linear parts of the respective deformation curves of the supraspinous/interspinous ligaments complex and of the isolated interspinous ligament. A similar comparison with the results of Pintar et al (Pintar *et al.*, 1992) showed the same trend. Therefore, the individual strain-tensile force curve of the isolated supraspinous ligament was reconstructed by dividing by a factor of two the last force value extracted from Adams et al (Adams *et al.*, 1980) for the supraspinous/interspinous ligament complex. The intermediate forces were estimated likewise from the ligament complex curve, assuming intermediate dividing factors that decreased proportionally with the current strains values. The individual ligaments cross-section data from Panjabi et al (Panjabi *et al.*, 1991) were used to calculate the mean stress associated respectively to the interspinous ligament and to the interspinous/supraspinous complex force values. Under the hypothesis that the total resisting stress offered by the complex is the sum of the stresses in each ligament weighted by its respective volume fraction (analogy with the parallel aligned structures mixing theory), the ligament volume fractions were estimated through the quantitative geometrical data of Panjabi et al (Panjabi *et al.*, 1991). Then for each interspinous ligament strain value, a corresponding stresses could be computed for the supraspinous ligament. Cross section data from Panjabi et al (Panjabi *et al.*, 1991) were used again to return from stress to force and the resulting posterior ligament individual strain-force curves are presented in Figure 2.12d. The mean tangent stiffness in the linear parts of the obtained supraspinous and interspinous ligament deformation curves were determined and according to Pintar et al (Pintar *et al.*, 1992), the supraspinous ligament was found to be about 2.8 times stiffer than the interspinous ligament. The maximum computed forces which should mark the end of the linear section in both ligaments (Adams *et al.*, 1980), were in a relation similar to that found by Myklebust et al (Myklebust *et al.*, 1988).

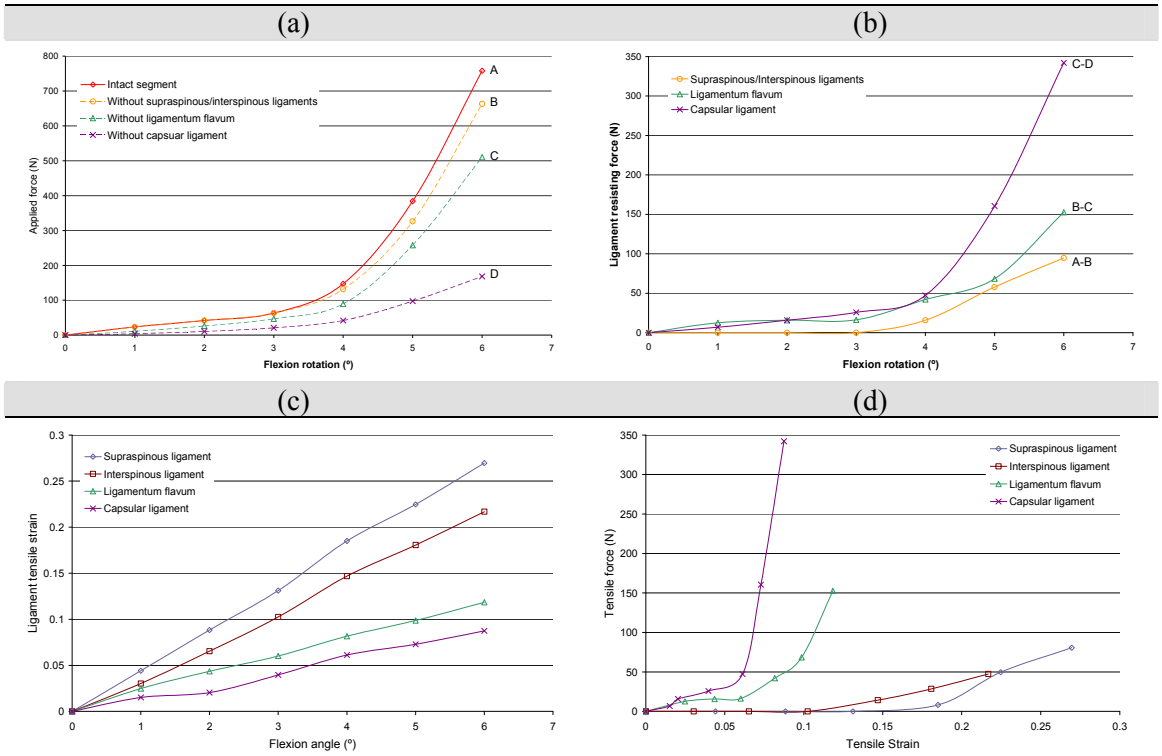

Figure 2.12: a) Experimental curves obtained by Adams et al (Adams et al., 1980) after successive resections of posterior ligaments (testing apparatus presented in Figure 1.22). b) Resisting force exerted by the removed ligaments, estimated by differences of the previously cited experimental curves.

For the intertransverse and the longitudinal ligaments, experimental mechanical data were obtained from the literature and directly expressed in terms of Green strain and 2nd Piola-Kirchhoff stress. As the available experimental data spread over a wide range and only few studies presented whole strain-stress curves, some characteristics of the ligaments stretching behaviour were used and mathematically interpolated. In accordance to the findings of Viidik (Viidik, 1980) on the mechanics of fibrous tissues with parallel collagen framework, the elastic domain of the ligament traction curve was divided into a toe part and a linear part (Fig. 2.13). The transition point between both parts marked in Figure 2.13 was quantified by Chazal et al (Chazal *et al.*, 1985) for most of the lumbar spine ligaments. The authors only reported mean values that included various levels. Hence, their data were combined with those of Pintar et al (Pintar *et al.*, 1992) who determined the mean slope of the force-deformation curve linear part for each ligament and at each level of the lumbar spine. For the intertransverse ligament, the lack of information led to use exclusively the data of Chazal et al (Chazal *et al.*, 1985). For the posterior ligaments, the computed strain-force curves of Figure 2.12 served to find the coordinates of the transition point and the stiffness of the deformation linear part. The conversion of all ligament data to level specific strain-stress values was performed by using the individual ligaments lengths and cross-sections provided by Panjabi et al (Panjabi *et al.*, 1991).

In order to have a smooth representation of the ligaments overall non-linear tensile behaviour, a power law of the form $S = BE^A$ was chosen. Such type of function has been used successfully by various authors for the description of the non linear static tensile behaviour of collagen reinforced soft tissues (Haut and Little, 1972). The parameters A and B of the power law were determined at the transition point of each ligament so that:

$$S_{transition} = BE^{A}_{transition} \tag{2.5}$$

$$\left.\frac{dS}{dE}\right)_{transition} = ABE^{A-1}_{transition} = C \tag{2.6}$$

where C is the tangent stiffness of the linear part (Fig. 2.13).

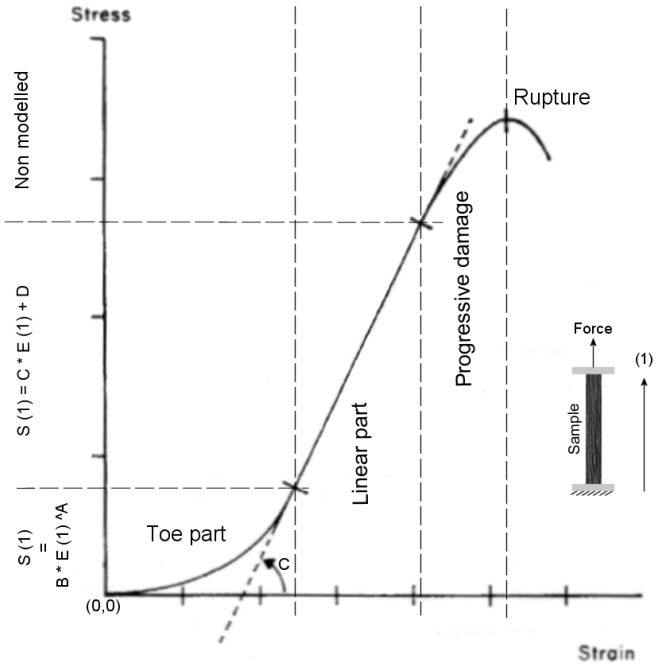

Figure 2.13: Modelling of the typical strain-stress curve for fibrous tissues with parallel aligned collagen framework (Adapted from (Viidik, 1980))

Table 2.3 gives the values of A, B and C calculated for each ligament of the lumbar spine bi-segment model, as well as the corresponding coordinates of the transition point between the power function toe part and the linear part. The final deformation curves computed for all the seven ligaments are represented in Figure 2.14 for each level of the lumbar spine bi-segment.

Table 2.3: Summary of the characteristic values used for the modelling of the bi-segment model ligaments

Ligament	Level	Transition point		Curve fit		
		Green strain	2nd Piola Kirchhoff stress (MPa)	*A*	*B* (MPa)	*C* (MPa)
Supraspinous	L3-L4	0.20	0.10	15.76	8.70×10^{9}	7.70
	L4-L5	0.20	0.09	15.76	8.08×10^{9}	7.14
Interspinous	L3-L4	0.16	0.25	4.07	4.66×10^{2}	6.52
	L4-L5	0.16	0.34	4.07	6.32×10^{2}	8.85
Ligamentum flavum	L3-L4	0.08	0.54	5.64	3.11×10^{5}	34.01
	L4-L5	0.08	0.50	5.64	2.83×10^{5}	30.98
Capsular	L3-L4	0.06	0.43	13.59	8.83×10^{15}	92.57
	L4-L5	0.06	0.44	13.59	8.94×10^{15}	93.84
Intertransverse	L3-L4	0.09	10.00	3.77	9.20×10^{4}	424.98
	L4-L5	0.09	10.00	3.77	9.20×10^{4}	424.98
Posterior longitudinal	L3-L4	0.12	1.84	1.68	68.4	26.60
	L4-L5	0.12	1.84	1.37	35.2	21.70
Anterior longitudinal	L3-L4	0.13	1.03	3.18	7.28×10^{2}	25.70
	L4-L5	0.13	1.03	2.96	4.58×10^{2}	23.89

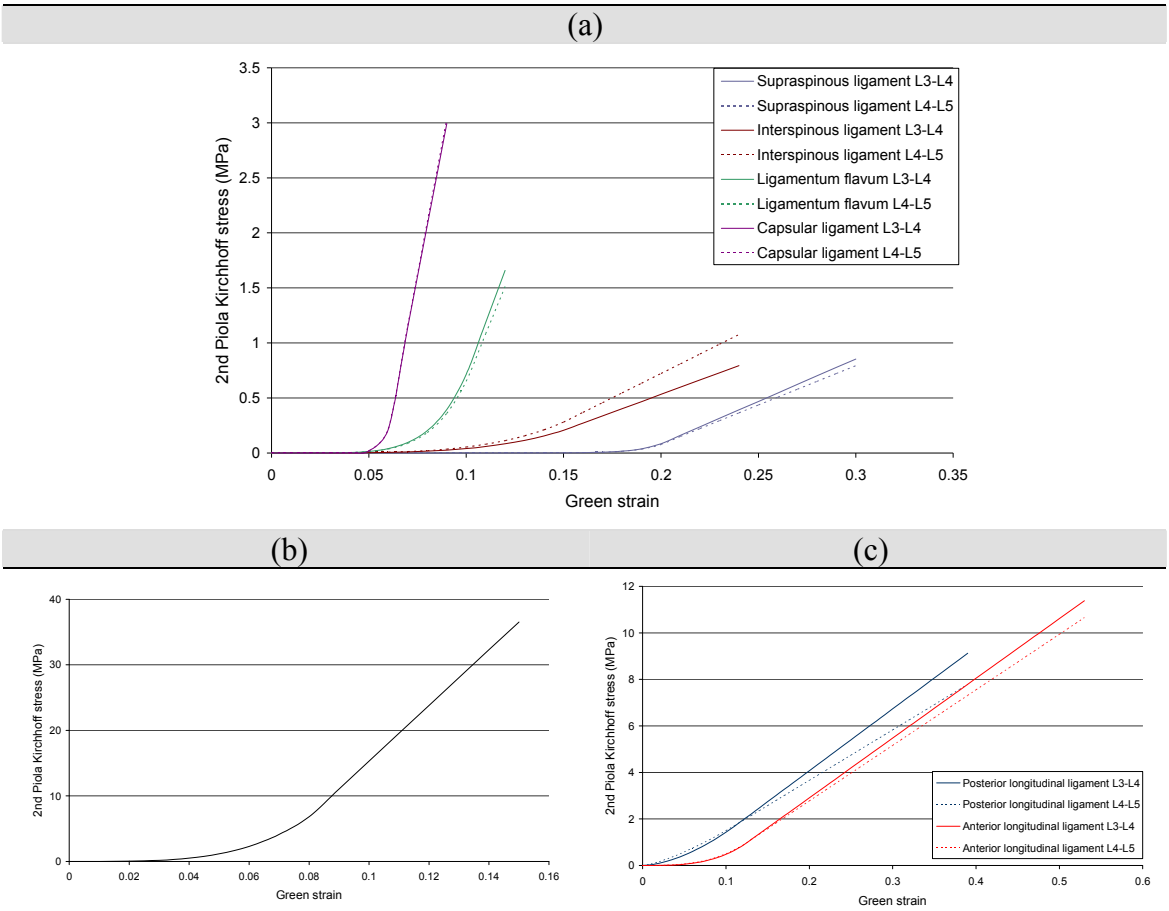

Figure 2.14: Deformation curves of the modelled ligaments (computed from data of Table 2.3)

d. Annulus fibrosus collagen fibres

According to the mechanical tests performed by Haut and Little (Haut and Little, 1972), the annulus fibrosus collagen bundles were also fitted to a power function of the type $S = BE^A$. Parameters B and A were fitted to the fibres traction curve used for collagen I by Sharma et al (Sharma *et al.*, 1995) and were found to be respectively 2.23×10^6 MPa and 3.15×10^6 MPa. Note that these values allow a phenomenological description of the collagen uniaxial non-linear stress-strain curve and taken individually, they do not have any physical meaning. The toe part of the deformation curve finished at 4.42% strain and 28.75MPa stress (values converted to Green strain and 2nd Piola Kirchhoff stress), and the linear part was characterized by a tangent modulus, C, of 847.76 MPa. The radial change of collagen I to collagen II content was modelled and the mechanical behaviour of collagen II was calculated by multiplying the tangent stiffness of collagen I by a factor of 0.77 that was estimated from the experimental work of Sun and Luo (Sun *et al.*, 2002) on human type II procollagen. Considering that the annulus fibrosus collagen bundles are composed by parallel fibres of collagen I and II, the resulting stiffness of the bundle will be given by the weighted sum of the collagen components tangent moduli. The relative contents of collagen I and II were taken from

the quantitative study of Bricley-Parsons and Glimcher (Brickley-Parson and Glimcher, 1984) for young adults and were used to compute the apparent stiffness pattern of the fibres through the thickness of the modelled annulus fibrosus. Table 2.4 gives the collagen bundle tangent stiffness in each radial zone of the annulus as a function of k_I, the general collagen I tangent stiffness, and Figure 2.15 compares the corresponding deformation curves with those computed for collagen I and collagen II only.

Table 2.4: presentation of the composition and corresponding tangent stiffness of the modelled annulus heterogeneous collagen bundles (see Figure 2.8a for the description of the radial areas).

Annulus radial section	OUT	MID(1)	MID(2)	IN
Collagen I to collagen II relative content	0.78	0.59	0.40	0.34
Bundle apparent stiffness	$0.95k_I$	$0.91k_I$	$0.86k_I$	$0.85k_I$
Collagen I deformation curve:		toe part	$k_1 = \frac{dS}{dE} = ABE^{A-1}$	
		linear part:	$k_1 = \frac{dS}{dE} = C$	

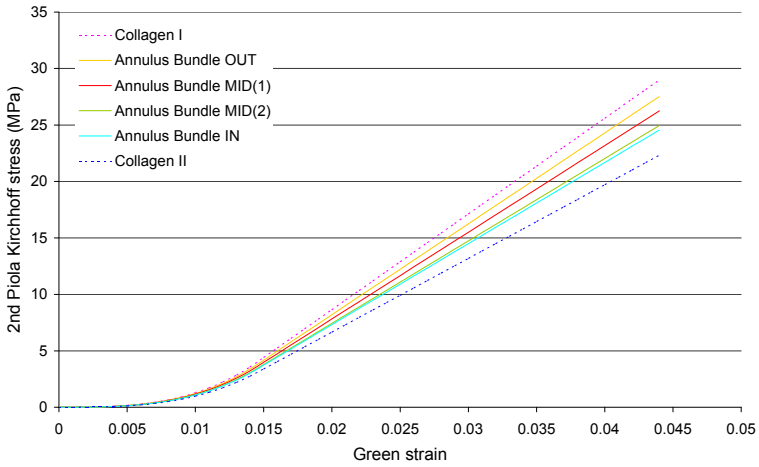

Figure 2.15: Deformation curves computed for the collagen I, II and the bundles of the different annulus radial areas.

C. Stress analysis – The significance of stress

The behaviour of the different modelled tissues will be studied by using a stress analysis of the model and through comparisons of the different information given by different types of stresses. The stress field acting on a normal vector to a surface plane of a deformable continuum body is the result of the action of external loads (traction, compression, shear forces, etc…). It translates the resistance of the body to the

deformations induced by the boundary conditions, and depending on these latter, different types of stress with different magnitudes will be generated. Consequently, in the case of load transfer from a body part to another, the study of the stresses can provide thorough information on how the different parts may mechanically interact. In accordance to the large strain option used in the finite element code, all the following descriptions are based on the current configuration of the body (material coordinates), which corresponds to the nature of the computed stresses that will be presented and discussed in the following sections. The mathematical formalism used in this section comes principally from Holzapfel (Holzapfel, 2000) and Crisfield (Crisfield, 1996). Therefore, for more details, the reader can refer to these books

I. Stress

In order to briefly introduce the notion of stress and the different types of stress that will be studied in the further sections, first we postulate that arbitrary external forces act on the boundary surface of a three-dimensional deformable body Ω. On a virtual internal surface that cuts the body in two portions, this situation results in the action of distributed internal forces (Fig. 2.16). Considering the force transfer across the internal plane surface that is due to the interaction of the two body portions, the infinitesimal force *df* that exerts on an infinitesimal surface element *ds*, centred at point $\boldsymbol{x}$ and whose normal is *n*, can be defined as follow:

$$df = tds \tag{2.7}$$

with $$t = t(x,n) \tag{2.8}$$

t is the force measured per unit surface area and represents the Cauchy traction vector that acts on *ds* with the outward normal *n*. The Cauchy stress theorem states that there exists a unique second-order tensor field, σ, so that:

$$t(x,n) = \sigma(x)n \qquad \text{or} \qquad t_i = \sigma_{ij}n_j \quad i,j = 1,3 \tag{2.9}$$

$\boldsymbol{\sigma}$ is called the Cauchy stress tensor that in matrix notation can be written as:

$$\sigma = \begin{bmatrix} \sigma_{11} & \sigma_{12} & \sigma_{13} \\ \sigma_{21} & \sigma_{22} & \sigma_{23} \\ \sigma_{31} & \sigma_{32} & \sigma_{33} \end{bmatrix} \tag{2.10}$$

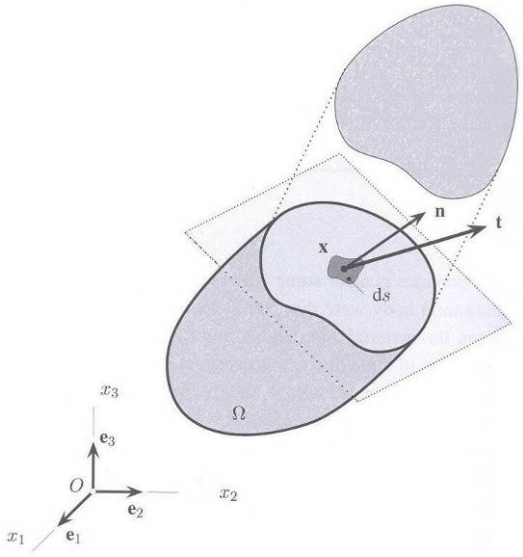

Figure 2.16: Traction vector acting on an infinitesimal surface element with outward normal unit (Adapted from (Holzapfel, 2000))

In order to express the stress components, the unique stress Cauchy tensor has to be projected along an orthonormal set of basis vectors, which gives:

$$e_i \bullet \sigma e_j = e_i \bullet t_{e_j} = \sigma_{ij}$$, where " $\bullet$ " represents the scalar product

By analogy with Equation (2.9), t_{e_j} represents the Cauchy traction vector acting on the surface element whose outward normal points in the direction $\boldsymbol{e_j}$, so that $t_{e_j} = \sigma e_j$, $j = 1,3$

Hence, the traction vectors on any surface elements are determined uniquely by the set of the given quantities σ_{ij} that are the stress components of the Cauchy stress tensor:

$$\begin{aligned} t_{e_1} &= \sigma e_1 = \sigma_{11}e_1 + \sigma_{12}e_2 + \sigma_{13}e_3 \\ t_{e_2} &= \sigma e_2 = \sigma_{21}e_1 + \sigma_{22}e_2 + \sigma_{23}e_3 \\ t_{e_3} &= \sigma e_3 = \sigma_{31}e_1 + \sigma_{32}e_2 + \sigma_{33}e_3 \end{aligned} \qquad (2.11)$$

As shown in Figure 2.17, the system of equations (2.11) can be graphically represented at the point $\boldsymbol{x}$ of Figure 2.16, within a volume element defined by the surfaces normal to the set of basis vectors. In order to respect a logical link between the subscripts used in Equations (2.9), (2.10) and (2.11), the first index of the stress components represents the plane on which t is acting, and the second index characterizes the component of the vector t_{e_i} at x in the orthonormal base $\{e_i\}$.

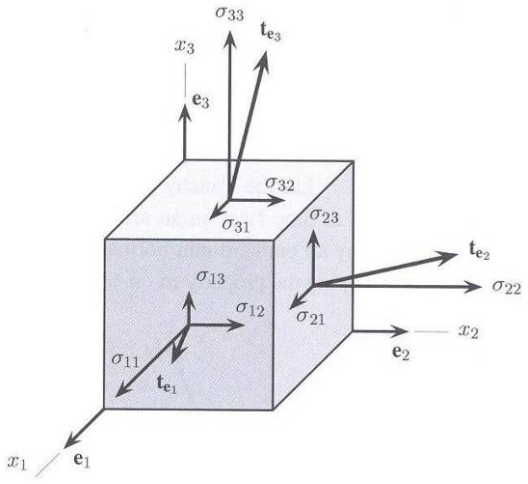

Figure 2.17: Positive stress components of the traction vector t acting on the faces of a cube (Adapted from (Holzapfel, 2000))

II. Normal stress & shear stress

The Cauchy traction vector t that appears at point $\boldsymbol{x}$ in Figure 2.16 can be divided into a normal and a tangential component with respect to the arbitrary oriented surface element (Fig. 2.18):

$$t = t_{//} + t_{\perp} \tag{2.12a}$$

$$t_{//} = (n \bullet t)n \quad , \quad t_{\perp} = (m \bullet t)m \tag{2.12b}$$

By using Equation (2.5), it is found that:

$$\begin{aligned} t_{//} &= n \bullet \sigma n = n_i \sigma_{ij} n_j \\ t_{\perp} &= m \bullet \sigma n = m_i \sigma_{ij} n_j \end{aligned} \tag{2.12c}$$

Therefore, while $t_{//}$ represents the diagonal elements of the Cauchy stress matrix (Eq. (2.10)), $t_{\perp}$ represents all the remaining components that act tangentially to a surface element. The lengths of $t_{//}$ and $t_{\perp}$ are respectively called the normal and shear stress. Positive normal stresses are "tensile stresses", and negative ones are "compressive stresses". For shear stresses, the sign has no physical relevance.

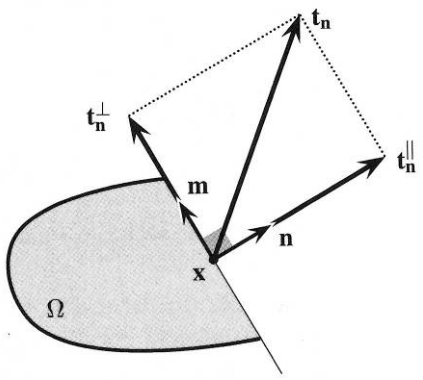

Fig. 2.18: Normal and tangential components of the Cauchy traction vector (Adapted from (Holzapfel, 2000))

III.Principal stress & Maximum shear stress

As shown in Figure 2.17, for a given point, and at given time, the normal and shear stresses vary in magnitude and direction, depending on the considered element surface. Therefore, in order to evaluate the effective stress state of a material, it is of interest to access to the magnitude and direction of the maximal compressive or tensile stress it has to support. For that, the Lagrange multiplier method, which consists in finding the extreme values of a lagrangian function, may be used. If λ and v (respectively the extreme stress value and its direction vector) are the searched items, the stationary position of the lagrangian function $L(v, \lambda)$ with respect to these parameters must be found. The problem can be mathematically expressed as follow:

$$L(v,\lambda) = v \bullet \sigma v - \lambda \left(|v|^2 - 1 \right) \tag{2.13}$$

After derivation, $|v|^2$-1 = 0 must characterize the constraint condition (see Equation (2.16) below) and λ is called the Lagrange multiplier. In index notation, Equation (2.13) becomes:

$$L(v_i,\lambda) = v_i \sigma_{ij} v_j - \lambda (v_i v_i - 1) \tag{2.14}$$

And the stationary position of L is given by the following conditions:

$$\frac{\partial L}{\partial v_k} = \sigma_{ij} \left(\delta_{jk} v_i + \delta_{ik} v_j \right) - \lambda \left(2 v_i \delta_{ik} \right) = 2 \left(\sigma_{ki} v_i - \lambda n_k \right) = 0 \tag{2.15}$$

$$\frac{\partial L}{\partial \lambda} = v_i v_i - 1 = 0 \tag{2.16}$$

From (2.15) and (2.16), the following eigenvalue problem can be expressed:

$$\left(\sigma - \lambda I \right) v = 0 \tag{2.17}$$

$$|v| = 1 \tag{2.18}$$

I is the identity matrix, and λ and v are respectively taken as the eigenvalues and eigenvectors of the problem. Taking into account that the eigenvectors are not zero, and replacing σ by its matrix expression (2.10), Equation (2.17) leads to a system of three equations that has a non trivial solution only if the determinant of $(\sigma - \lambda I)$ is zero:

$$\begin{vmatrix} \sigma_{11} - \lambda & \sigma_{12} & \sigma_{13} \\ \sigma_{21} & \sigma_{22} - \lambda & \sigma_{23} \\ \sigma_{31} & \sigma_{32} & \sigma_{33} - \lambda \end{vmatrix} = 0 \tag{2.19}$$

Equation (2.19) is a third degree equation with respect to λ, whose solution values are the three principal stresses that are usually described as follow:

$\sigma_I = \lambda_1 \equiv$ *Maximum Principal Stress*
$\sigma_{II} = \lambda_2 \equiv$ *Intermediate Principal Stress*
$\sigma_{III} = \lambda_3 \equiv$ *Minimum Principal Stress*

σ_I and σ_{III} are the extreme normal stresses among all planes passing through a given point at a given time. Since the Cauchy stress matrix is symmetric, the three eigenvectors, v_I, v_{II}, and v_{III}, resulting from (2.17) and (2.18) form an orthonormal basis that sets the principal stress directions along which the normal stress is stationary (Holzapfel, 2000). According to the well-known graphical representations of Mohr, it can also be shown that the maximum shear stress magnitude will be obtained with a half of the largest difference between the maximum stresses, and the corresponding direction is included within a plane that makes an angle of ± 45º with the maximum and minimum principal stresses planes.

IV. Strain energy density

When a body deforms under the action of external loads, it stores an internal potential energy that is function of the total energy and the potential brought by the external loading. For conservative systems, the total energy remains constant and the internal and external mechanical powers are the respective time derivatives of the internal and external energies. In this case, the internal energy at a given time can be expressed as:

$$\Pi_{\text{int}} = \int_{\Omega} \varphi \, dV \tag{2.20}$$

V is the volume contained in the space of the deformable body Ω and φ is the strain energy density or strain energy. As it appears in Table 2.2, the strain energy may also be denoted by W, especially when it represents the energy function for hyperelastic material.

Since the total or kinetic energy of the system is conserved, according to the relation between stress and external load presented above, the strain energy density is solely a function of strains, following the relation:

$$\varphi = \int \sigma : \delta\varepsilon \tag{2.21}$$

where σ is the Cauchy stress tensor (Eq. (2.10)), and ε is the associated log or true strain tensor.

V. Conclusion

The mathematical definitions of this section show the utility of using the different presented mechanical quantities. On one hand, the principal stresses allow identifying the way a material is loaded. Principal directions qualitatively indicate the interactions between geometrical components, and signs of the largest principal stress values may indicate if the considered material points are mostly under compression or under traction. If traction and compression are almost similar, then shear is maximal. If shear is minimal, the stress study can indicate which components favour uniquely traction or compression, etc…. On the other hand, the strain energy density takes into account the balance between stress and strain and would allow comparing the effective stress bearing of a body part. All these considerations are powerful tools in order to investigate how different materials may interact between each other within a common deformable structure, and what would be their contribution to the structure mechanical behaviour.

D. Finite element analysis

I. Boundary conditions

In order to study the role that played the different components of the model in the load transfer within the whole structure, the L3-L5 lumbar spine segment was loaded under sagittal flexion, and axial rotation with pure moments of 15Nm (Panjabi *et al.*, 1982). The effect of a 1000N axial compression follower load, known to produce physiological intradiscal pressure (Wilke *et al.*, 2001; Adams and Dolan, 1995) was also simulated. The lower bony endplate of the L5 vertebra was fixed in all directions and the loads were applied on the upper bony endplate of L3. Since solid hexahedral element nodes do not have any rotational degree of freedom, the rotations were induced by single pure moments centred in the horizontal plane of the L3 upper endplate. They acted on the bi-segment via shell elements that were glued to the surrounding endplate hexahedral elements through a contact procedure. In order to avoid the external punctual load to provoke stress concentrations in the L3 vertebra, the modelled plate

had typical steel material properties, and resulted much stiffer than the surrounding bone. In total the model contained 7902 nodes and 7266 elements. The detail of element types and number is given in Table 2.5.

Table 2.5: Element types and number of elements used in the model.

8 nodes isoparametric hexaedral elements	9 nodes isoparametric Hermann elements	8 nodes Rebar elements	2 nodes three dimensional truss elements	4 nodes bilinear thin shell
5526	848	640	146	106

II. Results

a. Principal stresses

1) Vertebral cortex

For all load cases the cortical shell mainly bore compressive and/or tensile stresses through the vertebral body (Fig. 2.19). In compression, the sign of cortical shell major principal stress changed in the areas close to the intervertebral disc and the bone passed to be under traction as in the surrounding annulus. The situation tended to be similar in flexion for the anterior shell. Figures 2.20a and 2.20b showed that in these cases, the surrounding bony endplate parts appeared also slightly tensed with fairly horizontal and outward pointing traction components. Dorsally in flexion and ventrally in extension, the vertebrae were axially stretched and the overall cortical shell bore axial tensile stresses (Fig. 2.20b,c). However, the stress magnitude decreased abruptly toward the bony endplates (Fig. 2.19a,b) and these latter bore outward pointing compressive loads (Fig. 2.20b,c). Under sagittal rotations, the anterior and posterior cortexes were not equally stressed and the cortical shell was generally about twice more tensed than compressed.

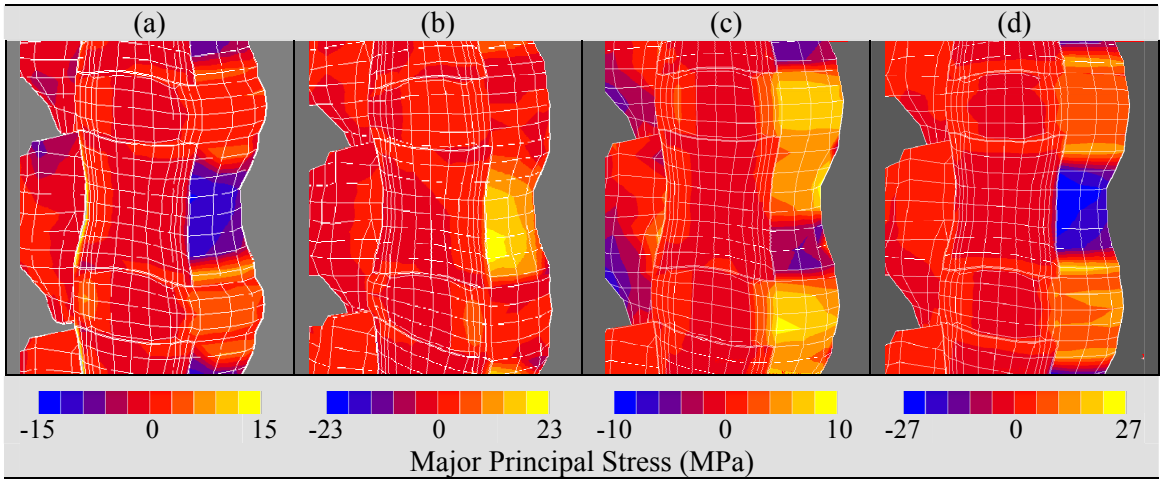

Figure 2.19: Major Principal Stress distribution in the L4 vertebra and its adjacent intervertebral discs (Sagittal cut frontal oblique views). a) Flexion; b) Extension; c) Right axial rotation; d) Axial compression

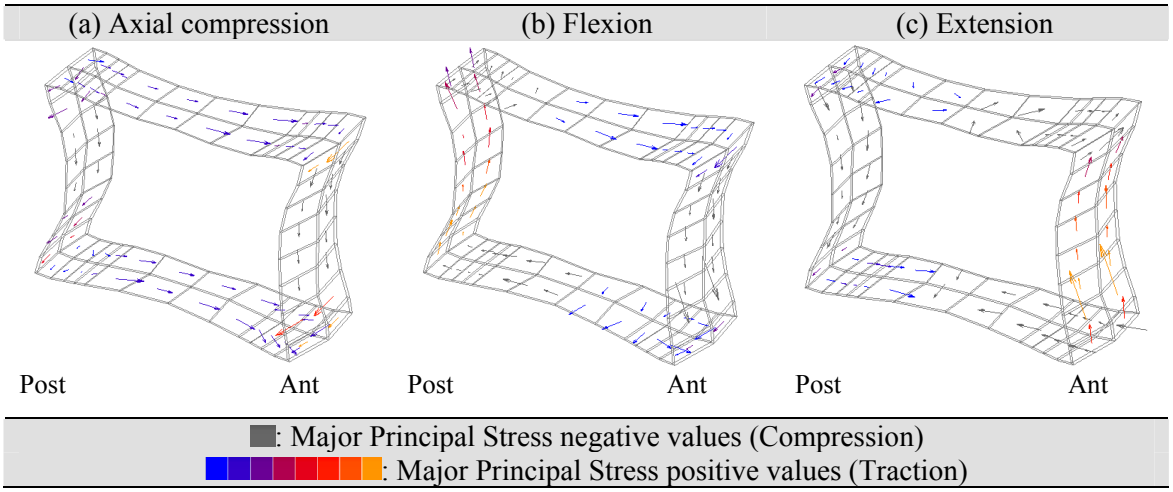

Figure 2.20: Major Principal Stress orientations in the L4 vertebra cortical shell and bony endplates (Oblique views of mid-sagittal plane slices). a) Axial compression; b) Flexion; c) Extension

2) Trabecular bone

As shown by Figure 2.19, the trabecular bone bore mainly compressive stresses and was generally less loaded than the other bony components. In axial compression, while the bony endplates were transversally tensed (Fig. 2.20a), nearly the whole trabecular bone was under axial compression (Fig. 2.19d). The major principal stress directions presented in Figure 2.21 show that most of the trabecular bone compressive stress came from interactions with the intervertebral disc, while the tensile stress components were principally induced by the reaction of the bony posterior elements through the pedicles. For all load cases except axial compression, the major amount of

posterior load seemed to be supported by the zygapophysial joints. Under axial compression, the greatest posterior tensile stress values were located near the superior intervertebral disc and ran obliquely to the bony endplate, pointing toward the nucleus pulposus area. In the anterior part of the trabecular bone, significant tractions were present only in extension and axial rotation, in the annulus fibrosus surrounding zone (Fig. 2.21b,c).

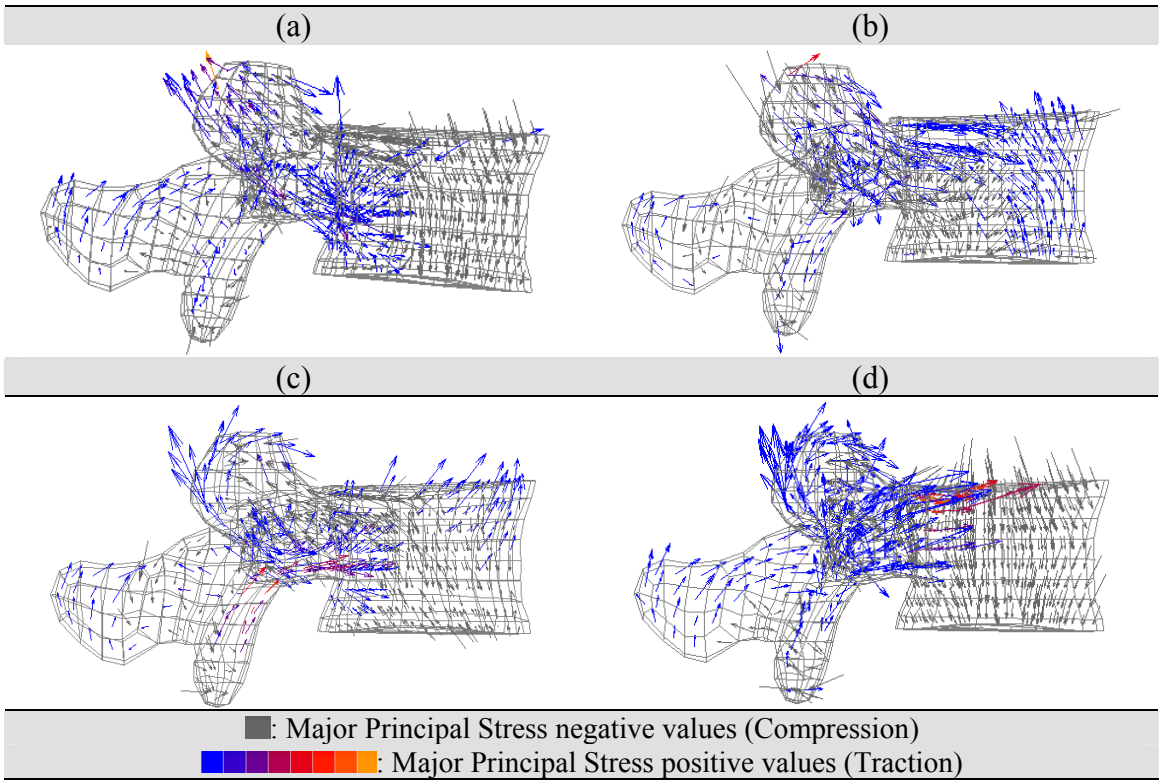

Figure 2.21: Major Principal Stress orientations in the L4 vertebra trabecular bone and bony posterior elements (mid-sagittal plane cuts). a) Flexion; b) Extension; c) Axial rotation; d) Compression

3) Intervertebral disc

The Major Principal Stresses distribution across the intervertebral discs transversal section is presented in Figure 2.22. Except in extension, while the nuclei pulposi were under compression, the annuli fibrosi were under traction. In extension, at the L3-L4 level, the posterior annulus fibrosus was mainly in compression and a large part of the nucleus pulposus bore a slight amount of tensile stresses. Axial compression and axial rotation were the load cases that more heavily loaded the annulus fibrosus and the largest tensile stresses were located in the most external layers. Nonetheless, the tractions were distributed all over the thickness of the annulus, up to the nucleus pulposus zone. In flexion, the same type of results as under compression was obtained for the annulus anterior area. However, in the posterior area as in the anterior area in

extension, the highest stresses were exhibited in the inner part of the mid annulus. In axial rotation, the amount of annulus stress at the L4-L5 level was highly dissymmetric with respect to the sagittal plane. On Figure 2.23a, this dissymmetry was translated by a large transversal component of the stress tensor in the lateral annulus and an axial component in the postero-lateral area. Finally, note that the major principal stress magnitude for the whole annulus corresponded exactly to those computed in the annulus fibre layers only (Fig. 2.23b).

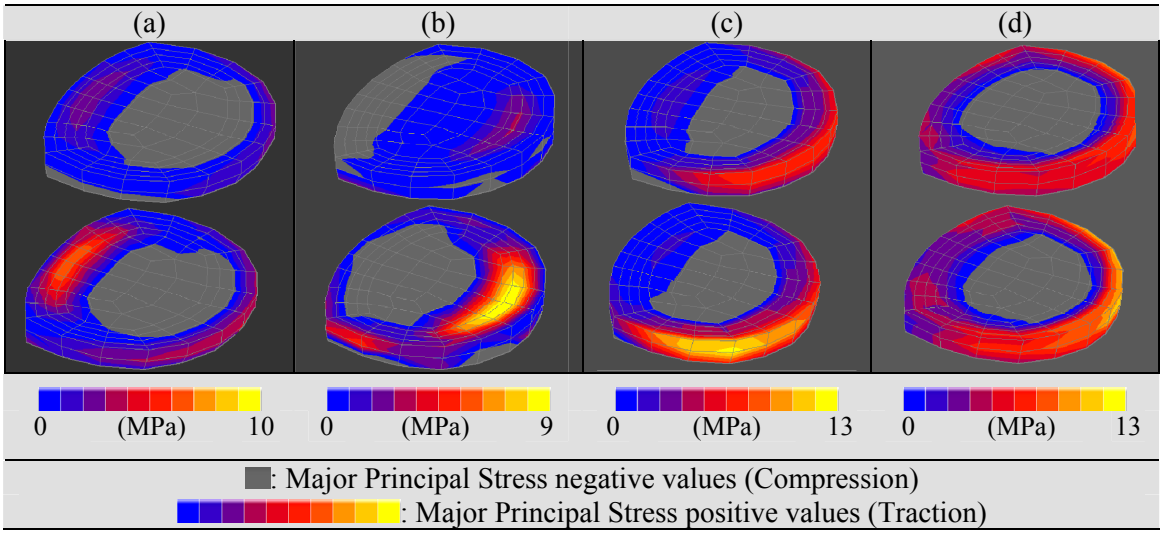

Figure 2.22: Major Principal Stress distribution in the L3-L4 (up) and L4-L5 (down) intervertebral discs (Oblique views of intervertebral discs mid-transversal plane cuts). a) Flexion; b) Extension; c) Right axial rotation; d) Axial compression

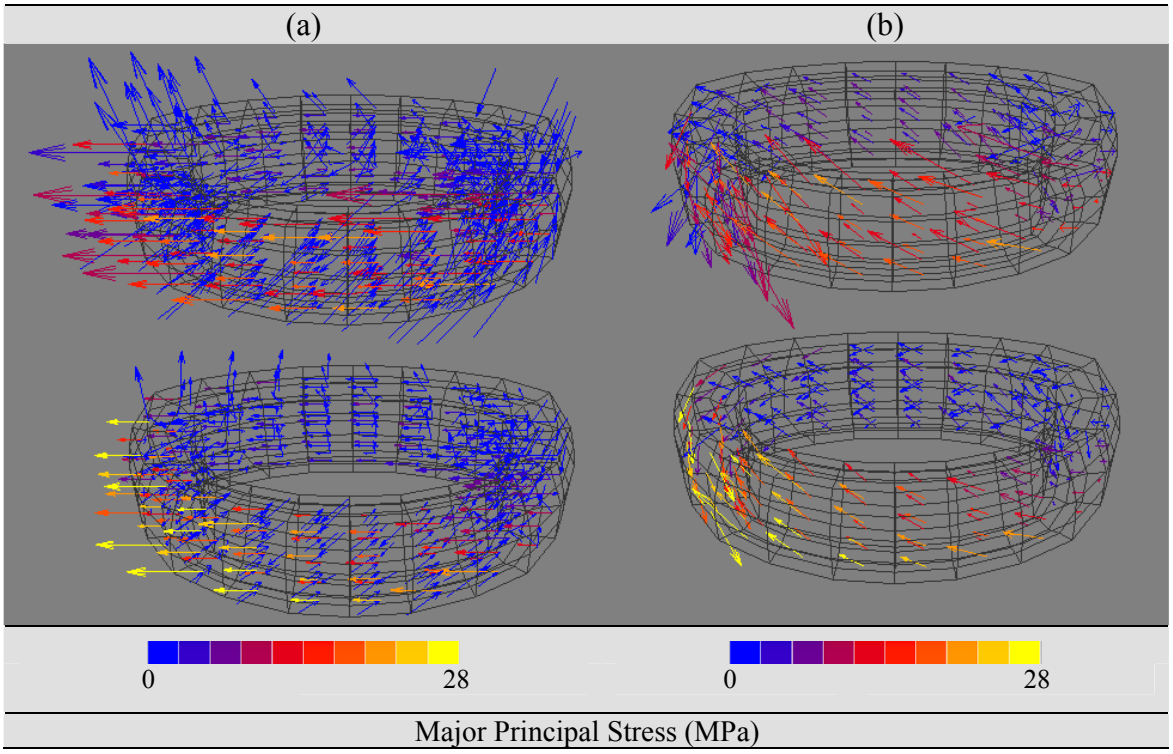

Figure 2.23: Major Principal Stresses in the L3-L4 (up) and L4-L5 (down) annuli fibrosi (Craneo-frontal views) under axial rotation. a) Whole annulus composite structure stresses; b) Fibre layers stresses

b. Shear stresses

The calculation of the shear stresses across the structure showed that in the ventral components (i.e. vertebral body, intervertebral discs) and for all load cases, shear is at least 60% lower than the maximum normal stresses (Fig. 2.24,2.25). The shear stresses were mainly bore by the cortical shell and the annulus fibrosus. In the trabecular bone, the predicted values were insignificant, and just few localised stresses were computed at the borderline of the bony endplates. In axial rotation, only low shear stresses were predicted in the cortical shell close to the intervertebral discs and the maximum values were calculated in the antero-lateral part of the outer annulus fibrosus (Fig. 2.24c). In compression and in flexion the annuli fibrosi ventral stress distributions were similar, although magnitudes were more than two times greater under compression (Fig. 2.24a,d). In extension, the shear stress was comparable to the values obtained under flexion, with the difference that the anterior annulus was not stressed except at superior and inferior edges (Fig. 2.24b). Figure 2.25 shows that dorsally, the major part of shear stresses was located around the bony posterior elements insertion points. In flexion and extension (Fig. 2.25,a,b), posterior shear stress was about twice greater than anterior shear, while in axial rotation and compression (Fig. 2.25c,d), they had similar magnitudes as those found ventrally and laterally in the intervertebral discs (Fig. 2.24). In general, the pedicles itself were not highly loaded; the dorsal shear stress

concentration was located at the anchoring point with the vertebra and around this point, the stresses extend preferentially in the posterior cortical wall.

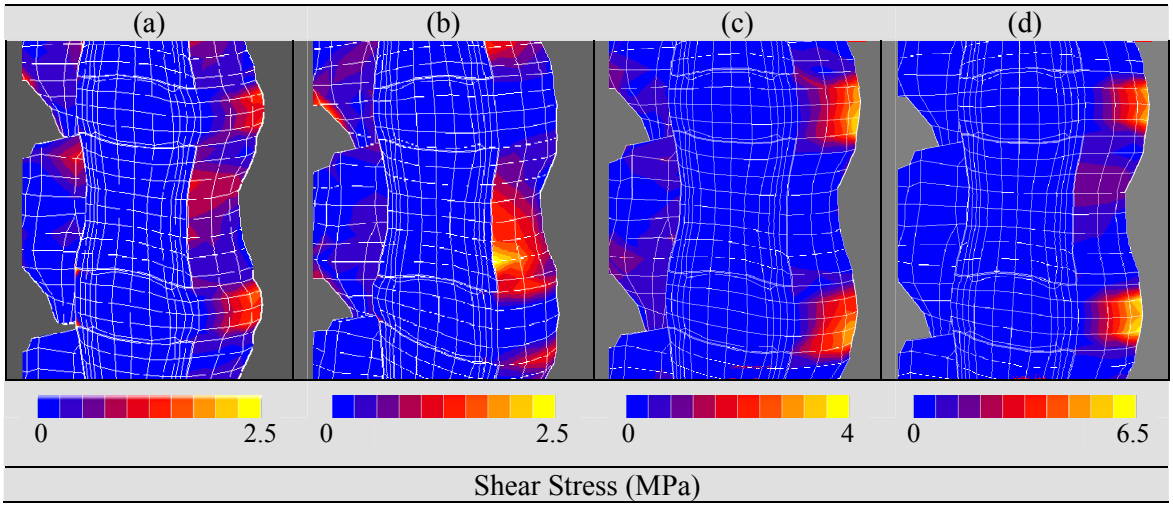

Figure 2.24: Frontal and sagittal plane shear stress distribution in the L4 vertebra and its adjacent intervertebral discs. a) Flexion; b) Extension; c) Right axial rotation; d) Axial compression

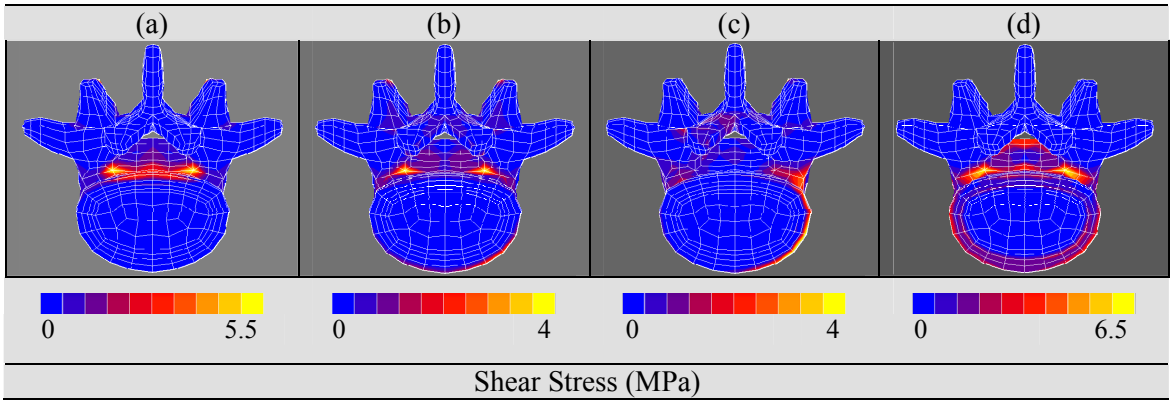

Figure 2.25: Caudal view of the dorsal shear stress distribution in the L4 vertebra. a) Flexion; b) Extension; c) Right axial rotation; d) Axial compression

c. Strain energy density

1) Vertebral body

As shown by Figure 2.26, the strain energy densities in the vertebral cortex were generally higher than in the trabecular bone. Nonetheless, although trabecular bone stresses were fairly insignificant when compared to the cortex (Fig. 2.19, 2.24), the strain energy densities had the same order of magnitude in both components. The

largest cortex strain energies were found in compression, followed by axial rotation and by flexion. Under flexion the greatest relative difference between cortex and trabecular bone strain energy density was predicted. In axial rotation, the strain energy density level within the bony endplate was lower than in the cortical shell, and was about as high as in the trabecular bone. Axial rotation was also the load case that involved the highest trabecular bone strain energy density, and the second largest trabecular bone strain energy density was given under axial compression. At the contrary to flexion, in extension, the smallest differences between trabecular and cortical bone were predicted.

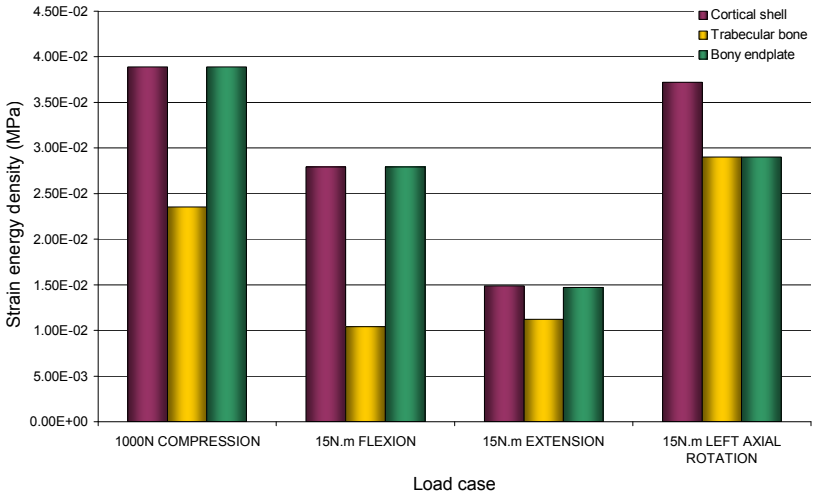

Figure 2.26: maximum values of strain energy density in the different components of the vertebral body.

2) Intervertebral disc

Figure 2.27 shows that annulus fibrosus was the most demanded intervertebral disc component for all the studied load cases followed by the cartilage endplate. The highest annulus and lowest cartilage endplate strain energy densities were predicted under flexion. Axial compression produced the second annulus fibrosus strain energy level and the largest energy values both in the cartilage endplate and the nucleus pulposus. Under compression and flexion, the cartilage endplate values resulted much closer to the nucleus pulposus ones than to the annulus fibrosus ones. Under extension and axial rotation, the situation was reversed, and the cartilage endplate predicted work was nearly similar to that of the annulus fibrosus. In these latter two load cases, the cartilage endplate energy densities were almost equivalent. However, in extension, the nucleus and annulus energies reached their minimum values and resulted lower than in rotation.

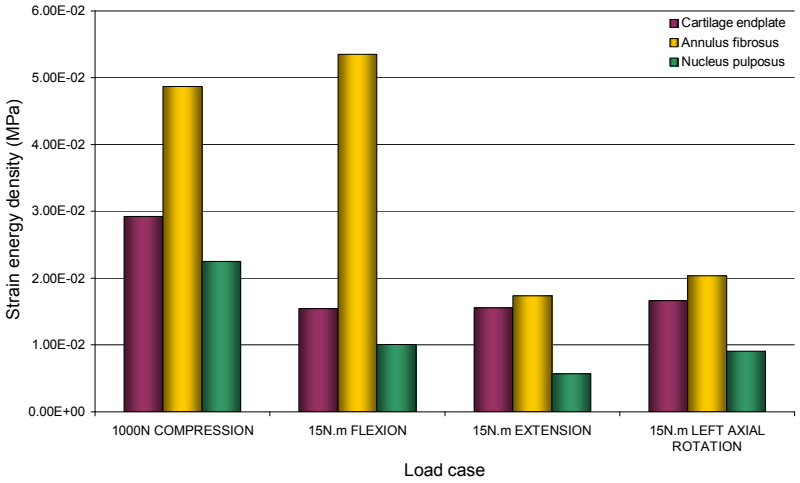

Figure 2.27: Maximum values of strain energy density in the different components of the intervertebral disc

3) Posterior bony components and zygapophysial joints

Except for flexion, the highest strain energy density values were computed within the facet cartilage layers and the maximum work was induced under axial rotation (Fig. 2.28). This latter external load also led to the largest bony elements energy level. In change, the capsular ligament had only a minor relative role in resisting axial rotation and it was mostly active under flexion. With respect to the facet cartilage layers and bony posterior elements, sagittal flexion was the most demanding load case after rotation and involved similarly all the bony and facet joint components. Extension and compression led to significantly lower strain energy level and under extension the role of the facet cartilage layers that was fairly predominant. The lowest strain energies were predicted under compression and the bony elements were the less working components.

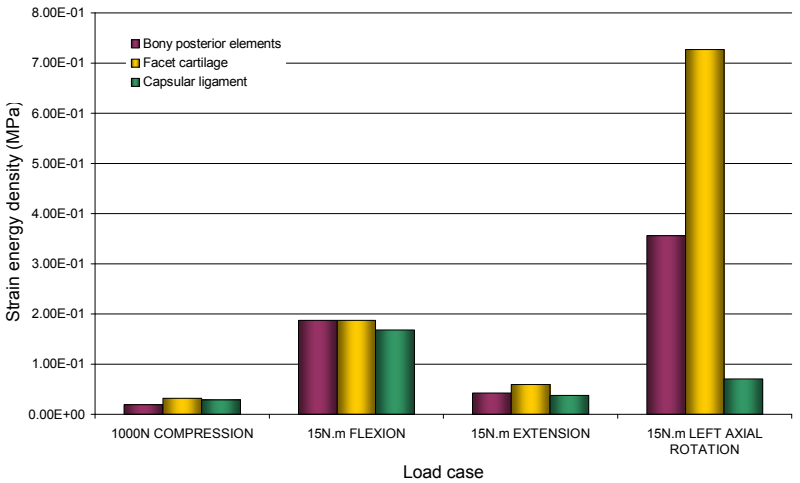

Figure 2.28: Maximum strain energy density values in the bony posterior elements and zygapophysial joints

4) Ligaments

Figure 2.29 shows the strain energy computed in the modelled ligaments. Note that the results concerning the capsular ligament were presented above and not repeated here. For all load cases, the ventral ligaments, namely the anterior longitudinal and posterior longitudinal ligaments store most of the energy of deformation. The maximum peak of energy was calculated for the anterior longitudinal ligament, under compression, followed respectively by flexion, extension and axial rotation. A similar pattern from load case to load case was found for the posterior longitudinal ligament from load case to load case. Nonetheless, the strain energy level of this ligament became insignificant under axial rotation, and the differences between compression, flexion and extension were not so pronounced as for the anterior longitudinal ligament. Flexion was the only load case that allowed the activation of the dorsal ligaments and among them the ligamentum flavum bore the maximum level of energy. The interspinous and supraspinous ligaments worked only slightly and the action of the intertransverse ligament was almost inexistent.

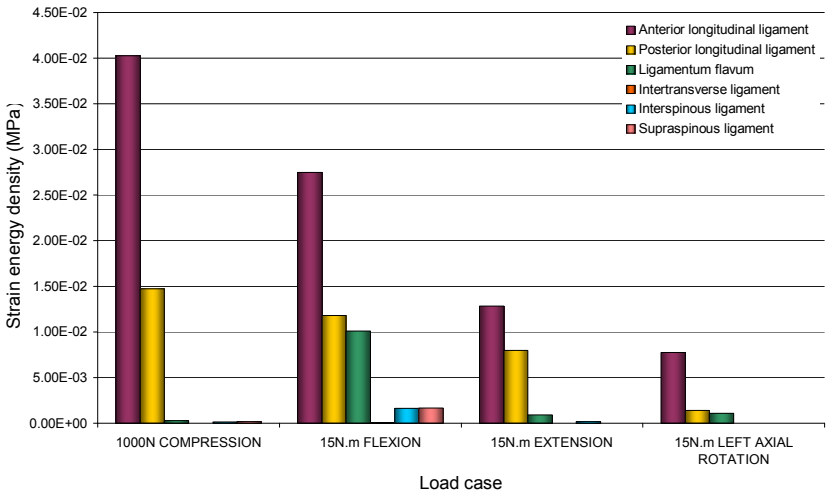

Figure 2.29: Maximum strain energy density values in the spinal dorsal and ventral ligaments (the capsular ligament was not included since it was studied as a component of the zygapophysial joint)

5) General strain energy distribution

Figure 2.30 compares the strain energy densities given in Figures 2.26 to 2.29, and provides a global view of the mechanical work induce by each load case in the different components of the lumbar spine bi-segment model. Axial rotation and flexion were the largest demanding load cases, and the greatest strain energy values were predicted in the bony posterior elements and zygapophysial joints. These components were also the most working ones in the case of extension. Excepting the posterior ligaments, axial compression was the load case that involved more equally the spine

components. Among all the tissues modelled for the anterior spine, the annulus fibrosus bore generally most of the energy. Nonetheless, and curiously, axial rotation involved a greater energy of deformation in the bony parts of the vertebral body than in the intervertebral disc.

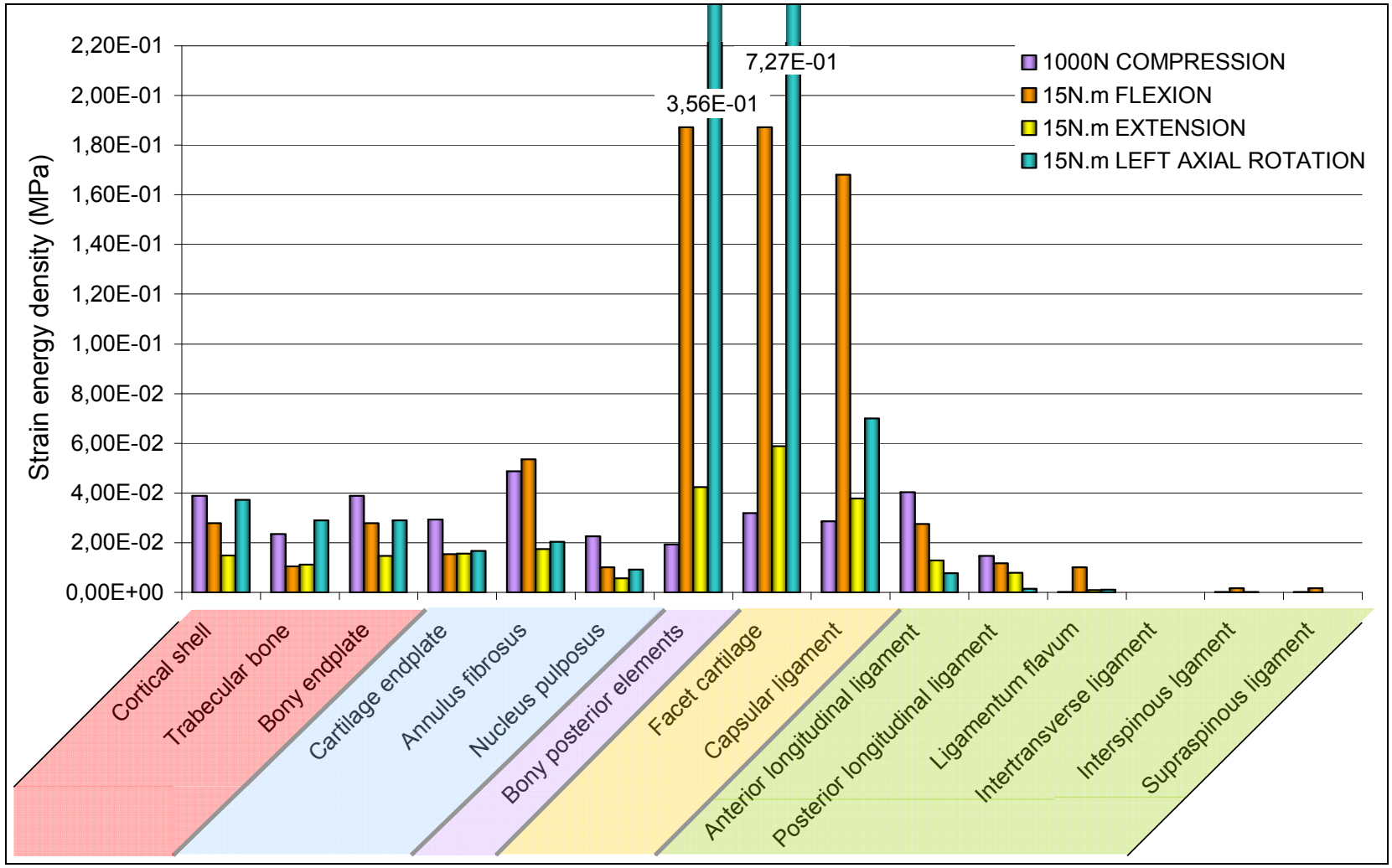

Figure 2.30: Comparison of the maximum strain energy density values computed for each component of the lumbar spine bi-segment model and for each studied load case

III.Discussion

a. Vertebral cortex and annulus fibrosus

For all load cases, it was found that the maximum normal stresses had the major magnitudes in the cortical shell and the annulus fibrosus. In the case of the cortical shell, although the shear stresses resulted at least 60% lower than the normal loads, the difference of magnitudes between the Coulomb and the Young's moduli lead to state that the shear solicitudes were proportionally comparable to the normal ones. Under axial rotation, Ueno and Liu (Ueno and Liu, 1987) predicted significant shear stresses in the vertebral cortex with peak stress at the postero-lateral rim of the bony endplate. According to the authors, higher shear stresses were locally calculated at the border of the bony endplate and in the surrounding area of the cortical shell. Nonetheless, the associated peak stress was rather antero-lateral instead of postero-lateral and otherwise, the computed cortex shear stresses were fairly insignificant. These differences might come from the fact that in the model of Ueno and Liu (Ueno and Liu, 1987), the cortical shell was nearly half of the annulus fibrosus thickness in which the poorly distributed strong fibres were likely to generate high shear states (Iatridis and Gwynn, 2004). Moreover, as the authors applied a combined compression, the interactions at the posterior facet joints may have influenced differently the location of the highest shear intensity.

In the intervertebral disc, the major load that was predicted in the annulus fibrosus was due to the action of the collagen fibres. As shown in the case of flexion and axial compression, disc bulge was highly responsible for the annulus fibres stress state and because of the large deformations undergone by the soft structure, the maximum principal stresses tended to be transversally oriented with respect to the cortical shell. Such situation illustrates the anatomical-based predictions of Humzah et al (Humzah and Soames, 1988) that the fibrous structure of the disc should be able to oppose stress in three dimensions in order to resist all types of deformations. It also may explain both the high shear and normal stress levels computed in the vertebral body bony shell. Given that the natural lumbar spine is mainly under compression, to the point of view of the bone remodelling process, these results are in good agreement with the axial concave shape of the lumbar vertebrae (Goel *et al.*, 1995b). The bulge and shrinkage of the annulus fibrosus, for example respectively predicted dorsally and ventrally under extension, contributed to put the bony endplates under compression or traction along their transversal plane. Under axial rotation, the annulus oblique fibres were directly stretched by the disc shear deformation and induced almost normal stresses within the cortical shell. These interpretations put in evidence a strong interaction between the annulus fibrosus and the vertebral body cortex, which contributes to transfer axially most of the loads along the anterior spine.

b. Trabecular bone and nucleus pulposus

Given the previous comments about the cortex mechanical role, the trabecular bone appears clearly shielded by the peripheral action of the cortical shell and bony endplates, and its low predicted stress level is quite adapted to its natural low dense structure. While the cortex bears any type of stress, the simulations revealed that the trabecular bone worked mainly under axial compression, which once more is in agreement with the porous structure of the bone that has been shown to be principally axially oriented and designed to resist mainly compressive loads (Smit *et al.*, 1997). For all load cases, and especially in the case of axial compression, the trabecular bone compressive state seems to come from the interaction with the intervertebral disc, in particular with the nucleus pulposus. In fact, the nucleus pulposus was almost always under compression. This was certainly due to the reaction of the annulus fibrosus fibres that bound together the bony endplates through the annulus matrix; the activation of the fibres makes them to pull down the superior moving vertebral of the segment, putting the nucleus pulposus under compression. The nucleus is confined and its lateral bulging is limited by the fibrous structure of the annulus; therefore, it acts as an important central supporting component. Since the bony endplates are laterally anchored to the stiff cortical bone, they may bend under the nucleus action and transfer the central compressive stress from the intervertebral disc to the trabecular bone. Note that axial compression generated one of the highest strain energy level within the trabecular bone and according to the previous interpretation the strain energy was similar in the bony endplates and in the cortical shell. Axial rotation induced the largest trabecular bone strain energy and the energy level was similar as in the bony endplates. In this case, no vertical displacements were introduced by the external loading. However, the large oblique reaction of the annulus fibres also put the nucleus under compression, resulting through the bony endplates in a wide area of axial compressive stress over the entire trabecular bone core. The fact that the bony endplate could transmit the intradiscal pressure generated either by direct compression of the disc or through the confining action of the strong annulus is in agreement on one hand with the experimental correspondence found by Nachemson (Nachemson, 1963) between the nucleus pulposus stress state and the annulus fibrosus tissue, and on the other hand with the greater bony endplate strength measured by Grant et al (Grant *et al.*, 2002) adjacently to the nucleus pulposus of non degenerated discs. Roberts et al (Roberts *et al.*, 1997) had also found that the central thickness of the bony endplate was positively correlated with the magnitude of the intradiscal pressure.

c. Nucleus pulposus and cartilage endplate

The stated mechanical link between the nucleus pulposus and the trabecular bone could also bring an explanation on the strain energy density results obtained for the different components of the intervertebral disc. Axial compression and flexion induced the largest axial compressions on the nucleus pulposus, which produced an axial load transfer to the cartilage endplate. The strain energy of this latter resulted then fairly close to that of the nucleus pulposus. In the case of extension or axial rotation, the nucleus axial compression was lower, and the cartilage endplate strain energy was

closer to that of the annulus. Nonetheless, it remained larger than that of the nucleus. This indicates that although the direct mechanical role of the cartilage endplate could not be clarified and has even been considered in the past as mechanically non relevant (Shirazi-Adl *et al.*, 1986), this component seems to act in the bi-segment model as an integrator for the loads transmitted by the nucleus pulposus, either directly or through the inner annulus fibrosus response. Some simulations performed during the model development without cartilage endplate showed that the absence of the subchondral cartilage, with an inner annulus linked directly to the bony endplates, contributed to slightly higher annulus maximum principal stresses (Fig. 2.31). According to our interpretation about the cartilage endplate, it appears on Figure 2.31 that the annulus was relatively more affected by the endplate under axial rotation, where it may play a larger role in the interaction nucleus pulposus – cartilage endplate.

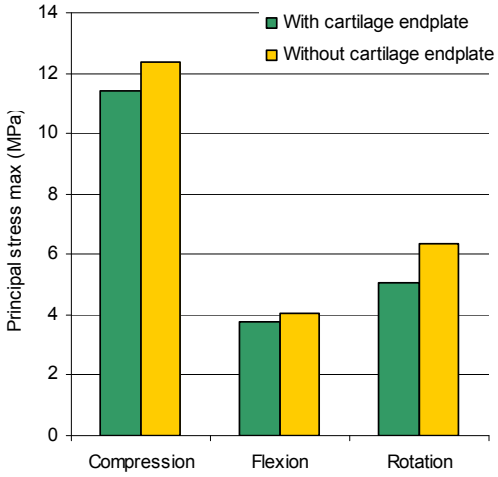

Figure 2.31: Comparison of the maximum principal stress peak values predicted in the annulus fibrosus with and without cartilage endplate (These results are based on calculations performed at an intermediate step of the model with annuli fibrosi modelled as in Figure 2.5 and with different material properties)

d. Zygapophysial joints and posterior bony elements

As shown by the strain energy density results, the role of the posterior elements in resisting the imposed external rotations is fundamental and the main involved tissues were part of the zygapophysial joints, namely the facet cartilage layer, the capsular ligament and the bony articular processes. Under axial compression, the facet joints were also activated. Nonetheless, the intervertebral disc remained the most load-bearing component. In fact, in any load case, there was a charge transfer between the posterior components and the intervertebral disc through the pedicles and the trabecular bone. The predicted principal stresses directions were in good agreement with the oblique trabecular structure found in the pedicle core of the lower lumbar spine (Pal *et al.*, 1988). Nonetheless, the modelled pedicles were considered as isotropic and the specific

orientation of their trabecular was not mechanically represented. The fairly high shear levels that were predicted at the pedicle bases may be a consequence of such approximation and could probably be minimized by the use of an anisotropic stiffness tensor. Nonetheless, the mechanical data on the bony posterior elements in general were limited and the properties used in this study came from a fit based on finite element simulations (Shirazi-Adl *et al.*, 1986). Under axial rotation, the large action of the facet joints obviously limits the deformation within the intervertebral disc, and in a more general sense, as shown by the largest anterior stresses within the annulus during rotational motions, the posterior joints seemed to induce more posterior intersegmental centres of rotation by limiting the axial or transversal displacements of the posterior part of the vertebrae. Hence, the bilateral action of the intervertebral disc and zygapophysial joints contributes to stabilize greatly the posterior part of the spine and lets the anterior annulus assuming the anterior stabilization. Given the previous interactions pointed out between the annulus and the vertebral cortex, it would explain the fact that in the lower lumbar spine, the anterior cortex is significantly denser than the posterior one (Fazzalari *et al.*, 2006). Moreover, this mechanism prevents large deformations to occur at the posterior aspect of the disc, near the spinal medulla area, and should imply a strong interdependence between the posterior annulus and the zygapophysial joints respective states. Such interaction is in agreement with the fact that posterior annulus ruptures occur in isolated discs unprotected by zygapophysial joints subjected to hyperflexion (Adams and Dolan, 1995). Otherwise, posterior prolapse of the disc may only occur under complicated load combinations (Adams and Hutton, 1985). Posterior facet contact may also be responsible for the slight tensile state predicted under extension in a large part of the L3-L4 nucleus pulposus. Note that the semi-experimental model of Goel et al (Goel *et al.*, 1987) led to a similar result.

e. Intervertebral disc

Under flexion and extension, the highest maximum principal stress values were predicted in the bulged parts of the annulus and not where the tissue was stretched. This in agreement with the *in vitro* study of Tencer et al (Tencer *et al.*, 1982), who found that after facet resection under extension, only damages introduced in the posterior bulged annulus had a further effect on the segment. Especially in the case of rotations, a gradient of deformation exists between the inner and outer annulus. Nonetheless, as shown by the maximum principal stress distribution, although maximal values were predicted at the external periphery, tensile stresses were distributed all over the thickness. In fact, in the case of axial rotation, the most inner fibre layer, that is oriented at 45º is already optimally designed to limit the shear deformations provoked by the motion. In the most outer layer, the fibres are more horizontal and therefore need some reorientation before aligning themselves in the maximum shear direction (Guerin and Elliot, 2006). Thus, these fibres allow a larger level of deformation within the soft matrix than the inner ones. Under flexion and extension, the same mechanism occurs in the stretched areas of the annulus; the more horizontal outer fibres reorient more than the inner ones, allowing a larger level of deformation. In change, the inner fibres limit strains in the nucleus surrounding zone. Note that the tension within the inner annulus fibre layers also contributes to restrict the nucleus lateral expansion, which may helps to

generate the intradiscal pressure necessary to the anterior spine stabilization. On one hand, the present interpretation is in agreement with the observations of Brickley-Parson and Glimcher (Brickley-Parson and Glimcher, 1984) who found that the inner annulus collagen bundles were the thickest ones; which points out the mechanical importance of this zone. On the other hand, the higher degree of collagen II measured by the authors, marks the influence of the interaction with nucleus pulposus discussed here, while the higher amount of collagen I at the external periphery is in agreement with the computed levels of deformation and tensile stress. Although in many previous published lumbar spine finite element models the most recent ones, the radial gradient of the annulus fibrosus fibres was not modelled (Goel *et al.*, 1995a; Natarajan and Andersson, 1999; Shirazi-Adl and Parnianpour, 2000; Eberlein *et al.*, 2004; Rohlmann *et al.*, 2006), it appears here to be an important requirement for the annulus fibres to stabilize the intervertebral joint. In fact, as performed in the present study, the choice of fibre angle variations across the annulus is motivated by the accessible anatomical data. Nonetheless, the description of the annulus fibre-induced anisotropy in non degenerated lumbar intervertebral discs is not unique and constant fibre angles across the annulus were reported (Marchand and Ahmed, 1990; Galante, 1967) as well as tangential (Eberlein *et al.*, 2001) or radial angle gradients (Cassidy *et al.*, 1989). Since the annulus fibres have the ability to reorient as a function of the tissue strain (Guerin and Elliot, 2006), as suspected by Humzah and Soames (Humzah and Soames, 1988), such structural aspect may be the result of a mechanical adaptation process for a particular loading history and a particular general morphology. Therefore, the present stress analysis on the lumbar spine bi-segment model could also be used in order to investigate the optimal annulus fibrosus configuration for the particular geometry of the model.

f. Ligaments

The ventral ligaments, together with the capsular ligaments from the zygapophysial joint seem to be the only ones to offer a significant work in resisting the motion. The limited role that was predicted for the supraspinous and interspinous ligaments within the chosen range of *in vitro* non destructive external loads correspond to the modelled ligament stress-strain curves and is in good agreement with various experimental studies about the effect of the ligaments resection on the spine kinematics under similar ranges of load (Schultz *et al.*, 1979; Adams *et al.*, 1980; Heuer *et al.*, 2007b). Opposed to that, Goel et al (Goel *et al.*, 1985) found that the supraspinous and interspinous ligaments were part of the components that had the major restraining effect on flexion. Nonetheless, their conclusions were based on a numerical extrapolation of experimental results in which the greater lever arm of these ligaments was taken into account but not their non linear behaviour. In fact, because of their extreme posterior position, the supraspinous and the interspinous ligaments would undergo rapidly very high stress levels if their behaviour would be linear and their stiffness was high enough to prevent efficiently risks of hyperflexion. Adams et al (Adams *et al.*, 1980) observed that even if these ligaments are fairly slack at small angles of flexion, they are the first to strain once the limit of flexion is exceeded. Therefore, as already hypothesised by some authors, the supraspinous/interspinous complex should behave in such a manner

that it allows the spine to deform and locks the motion only before this latter becomes traumatic (Panjabi *et al.*, 1982; Comín *et al.*, 1995). Even at 10N.m, Sharma et al (Sharma *et al.*, 1995) predicted that about 36% of the total resistance to flexion was provided by the supraspinous and interspinous ligaments of their L3-L4 lumbar spine segment finite element model. This may come from the fact that the non-linear strain-stress curves used by the authors for these ligaments have higher tangent stiffness than ours. In their study, the supraspinous, interspinous, and capsular ligaments had almost similar deformation curves, which may not correspond to the largest restraining role of the capsular ligament point out under flexion in several experimental studies (Adams *et al.*, 1980; Tencer *et al.*, 1982; Twomey and Taylor, 1983; Heuer *et al.*, 2007b). The present modelling of the ligaments mechanical non-linearity is based on crossed data from several in vitro tests on isolated ligaments and including the relative role of the ligament in a functional segment unit. It is interesting to note that the deformation-curves obtained for the posterior ligaments follow a logical order with respect to the distance of each ligament to the centre of rotation of the segment; such configuration allows optimizing the posterior passive resistance of the segment to the length of the lever arm represented by the bony posterior elements. Moreover, the consequent progressive recruitment of the ligaments with increasing deformation angles in flexion allows segment mobility at small levels of rotation without overloading the most external ligaments and ensures the protection of the spinal canal for large deflections.

When axial compression is compared to flexion and extension, the ventral ligaments appear more stretched under disc bulging than under direct axial traction. It may be therefore expected that the addition of a compressive follower force of the segment would contribute to raise significantly the stress in the longitudinal ligaments up to a point where they will become to work exclusively in the linear part of their deformation curves. Given that the annulus fibres have the same type of strain-stress curve and that they are also fairly loaded by disc bulge, this could bring an explanation to the linearization of the lumbar spine flexion-momentum curve found by Patwardhan et al (Patwardhan *et al.*, 2003) when adding an increasing compressive follower force on their L1-S1 multi-segments. Under extension, the capsular ligament together with the facet joint contacts contribute greatly to limit the load bore both by the anterior and posterior longitudinal ligaments, which is in agreement with the experiments of Tencer et al. (Tencer *et al.*, 1982), where an injury of the anterior annulus including the anterior ligament had only a slight effect on the segment behaviour in extension always when the zygapophysial joints remained intact. The large reaction of the posterior longitudinal ligament to bulging, once more should protect the spinal canal against the possible pressing action of the deformed intervertebral disc. Ventrally, the anterior longitudinal ligament which superficial fibres spread over various spine levels (Chapter 1) may contribute limit the traction exerted by the annulus fibres on the cortex.

IV. Conclusion

A complete L3-L5 lumbar spine bi-segment model was created and the stress distribution study that was carried out allowed identifying the mechanical interactions that exist between the different modelled tissues. Such investigation is useful to

extrapolate the *in vitro* experimental data obtained on ligamentous spines and it gives access to interpretations on the mechanical role of some tissues that do not participate directly to the motion and can hardly be experimentally studied. Some interpretations of experimental results can also be further performed on the basis of the predictions from the present study. For example, Farfan et al (Farfan *et al.*, 1970) found that under axial rotation, the annuli fibrosi of degenerated discs failed at lower torques than normal discs. Assuming that disc degeneration is always associated to a loss of nucleus water-binding capacity and lower intradiscal pressures (Walker and Anderson, 2004), it can be deduced from the simulations that the oblique traction exerted by the annulus fibres under axial rotation increases the vertical overall deformation of the disc. Consequently, larger annulus bulging is induced and for a given degree of rotation, annulus stresses rise dramatically. This could explain the lower strength of the degenerated discs and the annulus delaminating observed by Farfan et al (Farfan *et al.*, 1970). Nonetheless, while the authors excluded an eventual mechanical role of the nucleus pulposus, the finite element study shows that this component may have a large participation in the failure process.

In a general manner, a full analysis of multiple mechanical interactions that contribute to the biomechanical stabilization of the bi-segment could be performed. As shown for the ligaments, this even included the implication of introducing particular mechanical laws. Many of the predicted interactions could be directly related to the natural structure in the scope of an optimal relation between form and function. In this sense, the stress analysis could also be used for the self optimization of the model in the context of its particular geometry. Nonetheless, in the present case, despite the sub-structural upgrades performed on the original model (Smit, 1996), the L3 and L4 vertebrae were copies of L4, and the structural differences between the three vertebrae were not taken into account. The bony posterior elements shape had to be fitted to this geometrical approximation and therefore their modelling may also be inaccurate. Both intervertebral discs had the same shape, which does not correspond to reality. It appeared through this study that all these components play an important role in the stress transfer between the different modelled tissues and the impact of their geometrical approximation on the simulated biomechanical behaviour should be first investigated.